ABSTRACT

Title of Document:

MESENCHYMAL STEM CELL
ENRICHMENT AND DIFFERENTIATION
THROUGH FUNCTIONALIZED
BIOMATERIALS

Kimberly Marie Ferlin, Doctor of Philosophy,
2015

Directed By:

John P. Fisher, Ph.D., Fischell Family
Distinguished Professor
Fischell Department of Bioengineering

The use of mesenchymal stem cells (MSCs) for tissue engineering and cell-based therapies has great potential. MSCs are an adult stem cell population capable of undergoing multilineage differentiation into several key tissue types including bone, fat, and cartilage. However, despite key research and clinical advances, these therapies are still largely in the developmental phases. MSCs are typically isolated from the bone marrow using a multi-step process involving density centrifugation and adherence of the mononuclear fraction of cells to tissue culture polystyrene (TCPS). The majority of MSC-based approaches require *in vitro* cell expansion in monolayer to produce the cell numbers necessary for subsequent implantation. Recently, it has been suggested that expansion may cause significant changes to the MSC phenotype. In an effort to simplify the process of MSC isolation and use for such applications,

our goal was to develop a single-step 3D culture system for the capture, culture, and differentiation of MSCs. To this end, we focused on the adhesion of MSCs to an underlying substrate, specifically how adhesion could facilitate one-step isolation. We showed that there are distinct changes in MSC adhesion during differentiation that can be used to separate populations of differentiating cells to decrease the heterogeneity of the cell population for implantation. By tethering proteins typically found in the MSC extracellular matrix onto the surface of polymer scaffolds, we were able to increase the specific adhesion of MSCs over TCPS, the current gold standard. Additionally, surface functionalization could be used as a method to drive rapid and directed differentiation of MSCs. Upon exposure to the heterogeneous population of the bone marrow, cells captured on the functionalized material surface had a similar phenotypic signature to MSC controls. Using 3D printing technology, our polymer scaffolds were translated into a highly controlled 3D environment that supports MSC adhesion, proliferation, and differentiation. The techniques presented here represent the key criteria for the development of a one-step culture system for MSC isolation and subsequent implantation. This work highlights the feasibility of functionalized biomaterials as a means to simplify the current use of MSCs for regenerative medicine.

MESENCHYMAL STEM CELL ENRICHMENT AND DIFFERENTIATION
THROUGH FUNCTIONALIZED BIOMATERIALS

By

Kimberly Marie Ferlin

Dissertation submitted to the Faculty of the Graduate School of the
University of Maryland, College Park, in partial fulfillment
of the requirements for the degree of
Doctor of Philosophy
2015

Advisory Committee:

Dr. John P. Fisher   Professor, Fischell Department of Bioengineering,
                            Committee Chair
Dr. David Kaplan   Tissue Engineering Lab Coordinator, CDRH, Food and Drug
                            Administration
Dr. Adam Hsieh   Associate Professor, Fischell Department of Bioengineering
Dr. Steven Jay   Assistant Professor, Fischell Department of Bioengineering
Dr. Carol Keefer   Associate Professor, Department of Animal and Avian
                            Sciences

Dedication

To Griffin for his love and support throughout this journey.

Acknowledgements

Table of Contents

List of Tables

List of Figures

Chapter 1: Introduction

The use of mesenchymal stem cells (MSCs) for tissue engineering and cell-based therapies is increasing across all fields. However, despite key research and clinical advances, these therapies are still largely in the developmental phases. MSCs are an adult stem cell population capable of undergoing multilineage differentiation, and are known to reside in several tissues *in vivo* including the bone marrow. Isolation of MSCs from the bone marrow is executed through the use of density centrifugation and adherence of the mononuclear fraction of cells to tissue culture polystyrene. The majority of MSC based approaches require *in vitro* cell expansion in monolayer to produce the cell numbers necessary for subsequent implantation. As our knowledge of this stem cell population increases, it has become clear that this *in vitro* expansion phase results in significant changes to the MSC phenotype. These changes may result in significant implications for the effective use of MSCs for cell therapy applications.

To address the issue of *in vitro* MSC expansion, the research presented here is focused on the development of a single-step system on which whole bone marrow can be seeded directly, and MSCs can be subsequently isolated and differentiated on the same material surface. This can be achieved through the use of a three-dimensional (3D) culture system that serves as a more representative environment of the native MSC niche. Previous work has shown that there are many advantages to restoring 3D culture after expansion including the maintenance of MSC multipotency and the secretion of trophic factors. However, these systems only initiate 3D culture after an

expansion phase in monolayer; a 3D culture system for the immediate culture of freshly isolated bone marrow or mononuclear cells has not yet been successfully developed. Such a device would have great implications in the field of cell therapy, particularly as a means to avoid treatment delays and extensive costs accrued as a result of long or complex *in vitro* culture conditions. In order to create a one-step system for the direct culture of MSCs from the bone marrow, we must first gain a greater understanding of the nature of MSC adhesion to the underlying substrate. Cell adhesion is critical to many cell functions including cell survival, proliferation, migration, and differentiation. In the case of MSCs isolated from the bone marrow, cell adhesion is a key characteristic of MSCs that is vital to their isolation. A thorough understanding of MSC adhesion under various culture conditions can serve as a guide for the development of a biomaterial substrate that encourages specific MSC adhesion.

In this work, we use previously established protocols to assess changes in MSC adhesion as cells differentiate down the three main mesenchymal lineages. The understanding of MSC adhesion is used as a guide for the development of a biomaterial platform that encourages MSC adhesion and differentiation and is readily translated into a 3D culture system. The objectives of the presented research are to:

(1) Characterize the adhesive changes of MSCs as a result of *in vitro* culture through the use of a simple and reproducible adhesion assay.

(2) Develop a biomaterial platform that encourages specific MSC adhesion, proliferation, and differentiation.

(3) Translate the biomaterial platform into a relevant 3D culture system using 3D printing technology to elucidate the response of MSCs to 3D scaffold geometry.

The presented objectives will further the understanding of MSCs and the phenotypic changes that occur during *in vitro* culture, specifically changes that relate to cell adhesion. The multipotent nature of MSCs suggests that a one-step system could be used for a wide range of applications, including the repair of cartilage defects. By tuning the material properties to mimic the chemical characteristics of the native extracellular matrix (ECM) and the mechanical properties of the tissue *in vivo*, autologous bone marrow could be seeded onto the device and directly implanted at the injury site in one surgical intervention. The development of a single-step device that will simplify the use of MSCs would offer both economic and clinical advantages compared to current protocols

Chapter 2: Characterization of the Adhesive Interactions between Cells and Biomaterials[1]

Cellular adhesion is critical for many cellular functions, including spreading, proliferation, and migration. The interactions between cells and their environment are mediated by adhesion receptors located on the cell surface. Adhesive interactions can take place between cells, or between a cell and the surrounding extracellular matrix (ECM). Adhesion receptors are responsible for both types of interactions. Biomaterials have been introduced as a means to facilitate cell adhesion and infiltration during the repair or replacement of damaged or diseased tissues. In order for biomaterials to successfully act as an alternative ECM, the interactions between cells and biomaterials must mimic the adhesive interactions in native tissue. Therefore, the control and optimization of adhesive interactions is an important aspect of material fabrication. Cell-material interactions can be regulated through material design and processing. Here we will highlight the adhesion receptors responsible for the interactions that occur within native tissue; current biomaterial fabrication methods that attempt to mimic these interactions for tissue engineering applications, and measurement techniques that investigate cell-substrate adhesion strength.

---

[1] Adapted from: KM Ferlin, DS Kaplan, and JP Fisher. Characterization of the Adhesive Interactions Between Cells and Biomaterials. In: Micro and Nanotechnologies in Engineering Stem Cells and Tissues. (Ramalingam, Jabbari, Ramakrishna, and Khademhosseini, eds.) Wiley – IEEE Press, Hoboken, NJ. 159 – 182 (2013).

2.1 Adhesion Receptors in Native Tissue

Cells form connections with the ECM as well as with each other through adhesion receptors that are present on the surface of the cell. There are three major classes of adhesion receptors: integrins, cadherins, and members of the immunoglobulin family. While the exact functions of each class of receptor may vary, many adhesion receptors share some common properties including the formation of receptor clusters after binding with an extracellular ligand, and the formation of connections to the underlying cytoskeleton. In this work we will focus on integrins, particularly those found on the MSC cell surface.

Integrins are a superfamily of cell adhesion receptors that exist as 24 distinct transmembrane $\alpha\beta$ heterodimers [1], which can be found in Table 2.1. Currently, there are 18α and 8β subunits identified, which associate through noncovalent interactions [2]. The term integrin originates from the importance of such receptors at maintaining the 'integrity' of the cytoskeleton. Integrins primarily interact with extracellular matrix ligands, but also have the ability to interact with cell surface ligands. Integrins serve as a connection between the extracellular environment, where they bind to a ligand or adjacent cell surface, and the intracellular environment, where they bind to the cytoskeleton. Individual integrins may bind to multiple ligands and multiple integrins can share the same ligand [3]. Integrin activation results in alterations of cell behavior, for example adhesion, proliferation, shape, survival/apoptosis, motility, gene expression and differentiation [1]. Due to the importance of integrin activation on cell function, biomaterials can be designed to mimic integrin interactions and achieve specific cell functions. The function of

integrins as transmembrane links between their extracellular connections and the cytoskeletal elements within the cell often plays an important role in mechanosensing. With the exception of α6β4, which links to the intermediate filaments of the cytoskeleton, most integrins form intracellular connections with the actin cytoskeleton [2]. This anchoring function of integrins plays an important role in several cell functions including blocking apoptosis and triggering the progression of the cell cycle.

Current research has supported the function of integrins in mechanotransduction, indicating that integrin activation and initiation of downstream signaling pathways can result in multiple cellular responses including ECM remodeling, differentiation, and survival signaling. Similarly, intracellular integrin activation can occur through the deformation of the underlying cytoskeleton due to stress [4]. Structural alterations of the actin-filamin cytoskeleton exposed binding sites for the β tails of integrins, causing activation and stimulation of downstream signaling pathways.

Integrin activation as controlled through substrate stiffness has recently been shown to play a role in osteogenic differentiation. The differentiation of mesenchymal stem cells into osteoblasts varied with the stiffness of the matrix, resulting in greater differentiation on stiffer substrates [5]. Additionally, a similar correlation was found for α2 integrin expression, indicating that this integrin subunit may play a role in transmitting the mechanical stiffness into differentiation signals. This hypothesis was confirmed through a knockdown of α2 by siRNA that resulted in a downregulation of osteogenic differentiation [5].

The role of integrins in mechanotransduction should be exploited in order to initiate or inhibit downstream signaling in response to integrin activation from mechanical stress. Biomaterial design, specifically material properties and three-dimensional structure, should address ways to promote integrin activation in situations where activation can lead to positive effects such as cell survival or differentiation, but also address means to inhibit integrin activation. Inhibition of integrin responses to mechanical changes that occur during the progression of cancer could have significant therapeutic implications.

In addition to being regulated by ligand binding, integrin function can be controlled intracellularly. For many integrins, the active state is not constitutive. These integrins exist on the cell surface in an "off" or inactive state, in which no ligand binding or downstream signaling can occur until there is activation by an intracellular signal [2]. Platelet activation is an example of this type of integrin regulation. In order to be capable of binding to fibrinogen, von Willebrand factor and fibronectin, the integrin αIIbβ3 must be internally activated. Inside-out activation can occur through several different routes, including through thrombin, ADP, or epinephrine signaling, which function through G protein-coupled receptors; through von Willebrand factor (VWF) signaling which occurs through the VWF receptor; or through collagen signaling which occurs through the collagen receptor and the integrin α2β1 [2]. Recently, it has been shown that the cytoskeletal protein α-actinin plays an important role in the "inside-out" signaling that activates the platelet ligand αIIbβ3 [6]. An understanding of integrin activation in platelets could lead to the

development of drugs and biomaterials that can help initiate clotting from both the inside and the outside.

Some integrin-ligand pairings are more common than others, and specific sequences that appear frequently have been identified. Among the most common of these is the arginine-glycine-aspartic acid (RGD) sequence. Approximately one-third of integrins have binding sites for the RGD tripeptide which can be found on many ECM proteins including fibronectin, vitronectin, fibrinogen, and the LAP complex part of inactive transforming growth factor β. Although the RGD sequence is not readily exposed by collagen or laminin, there are cases where denaturation or cleavage of these proteins results in exposure of the RGD sequence and subsequent integrin binding [7]. The RGD-binding integrins include all five of the αV integrins, two β1 integrins and the αIIbβ3 integrin. RGD binding integrins can bind a large number of ECM and soluble vascular ligands. The ligands that contain the specific tripeptide active site bind with the integrins through an identical atomic basis [8]. The affinity of integrins to the RGD sequence has been exploited extensively in tissue engineering research and therapy development. Recently, nanocarriers with RGD tethering on the surface have been shown to use the integrin-ligand specificity to target tumors that are rich with RGD-binding integrins [9]. Optimization of this drug delivery vehicle to increase the specificity, targeting, and loading efficiency of the nanocarrier can have a significant therapeutic impact. RGD peptides have also been shown to positively influence the differentiation of mesenchymal stem cells into articular chondrocytes [10] as well as the development of functional cardiac tissue from neonatal cardiac cells [11].

Similar to the RGD sequence, the tripeptide leucine-aspartic acid-valine (LDV) is a common ligand among a group of integrins. LDV is an acidic motif that is functionally related to RGD and is suggested to bind to integrin receptors in a similar fashion [12]. LDV is present on fibronectin, and a related sequence is present on vascular cell adhesion molecule-1 (VCAM-1). The β2 integrins as well as α4β1, α9β1, and α4β7 [7, 12, 13] contain a binding site for the LDV ligand.

Although RGD-binding integrins can recognize the RGD sequences that are exposed when collagen is degraded or cleaved, there is another specific amino acid sequence that can be recognized by integrins when collagen structure is intact. The glycine-phenylalanine-hydroxyproline-glycine-glutamic acid-arginine (GFOGER) sequence exists on triple helical collagens. The sequence is recognized by a group of collagen-binding integrins, including α2β1, an important integrin in hemostasis. It is speculated that the GFOGER sequence is exposed once per microfibril unit of collagen [7]. The proximity of the ligand sequences on a microfibril of collagen promotes integrin clustering and focal adhesion formation, the importance of which has already been discussed.

Similar to collagen, binding sequences on laminin are only recognized by RGD-binding integrins if the ECM protein has been disrupted. The integrin binding sequence tyrosine-isoleucine-glycine-serine-arginine (YIGSR) has been discovered as the minimum sequence necessary to promote binding and adhesion between integrin receptors and epithelial cells on intact laminin [14]. YIGSR is found to be highly active in epithelial cells yet much less active in chondrocytes, osteoblasts, and fibroblasts.

Due to the lack of a unique surface marker for MSCs, the cell surface proteome has been studied extensively, and the integrin population is well documented [15]. Major ligands for the integrins present on the MSC surface include laminin, collagen, and fibronectin. CD44, one of the positive cell surface markers for MSCs, readily binds to hyaluronic acid, a molecule that is also a major player in the cartilage ECM. There are also receptors of the MSC surface for fibrinogen, ICAM-4, vitronectin, and E-cadherin, though these exist in a lower abundance.

β subunit	α subunit	ECM binding site
β₁	α₁	laminin, collagen (GFOGER)
	α₂	collagen (GFOGER), laminin, E-cadherin
	α₃	laminin
	α₄	VCAM-1, ICAM-4, fibronectin
	α₅	fibronectin (RGD)
	α₆	laminin
	α₇	laminin
	α₈	fibronectin (RGD)
	α₉	VCAM-1
	α₁₀	collagen (GFOGER), laminin
	α₁₁	collagen (GFOGER)
	αᵥ	fibronectin (RGD)
β₂	α_D	ICAM, VCAM-1, fibronectin, fibrinogen
	α_L	ICAM, ICAM-2, ICAM-4
	α_M	ICAM, ICAM-4, fibrinogen
	α_X	ICAM, ICAM-4, fibrinogen, collagen
β₃	αᵥ	fibrinogen, fibronectin (RGD), ICAM-4
	α_IIb	fibrinogen, fibronectin (RGD)
β₄	α₆	laminin
β₅	αᵥ	vitronectin (RGD)
β₆	αᵥ	fibronectin (RGD)
β₇	α₄	VCAM-1, fibronectin
	α_E	E-cadherin
β₈	αᵥ	vitronectin (RGD)

Table 2.1: Integrin heterodimers and their ECM binding sites

2.2 Optimization of Cellular Adhesion through Biomaterial Modification

Degradable polymeric scaffolds are typically used in vitro and in vivo in the field of tissue engineering, and serve as a temporary matrix that can be seeded with cells to promote healing, proliferation, and differentiation at an injury site. Polymeric scaffolds must meet certain criteria before being employed including having the degradation, mechanical, adhesive, and biocompatible properties that will result in proper healing and regeneration of tissue at the implant site [16]. Some of the commonly used natural and synthetic polymers will be discussed here briefly, with a focus on poly(ethylene glycol) (PEG) and poly(propylene fumarate) (PPF)-based materials and modification techniques.

Several factors play a role in how cells adhere and respond to biomaterials. On a basic level, the hydrophilicity of a material has an effect on cell adhesion. PEG is an example of a hydrophilic synthetic polymer that resists protein adsorption. This quality is exploited for applications in which cell adhesion is not ideal. PEG can also be modified to contain specific adhesive moieties of interest, resulting in a high level of control over cell-material interactions. As a linear chain, PEG has poor overall material properties, but as a network, its properties are greatly improved. PEG is nondegradable in vivo, but this shortcoming can be overcome by copolymerization. Copolymerization with degradable moieties such as lactic acid has been shown to result in degradation of these modified PEG scaffolds. In such scaffolds, the bioactive moieties degrade rapidly, breaking apart the PEG polymer into monomer degradation products [17]. While the degradation of modified PEG varies based on the material chemistry, average rates tend to reach 100% degradation after the first

month following implantation [17]. Modifications and copolymerization of PEG is common for tissue engineering applications. For example, an injectable modified PEG was recently used as an injury specific scaffold for cartilage tissue engineering [18].

In contrast, PPF is a hydrophobic polymer which undergoes ester hydrolysis to form fumaric acid and propylene glycol. Scaffolds of PPF are manufactured via covalent crosslinking, and the resulting scaffolds show good compressive and tensile strength [19]. Due to its mechanical properties, it is often used in bone tissue engineering applications. PPF discs have been shown to support cell adhesion and stimulate osteogenic differentiation of bone marrow stromal cells in vitro [20]. The photocrosslinkng properties of PPF allow the polymer to be used in rapid prototyping applications, such as 3D printing, resulting in highly controlled architecture scaffolds. PPF scaffolds can undergo chemical surface modifications to introduce bioactive moieties to increase cell adhesion and function [21]. Methods for altering surfaces with bioactive molecules will be discussed in the sections following.

Perhaps one of the simplest ways to improve cell adhesion on the surface of a material is through the adsorption of ECM proteins onto the biomaterial surface. The adsorption process can be increased by employing the use of culture medium that contains serum. In general, the major components of serum are albumin, vitronectin, and fibronectin. Protein absorption on a biomaterial surface as a mediator of cell adhesion has been demonstrated extensively in the literature [22-25]. A study conducted using a hydrophobic self-assembled monolayer was incubated in a fibronectin solution before cell seeding and showed that due to the fibronectin

adsorption, fibroblasts were able to strongly adhere to the scaffold and maintain adhesion under applied shear stress conditions [26]. In addition to serum, a more specific protein solution can be used to pre-treat a tissue engineering scaffold in order to promote cell adhesion. Use of a specific protein solution adds an additional layer of control or targeting, and can result in interactions between the cell and the material which can in turn mediate desired downstream effects on cell behavior.

A more specific method of optimizing cell adhesion to a tissue engineering scaffold is to incorporate adhesion motifs within the scaffold composition. As mentioned above, there are known adhesive domains such as RGD and YIGSR which are present within the ECM and promote adhesion in the native environment via integrin binding. Interactions between the cell and one of these domains can promote anchorage, migration, and signal pathway activation, which in turn mediates numerous intracellular reactions. To exploit these adhesive domains for tissue engineering applications, short bioadhesive peptides have been tethered onto the surface of synthetic and natural polymers. Molecules are typically tethered through the use of PEG or poly (ethylene oxide) polymer spacers so that the bioactive molecule can be presented to a cell [27, 28].

Bioadhesive peptides can be derived from natural or synthetic sources, each with advantages and disadvantages. Naturally derived bioadhesive peptides have been successfully used in biomimetic material studies, but are very difficult to isolate and purify, especially while maintaining functionality. Due to this shortcoming, synthetic bioadhesive peptides are commonly fabricated and used for biomimetic applications [29].

Adhesive peptides can be added to the material surface in a variety of ways, including biofunctionalization through covalent binding. One method for tethering reactive amine groups onto the surface of a biomaterial is through aminolysis [30]. Aminolysis is achieved through the use of a bifunctional molecule, such as hexamethylene diamine, which works to cleave ester links on the polymer surface, replacing the ester bond with a covalent amide bond. Following aminolysis, the surface of the polymer can be further modified to attach proteins or bioadhesive peptides to the surface. Tan et al [31] recently utilized this method to attach a gradient of collagen for investigation of chondrocyte distribution. Another method commonly used is modification using 1-Ethyl-3-(3-dimethylaminopropyl)carbodiimide (EDC) chemistry, which works though EDC coupling to a carboxylic acid group on the material surface, followed by subsequent steps to attach adhesive molecules of interest. Reactive groups formed by the initial EDC reaction can be stabilized through a secondary reaction with N-Hydroxysuccinimide (NHS) [32] which is highly reactive with the N-terminus of a protein structure.

The inclusion of bioadhesive peptides has shown significant enhancement of cellular activities [28, 33]. Peptides are typically tethered in a random yet spatially uniform manner across the surface of the biomaterial. Recently, studies have shown that if the peptides are arranged within clusters, the cellular response is increased [33]. As discussed above, integrin clustering occurs during adhesive interactions to promote stronger or multiple simultaneous downstream effects. In a study investigating how cell adhesion with an orthopedic implant can be employed to promote better tissue integration, Petrie et al [33] showed that clustering of

bioadhesive ligands on the surface of the implant upregulated osteogenic signaling and differentiation of human mesenchymal stem cells.

There are still some inherent limitations with the use of adhesive oligopeptides, however. Synthetic peptides have much lower activity than that of the native ligands, and also have limited specificity. There are also several conformational differences between the native adhesive domains and the synthetic ones, which can similarly result in lower adhesion activity and specificity.

The consideration of cell-substrate interactions in biomaterial design has resulted in the successful creation of materials that are able to elicit downstream cellular responses such as differentiation and proliferation. In the following section, methods to quantify cell-substrate interactions will be discussed. Quantification of cell adhesion can provide another means to characterize the interactions between cells and an underlying substrate.

2.3 Measurement of Cell Adhesion

The adhesion of cells to an underlying substrate can be quantified through the use of cell adhesion assays. In general, cells are allowed to establish adhesive interactions to a substrate of interest and then are exposed to a detachment force. Adhesion assays are often categorized based on the type of force that is applied, resulting in three major categories: micromanipulation, hydrodynamic stress, and centrifugation [34, 35]. Currently, the vast majority of cell adhesion measurements are studied in two-dimensional systems. In the future, the field would benefit greatly

from the development of quantitative assays that could characterize cell adhesion in a three-dimensional environment, as this is a more relevant configuration and representation of the native tissue.

Prior to the development of assays based on detachment force, "stick and wash" assays were commonly used for the study of cell adhesion [35, 36]. In a stick and wash assay, cells were allowed to adhere to a surface and then were simply subjected to washing over the surface with buffer. While many of the first discoveries involving cell adhesion ligand-receptor interactions were made utilizing this technique, there are inherent limitations. Stick and wash assays had poor reproducibility and applied uneven and unknown detachment forces [35, 36]. These limitations led to the development of the measurement techniques that will be discussed below.

2.3.1 Micromanipulation

In micromanipulation techniques, the detachment force can be applied as either a vertical force pulling cells normal to the surface, or a shear force, pulling cells tangential to the surface [34]. Micromanipulation covers a range of techniques including micropipette aspiration, atomic force microscopy (AFM), and laser tweezers [35]. With these techniques, it is possible to collect real-time force-displacement measurements on a single cell and investigate specific interactions between cell adhesion receptors and the substrate.

AFM can be used to evaluate morphological changes occurring during cell adhesion, adhesion strength measurements, and interaction forces between cells. AFM images are capable of showing cell flattening and spreading, and it is generally

accepted that the flatness of a cell designates good adhesion [37]. A typical morphological change related to adhesion is the appearance of structured stress fibers, indicating the stability of the cells on the underlying substrate. The adhesion strength of cells to an underlying substrate can be quantitatively measured on a single cell level using AFM techniques. The force necessary to laterally displace a cell with the AFM cantilever can be measured in real time by recording the deflection of a laser beam versus the lateral displacement of the AFM cantilever [37]. In addition to measuring the adhesion strength, the AFM technique can also estimate the timescale over which adhesion occurs and eventually saturates.

AFM techniques can have several practical difficulties [38]. The underlying substrate as well as surrounding cells can influence the force measurements which are collected from a single cell. Additionally, the user must be sure that the forces being measured are the attachment forces of the cell and not simply a measure of cell membrane strength. Other practical issues include z-axis restrictions and protein adsorption to the AFM cantilever.

Micromanipulation assays offer a sensitive and quantitative means to investigate cell-substrate and cell-cell interactions at the molecular level. However, these assays are limited to applying small forces, and can only be used for individual cell studies in which the seeding time is short. For longer adhesion times or for quantification of a larger cell population, assays that provide a greater distractive force must be considered.

2.3.2 Hydrodynamic Shear Stress

Flow systems have been developed to apply a wide range of shear detachment forces to large adherent cell populations, and are generally considered a more reliable adhesion measurement system [35]. Hydrodynamic shear stress assays are classified according to the geometry of the flow responsible for generating the shear detachment force. There are three basic flow cell configurations: the parallel plate, the rotating disc, and radial flow between parallel disks. Of these geometries, the parallel plate has been studied extensively studied, specifically in combination with microscopy [35]. The parallel plate configuration permits the observation of attachment and detachment throughout the assay, and has been used frequently in the characterization of leukocyte-endothelial cell adhesion events [39, 40]. A typical parallel plate flow cell is designed so that a) flow is laminar (Reynolds number less than 2300), and controlled through the use of a syringe pump, and b) the entrance length is minimized so that entry effects can be neglected, and flow can be considered fully developed and parabolic [40].

While hydrodynamic shear stress assays provide a reliable and reproducible means for quantifying cell adhesion *in vitro*, there are some limitations related to the measurement of shear stress. In general, the adhesion strength is reported as a shear stress with units of force per area. Even though this is a useful measure for the investigation of adhesion strength, the net force that is applied is not simply the shear stress, but includes parameters such as hydrodynamic drag and torque [35]. Therefore, results of such assays must be carefully examined. There are several practical difficulties of hydrodynamic shear stress assays including complications

with the system set-up, preventing the inclusion of air bubbles in the stream of flow, and preventing non-laminar flow through the chamber [38].

2.3.3 Centrifugation

For larger cell populations, centrifugation assays offer a simple and reproducible means to quantify cell adhesion. In general, cells are seeded onto a substrate and allowed to adhere for a period of time, typically no longer than one hour [35]. After adherence, cells are subjected to a perpendicular detachment force generated by spinning at a specified speed in a standard laboratory centrifuge [35]. A schematic of a typical centrifugation assay procedure can be seen in Figure 2.1. The ratio of post-spin cell count to pre-spin cell count results in the adherent fraction of cells at the designated force set by the centrifugal speed.

Centrifugation assays have also been used to quantify differences between initial adhesion and "strengthened" adhesion [36]. Strengthened adhesion is defined as adhesion that occurs while cells are incubated on a substrate. As with the micromanipulation assays, adhesion strength increased with longer seeding times (for example 30 versus 60 minutes) [36, 41], showing that adhesion is time dependent. Reyes et al. [41] further modified the centrifugation assay and developed the mean adhesion strength value, which is the force that causes 50% cell detachment, for fibrosarcoma cells seeded on fibronectin coated 96 well plates. Centrifugation assays offer a simple and reproducible method of characterizing biomaterials based on the ability of the material to successfully initiate cell adhesion.

Despite the success of centrifugation assays, there are limitations, including the fact that only one speed can be subjected to cells at a time, and that at longer adhesion times (> 1 hour) [35], the distraction forces generated by the centrifuge may not be large enough to displace large cell populations.

All of the above adhesion assay techniques have advantages and disadvantages, making it clear that there is no perfect solution when it comes to quantifying cell adhesion. A measurement system must be chosen based on the cell system in place and the desired results. Results of adhesion assays must be taken as relative to the cell population and the particular experiment, and not as an absolute measure.
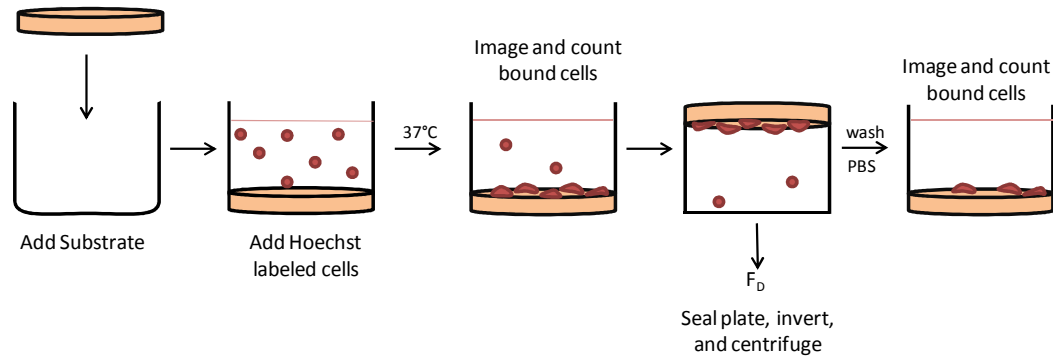
Figure 2.1. Schematic of a centrifugation cell adhesion assay. The incubation time and F_D can be varied based on the substrate and cell population of interest.

2.4 Conclusion

Adhesion receptors function to modulate cell behavior in a variety of ways, and these functions are desirable to incorporate into the design of biomaterials that will be used for tissue engineering applications. A common method is the tethering of integrin binding domains such as RGD, LDV, GFOGER, and YIGSR onto the surface of the biomaterial to promote cell adhesion. The inclusion of adhesion receptor ligands into biomaterials enhances cell adhesion and can potentially mediate a desired intracellular reaction to ligand binding.

Research involving the modification of biomaterials to optimize cellular adhesion has made strides including bioactive molecules on the material surface to control cell phenotype and induce changes such as increased spreading, proliferation, and differentiation. Patterning techniques have allowed for control over adhesive domain inclusion on the surface of biomaterials at the micro and nanoscale. Optimizing biomaterial design to mimic the native adhesive interactions of a cell population provides a method for controlling downstream cell responses, and could have significant impacts for therapeutic applications.

The quantification of cell adhesion through the use of a detachment force offers a means to further characterize and optimize cell-cell and cell-substrate interactions. Results of such assays can be used as feedback for biomaterial designs, and encourage further manipulation of biomaterials to achieve desired levels of cell adhesion.

Chapter 3: Centrifugation Assay for Measuring Adhesion of Serially Passaged Bovine Chondrocytes to Polystyrene Surfaces[2]

3.1 Introduction

Isolated chondrocytes are a common cell source for repair of cartilage defects. Mature autologous chondrocytes retrieved from regions of the knee cartilage that are less load-bearing have been used to repair well-defined cartilage defects in younger patients [42]. This strategy has been commercialized for repair but remains limited to defined cartilage defects. The advantage of using isolated chondrocytes is that they can be propagated under different culture conditions to facilitate proliferation and/or ECM production. For example, chondrocytes can be grown in low- or high-density monolayer culture [43] or, alternatively, in a constrained environment such as pellet culture, alginate culture or seeded in three-dimensional matrices [44, 45]. Growth in alginate beads helps maintain the chondrocyte phenotype, but limits cell multiplication [46]. The more commonly used monolayer culture method facilitates transport of nutrients and cell proliferation. However, this method to propagate the cells causes the chondrocytes to undergo phenotypic changes and assume "fibroblastic" morphologic and biochemical characteristics [47]. They shift from making type II to type I collagen and decrease their synthesis of high-molecular-weight proteoglycans [48].

Although changes in phenotype have been well characterized when chondrocytes were propagated in monolayer cultures, little information is available about alterations in adhesion characteristics with passage of the cells. The ability of cells to adhere to surfaces in both two and three dimensions is critical for their survival. In this study, we examined the alterations in cell adhesion characteristics of chondrocytes cultured as monolayers as a function of cell passage using a centrifugation cell adhesion assay, based on the method described by Reyes and Garcia [41]. Furthermore, quantitative reverse transcriptase–polymerase chain reaction (qRT-PCR) and immunostaining were also used to compare the relative expression of type I and type II mRNA expression and biomarkers, respectively. Our hypothesis is that the physical cell adhesion assays will detect changes in adhesion properties that correlate with changes in morphology as the chondrocytes de-differentiate in passage as monolayer cultures.

3.2 Materials and Methods

3.2.1 Preparation of Articular Chondrocytes

Articular chondrocytes were isolated from the knee joints of immature steer (2–4 weeks old; Farm-to-Pharm, L.L.C., Warren, NJ) by digestion of the tissue with 11,000 U collagenase (type II from *clostridium histolyticum*, Sigma Chemical, St. Louis, MO) suspended in 100 mL Dulbecco's modified Eagle's incomplete medium: nutrient mix F-12 (DMEM/F-12; Invitrogen, Carlsbad, CA) containing 50 μg/mL L-ascorbic acid, 50 μg/mL gentamicin (Invitrogen), and antibiotic-antimycotic solution

(100 U/mL penicillin, 100 µg/mL streptomycin, 0.25 µg/mL amphotericin B; Invitrogen), but without fetal bovine serum (FBS). The tissue was incubated for 22–24 h on a rocking platform at 37°C in a 5% CO_2–95% air incubator to obtain primary chondrocytes. The isolated cells were filtered (40 µm Nylon cell strainer; BD Falcon, Bradford, MA), subsequently assessed for viability, and counted using the Trypan-blue dye exclusion method and a hemocytometer. The chondrocytes were plated at 5×10^6 cells per T-75 tissue culture flask and incubated for 5–7 days at 37°C at 95% air/5% CO_2/90% relative humidity (R.H) in DMEM/F-12 complete media supplemented with 10% FBS (HyClone, Logan, UT) and the other supplements. The retrieved chondrocytes were serially passaged, approximately every 3–5 days, when about 90% confluent, for five passages (starting at passage 0). Chondrocytes were harvested from eight separate knee joints. The resultant chondrocytes from each joint were kept separate and assayed as described next.

3.2.2 Mouse Fibroblasts (L929)

L929 fibroblasts were used as a control cell line with high expected adhesion in the centrifugal test system. The cells were cultured at 37°C at 95% air/5% CO_2/90% R.H. in RPMI-1640 complete medium (Invitrogen) supplemented with 10% FBS and without antibiotics or antimycotics. The sub confluent cells were passaged twice to thrice weekly.

3.2.3 Centrifugation Cell Adhesion Assay

Four wells of a 96-well plate (Costar, St. Louis, MO) were coated with

100 µg/mL fibronectin (Sigma Chemical) and incubated for 1 h at room temperature.

After removing the excess fibronectin solution from the wells, 5×10^3 bovine

chondrocytes in complete DMEM/F-12 medium with 10% FBS, or L929 (control)

cells in RPMI-1640 medium with 10% FBS were premixed with Hoechst 33342

fluorescence stain (10% of volume). The labeled cells were added to the wells and

incubated, after being covered in aluminum foil to prevent photobleaching, for 1 h at

37°C at 95% air/5% CO2/90% R.H. Chondrocytes from serial passages for each of

the eight joints were examined to determine adhesive properties using the

centrifugation cell adhesion assay. At each serial passage, the centrifugation cell

adhesion assay was used to obtain three replicate sample measurements. An

additional fourth well was used to adjust the microscope parameters, such as

exposure. Measurements from this fourth well were discarded.

Using an inverted microscope (Zeiss AxioVert, equipped with an AxioCam

MRm digital camera; Zeiss, Inc., Thornwood, NY) and AxioVision Software

(Version 4.8.2; Zeiss, Inc.), 5×5 digital tiled images (total tiled image

area=3.177 mm^2) were captured for each of the three wells before centrifugation

(prespin). The combined number of cells counted per sample was 2400–3600 (800–

1200 cells/well × 3 wells). The wells were filled with D-PBS, purged of air bubbles,

and covered with acetate sealing tape (Fisher Scientific, Atlanta, GA). The plates

were centrifuged (upside down) at either a RCF of 120 g or 350 g for 5 min at 22°C.

26

The cell detachment forces (FD) were 150 pN (for 120 g RCF) and 440 pN (for 350 g RCF) and were calculated by the following formula: [51]

$$FD = V \cdot d \cdot RCF$$

Where, V = cell volume = $1800\mu m^2$, d = (cell density – media density) = $0.07 g/cm^2$, and RCF = 120 or 350.

The supernatant was removed from the wells, washed $1\times$ with D-PBS, and 100 µL D-PBS was added to each well. A total of 25 tiled digital images (5×5 matrix) were captured for each of the three wells after centrifugation (postspin). The cell number pre- and postspin were determined by stitching together the tiled images and subsequently using an automated cell counting (AxioVision) routine to count the number of fluorescently labeled nuclei. The percent adhesion was determined by dividing the postspin cell count by the prespin count, and multiplying by 100.

3.2.4 RNA Isolation

RNA was isolated using the RNeasy Plus Mini Kit (Qiagen, Valencia, CA). Total RNA was eluted into RNase free water and then detected using a NanoDrop ND-1000 Spectrophotometer (NanoDrop Technologies, Wilmington, DE).

3.2.5 Quantitative RT-PCR

The isolated RNA for all joints at all passages was reverse transcribed using a cDNA Archive Kit (Applied Biosystems, Foster City, CA), which can convert up to 10 µg of RNA to cDNA. The cDNA was combined with a Universal Master Mix (Applied Biosystems), oligonucleotide primers, and Taqman probes (Applied

Biosystems) for the genes of interest as well as a control gene. The genes of interest were type I collagen, type II collagen, and aggrecan, and the endogenous control gene was glyceraldehyde 3-phosphate dehydrogenase (GAPDH). The sequences for the forward primers for type I collagen, type II collagen, aggrecan, and GAPDH are 5′ AGAACCCAGCTCGCACATG 3′, 5′ CGGGCTGAGGGCAACA 3′, 5′ GGGAGGAGACGACTGCAATC 3′, and 5′ TGCCGCCTGGAGAAACC 3′. The reverse primer sequences for type I collagen, type II collagen, aggrecan, and GAPDH are 5′ CAGTAGTAACCACTGCTCCATTCTG 3′, 5′ CGTGCAGCCATCCTTCAGA 3′, 5′ CCCATTCCGTCTTGTTTTCTG 3′, and 5′CGCCTGCTTCACCACCTT 3′. The probe sequences for type I collagen, type II collagen, aggrecan, and GAPDH are 5′ AGACTTGAGACTCAGCC 3′, 5′ CAGGTTCACATATACCG 3′, 5′ CAGGCTTCACCGTTGAG 3′, and 5′ CCAAGTATGATGAGATCAA 3′. The reaction volume was 20 μL, and the reaction was performed in technical triplicates on a 7900HT Fast Real-time PCR System Prism 7000 sequence detector (Applied Biosystems). The thermal profile followed was 2 min at 50°C, 10 min at 95°C, 40 cycles of 15 s at 95°C, and 1 min at 60°C. Gene expressions were analyzed using the comparative C_t method, with GAPDH used as the endogenous control gene. The passage 0 cells were used as the calibrators in all analyses. Fold changes in gene expression were calculated and are reported as the mean RQ values with associated standard deviations (SDs; n=3), in accordance with the methods previously described [49].

3.2.6 Statistical Analysis

For the centrifugation assay, the mean percent adhesion for each of the three wells at each RCF and passage number was calculated. The data were subsequently analyzed using a two factor analysis of variance (ANOVA) at a confidence level of 0.95 for the effects of passage number and RCF, with a Tukey Test post hoc all pairwise comparison (SigmaStat, Systat Software, Inc., Richmond, CA). Quantitative RT-PCR data were analyzed using a one-way ANOVA and Tukey's multiple-comparison test to determine statistical differences. A confidence interval of 95% (α=0.05) was used for all analyses, and means and SDs are shown in each figure.

Figure 3.1. The percent adhesion of serially passaged chondrocytes at 120 and 350*xg*. Chondrocytes were harvested from eight separate knee joints. The resultant chondrocytes from each joint were examined separately. Three replicate sample measurements were presented for each serial passage. A two-way analysis of variance (ANOVA) with Tukey's test for pairwise comparison indicated at '*' $p<0.001$ that cell adhesion at P0 $\neq$ P1-5, L929; at $p<0.05$, '#' P1 $\neq$ P0, P3-5, L929; '**' P2 $\neq$ P0, P4-5, L929; and P3 $\neq$ P0-1. Passage 3 showed a trend to be different than passage 2 (p = 0.090).
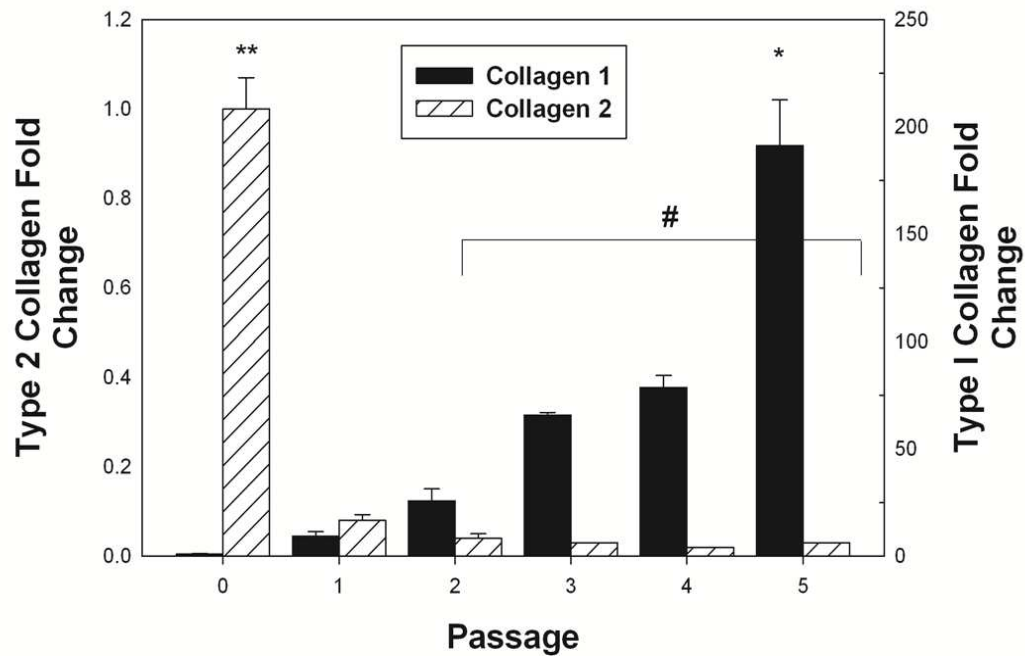
Figure 3.2. Type I and II collagen mRNA expression of chondrocytes cultured in monolayer. qRT-PCR was performed on chondrocytes taken from each joint at P0-P5 and evaluated for type I and type II collagen mRNA expression, using GAPDH as an endogenous control. Data were analyzed using a one-way ANOVA and Tukey's multiple-comparison test to determine statistical differences. A confidence interval of 95% ($\alpha = 0.05$) was used for all analyses, and means and standard deviations are shown here. '*' indicates the largest type I collagen expression group; '**' indicates the largest type II collagen expression group; and '#' indicates no statistical differences between the type II collagen expression for passages 2-5.

3.3 Results and Discussion

3.3.1 Chondrocyte Adhesion Characteristics in Monolayer Culture

The centrifugation cell adhesion assay compared the adhesion of chondrocytes serially passaged for passage (Ps) 0 to passage 5 to the adhesion of a control L929 fibroblast cell line to determine whether, over passage, the chondrocytes were taking on the adhesive characteristics of the fibroblasts. L929 fibroblasts routinely showed 87%–100% adhesion in the centrifugation assay at both 120 and 350 g (See Figure 3.1). Chondrocytes at passages 3–5 appeared to be taking on the adhesion characteristics of the L929 fibroblast control cells, as the percent adhesion of the passage 3–5 chondrocytes was increased compared with Ps 0–2 and was statistically the same as that of the L929 cells. Only the adhesion of chondrocytes for passages 0–2 was significantly different ($p<0.05$) from the adhesion of the L929 cells.

The centrifugation assay demonstrated that chondrocyte adhesion at passages 0 to 2 was significantly less than at the later passages 4 and 5 (See Figure 3.1). Two-way ANOVA with Tukey's test for pairwise comparison indicated at $p<0.001$ that cell adhesion at Ps0≠Ps 1–5, L929; at $p<0.05$, Ps1≠Ps0, Ps 3–5, L929, Ps2≠Ps 0, 4–5, L929; and Ps3≠Ps0-1. Passage 3 showed a trend to be different than passage 2 ($p=0.090$). There was statistically no difference in the adhesion of the chondrocytes at 120 g vs. 350 g ($p=0.117$). The centrifugation assay was very sensitive, in that it detected differences in adhesion as early as passage 2.

We compared the relative mRNA expression of type I and type II collagen using qRT-PCR. As shown in Figure 3.2, type II collagen expression decreases

32

rapidly after passage 0, while type I collagen mRNA expression started increasing after passage 2. Immunostaining for markers for collagen I and collagen II showed significant staining for collagen II in passage 0, while passage 5 showed significant staining for collagen I.

Centrifugation adhesion assays have been used in the past to monitor cell-substrate interactions, [41, 50] as well as to assess the distribution and function of cell adhesion molecules. In the current study, the cell adhesion assay was shown to provide a consistent and predictive method to evaluate the performance of cells that will be used to repair defects caused by trauma or sickness. As chondrocytes become more adhesive when cultured *in vitro*, this cell adhesion assay could be very useful as a screening tool for tissue-engineered products, especially to compare the adhesive properties of chondrocytes grown under different oxygen tension, mechanical stress, or culture conditions (such as 3D vs. monolayer). Although at later passages the change in cell phenotype was visible morphologically and biochemically, the cell adhesion assay provides another tool to measure changes in cell phenotype that is mechanical in nature and independent of other available methods.

It is not clear why chondrocytes become more adherent with passage number in monolayer culture. It has been proposed that as chondrocytes become more fibroblastic, alterations in the production of ECM molecules may occur. Previous investigations have focused on several ECM molecules and their adhesion receptors (integrins, cadherin, Igs) involved in chondrocyte adhesion [35, 47, 51]. Those studies reported on the role of cell adhesion molecules in maintaining the chondrocyte phenotype exemplified by interactions among integrins and type II and type VI

collagen [52, 53]. They also examined the regulation of expression for different integrins during the process of chondrocyte proliferation and de-differentiation. Other investigators evaluated the strength of cell adhesions in cultured chondrocytes [35, 47, 51]. Kino-Oka *et al*. [54] studied the influence of solid phase materials on the events that regulate cellular phenotypes and modulate cell shape. These previous studies described different methods to evaluate adhesion properties and proposed the role of adhesion molecules in regulating cell shape, phenotype, and proliferation.

The key finding of the present study is that the modified centrifugation adhesion assay identified changes in adhesion properties with the passage number of the cells. Chondrocytes appeared to be more adherent with passage number (See Figure 3.1). These changes in adhesion properties correlated with phenotypic alterations indicated by changes in cell morphology, qRT-PCR gene expression (See Figure 3.2), and immunostaining. This assay is simple to perform, uses known RCFs to dislodge weakly adherent cells, and allows the user to run multiple replicates simultaneously. The centrifugation assay applies a force to pull the cells in a perpendicular direction away from the surface. The present study is the first that measures changes in actual cell adhesion over sequential passages 0 through 5.

In conclusion, the present study demonstrates that chondrocytes become more adherent and fibroblastic with passage number using the centrifugation assay. Additional studies are necessary to determine correlations among the expression of specific chondrocyte phenotype markers such as collagen type II and aggrecan, morphology, proliferation, and cell adhesion molecules. The analysis of phenotype markers, including cell adhesion and morphological endpoints, may serve as useful

indicators to identify culture conditions that may help preserve chondrocyte

phenotype and function for use in therapeutic applications.

Chapter 4: A Centrifugation Assay for the Separation of Differentiating Mesenchymal Stem Cells

4.1 Introduction

Mesenchymal stem cells (MSCs) are an adult stem cell population capable of multilineage differentiation into cells of the mesoderm including osteoblasts, adipocytes, and chondrocytes. The use of MSCs for therapeutic applications has great potential due to their properties of self-renewal and differentiation, but there remain questions about population purity and instability following implantation. There has been much evidence of cell heterogeneity *in vitro*, particularly heterogeneity in MSC differentiation potential [55, 56].

It is well documented that MSCs undergo changes following culture *in vitro,* and the relationship between the adhesive cells that are recognized as MSCs *in vitro* and their *in vivo* counterpart remains a critical question. Increasing passage number is associated with many crucial changes including decreased proliferation potential, an increase in cell size, and a loss of multipotency [57-59]. Muraglia et al. [57] found that as population doublings increase, there is first a significant loss of adipogenic potential, followed by chondrogenic potential. This was one of the first indications of a linear hierarchical model of MSC differentiation. A complete understanding of the hierarchy of MSC differentiation has yet to be elucidated, though it is hypothesized to include asymmetrical cell division, leading to the rise of a heterogeneous cell population made up of stem cells, precursors and progenitor cells [55].

The use of MSCs for therapeutic purposes relies on the potential of MSCs to differentiate into the tissue of interest either prior to or following implantation. However, the heterogeneity of MSCs during differentiation may lead to low levels of differentiation following implantation. Current methods of *in vitro* differentiation result in somewhat low levels of overall differentiation with reports showing that the area-times-intensity score (defined as the product of the percent stained area and its optical density) was less than 30% for osteogenesis, less than 24% for chondrogenesis, and less than 10% for adipogenesis [60]. Similarly, the use of histological analysis techniques combined with automated microscopy has shown that less than 15% of cells stain positively for lipid deposits after 21 days of induction [59]. These low levels of differentiation may be due to the heterogeneous nature of MSCs.

The development of methods to prime or purify differentiating MSCs is of ongoing importance to the field. Currently, a number of techniques to enrich an MSC population prior to differentiation have been developed, including separation based on cell size and shape [61], selection based on cell plating density [62], and the use of additional cell surface markers [63]. Adhesion based assays have previously been shown to be a simple, reproducible, and non-destructive means to evaluate the phenotype of a cell population [35, 64]. Cell adhesion assays have also been used to separate distinct cell populations. Singh et al. [65] has shown that using a shear stress based adhesion assay, it is possible to definitively isolate induced pluripotent stem cells without the use of traditional labeling techniques. Adhesion is critical to many

cell functions, and changes in integrin expression have been hypothesized as a key factor in MSC differentiation [66-68].

Here, we propose the use of a centrifugation cell adhesion assay, first as a technique to identify changes in adhesion during differentiation, and second as a way to purify a differentiating population of MSCs. We hypothesize that cell adhesion can be used to isolate a more homogenously differentiated cell population. To investigate this hypothesis, we first varied the assay parameters to identify changes in cell adhesion, and relate these to cell phenotype using quantitative histological analyses. Using these results, we were able to identify a critical point of intervention, where the application of centrifugation resulted in cell populations that were separated by differentiation potential. The centrifugation assay developed here can be used as a technique to decrease population heterogeneity of differentiating MSCs for cell therapy applications.

4.2 Materials and Methods

4.2.1 Human Mesenchymal Stem Cell Culture

hMSCs (Lonza, Walkersville, MD) were expanded prior to the study on TCPS in media consisting of DMEM supplemented with 10% fetal bovine serum, 1.0% v/v penicillin/streptomycin, 0.1mM non-essential amino acids, and 4mM L-glutamine (all from Life Technologies, Frederick, MD) using protocols set forth by the manufacturer and previously described [69]. Media was changed every 3 days according to the manufacturer's specifications, and cell cultures were incubated at

38

37°C, 5% CO2, and 80% humidity. hMSCs at passage 4 were used for all experiments.

4.2.2 Induction of hMSC Differentiation

Prior to the start of differentiation, hMSCs were seeded at 3500 cells/cm^2 for osteogenesis, and 35,000 cells/cm^2 for adipogenesis and chondrogenesis. Following incubation for 24 hours in growth medium, cells were cultured for 21 days in osteogenic (DMEM with 10% FBS, 1mM sodium pyruvate (Life Technologies), 100U/100µg penicillin-streptomycin, 10^{-7}M dexamethasone (Sigma-Aldrich), 50µg/mL ascorbic acid (Sigma-Aldrich), and 10mM β-glycerophosphate), chondrogenic (high glucose DMEM supplemented with ITS (BD, Franklin Lakes, New Jersey), 4mM L-proline (Sigma-Aldrich), 50µg/mL ascorbic acid, 1% sodium pyruvate, 10^{-7}M dexamethasone, and 100U/100µg penicillin-streptomycin, and 10ng/µL TGF-β3 (R&D Systems, Minneapolis, MN)), or adipogenic (DMEM with 10% FBS, 1mM sodium pyruvate, 100U/100µg penicillin-streptomycin, 10^{-6}M dexamethasone, 10µg/mL insulin (Sigma-Aldrich), 0.5mM IBMX (Life Technologies), and 200µM indomethacin (Life Technologies)) media as described previously [70]. hMSCs cultured in growth media served as a control. All media were changed every 3 days.

4.2.3 Centrifugation Assay

To quantify the relative adhesion of hMSCs throughout differentiation, a centrifugation cell adhesion assay was performed as described in Section 3.2.3. At

days 7, 14, and 21, cells were lifted, counted, and approximately 5000 hMSCs were added to each well of a 96 well plate (Costar, St. Louis, MO). Prior to seeding, cells were pre-mixed with Hoechst 33342 fluorescence stain (10% of volume). Cells were incubated for 20 or 200 minutes at 37°C, 5% CO2, and 80% humidity. A schematic of the centrifugation cell adhesion assay, which was modified from Kaplan et al [64] is shown in Figure 4.1A. Images were collected as described in 3.2.3. The wells were filled with PBS, purged of air bubbles, and covered with acetate sealing tape (Fisher Scientific, Pittsburgh, PA). The plates were centrifuged (upside down) at a relative centrifugal force (RCF) of 50, 200 or 500xg for 5 minutes at 22 °C. The force of detachment (FD) was calculated by the following formula (Reyes and Garcia, 2003[41]):

$$FD = V \cdot d \cdot RCF$$

where V = cell volume = 5000μm^2, d = (cell density – media density) = 0.07g/cm^2, and RCF = 50, 200, or 500.

The percent adhesion was calculated as described in 3.2.3 (n = 6). For the initial investigation of adhesive changes during differentiation, cells were incubated for 30 minutes and centrifugation was applied at 200xg for 1 minute (results shown in Figure 4.2).

4.2.4 Histological Analysis

At days 7, 14, and 21, cells were lifted and subjected to the centrifugation assay as described above with one exception. In addition to keeping the attached fraction of cells for analysis, the detached fraction of cells were also collected

following centrifugation and reseeded into wells of a 96 well plate for 24 hours. At this time cells were fixed with 10% formalin for 10 minutes, and stored at 4°C in PBS. Histological staining was completed to show calcification, glycosaminoglycan production, and the presence of lipid droplets. Mineralization was visualized using Alizarin Red (Sigma) staining following standard protocols. Briefly, freshly prepared 2% w/v alizarin red solution was added to cell monolayers for 5 minutes. Cells were washed 3 times in DI water and imaged immediately. Glycosaminoglycan production was visualized by staining with 0.5% Alcian Blue solution (Poly Scientific) followed by a nucleic counter stain with Nuclear Fast Red (Poly Scientific). For the visualization of lipid vacuoles in adipogenic samples, a working solution of Oil Red O (Poly Scientific) was prepared and applied to fixed monolayers, followed by counterstaining with hematoxylin. For quantification, 5 x 5 tiled images were captured of each well (n = 3) using an inverted microscope (Zeiss) and AxioVision Software. A routine was created in Axiovision for each stain to capture and calculate regions positively stained for calcification, lipid deposits, or proteoglycans.

4.2.5 Application of Centrifugation at Day 14 to Separate Cell Populations

Based on the data derived from the first experiment, an incubation time and centrifugation speed was chosen that resulted in an appropriate separation of cell number (around 50% adhesion) and exhibited large differences between the histological staining of the attached and detached populations at day 14. hMSCs were cultured and differentiated down the three main lineages until day 14. After 14 days, cells were lifted and subjected to centrifugation following methods similar to those

described above. Following centrifugation, both the attached and detached

populations were reseeded and differentiation continued until day 21 (an additional 7

days post centrifugation). At this time, cells were collected from all groups for

analysis using histological methods as described in 4.2.4 and qRT-PCR. hMSCs that

were differentiated under identical media and cell density conditions but were not

subjected to centrifugation served as a control.

4.2.6 Quantitative Reverse Transcriptase-Polymerase Chain Reaction

RNA was isolated using an RNeasy Mini Plus Kit (Qiagen, Valencia, CA)

following standard protocols. Isolated RNA was then reverse transcribed to cDNA

using a High Capacity cDNA Archive Kit (Applied Biosystems, Foster City, CA).

The sequences of the gene expression assays used (Applied Biosystems) are

proprietary. Glyceraldehyde-3-phosphate dehydrogenase (GAPDH, Hs99999905_m1)

served as an endogenous control gene for all samples. Osteopontin

(Hs00960641_m1), adiponectin (Hs00605917_m1), and type II collagen

(Hs00264051_m1) were assayed as markers for osteogenesis, adipogenesis, and

chondrogenesis, respectively. Gene expression assays were combined with the cDNA

to be analyzed and TaqMan PCR Master Mix (Applied Biosystems). The reaction

was performed on a 7900HT real-time PCR System (Applied Biosystems) using

thermal conditions of 2 minutes at 50°C, 10 minutes at 95°C, and 40 cycles of 15

seconds at 95°C and 1 minute at 60°C. The relative gene expression level of each

target gene was then normalized to the mean of the GAPDH in each group. Fold

change was calculated using the ΔΔCT relative comparative method as described

previously [69]. Samples were completed in triplicate and standard deviations are reported (n = 3).

4.2.7 Statistical Analysis

All data was analyzed using one-way analysis of variance and Tukey's multiple-comparison test to determine statistical differences between hydrogels. A confidence interval of 95% (α=0.05) was used for all analyses, and means and SDs are shown in each figure.

4.3 Results

4.3.1 Identification of Adhesive Differences between Lineages over 21 Days

As an initial investigation into the potential adhesive differences between the three main mesenchymal lineages and an undifferentiated control, adhesion was evaluated using centrifugation over 21 days (see Figure 4.2). Results showed significant differences between lineages, specifically between the chondrogenic group and all other groups. There were also significant changes within a group over the three timepoints. At day 7, the control group was significantly less than the osteogenic and chondrogenic groups, but not statistically different from the adipogenic group. On day 14, both osteogenic and adipogenic samples showed statistically greater adhesion than the control, with the osteogenic group showing the highest percent adhesion. The chondrogenic group experienced a dramatic decrease in percent adhesion between day 7 and day 14, and was statistically lower than all other

groups on day 14. This trend continued on day 21, with the chondrogenic group exhibiting the lowest percent adhesion. The osteogenic group remained statistically higher than all other groups, and the control and adipogenic group showed no statistical differences.

4.3.2 Impact of Incubation Time and Centrifugation Speed on Differentiating hMSCs

Overall, the osteogenic group exhibited high levels of adhesion, particularly when incubated for 200min prior to centrifugation (see Figure 4.3). On day 7, all groups showed very high levels of adhesion at the 200min incubation condition (>90% for all speeds). At the 20min incubation condition, there is a decreasing trend with increasing detachment force. At day 14, similar trends are present, with an overall decrease in the percent adhesion of all groups. By day 21, cells have become fully differentiated and there is a distinct overall drop in the percent adhesion for both incubation conditions. For the adipogenic group (Figure 4.4) on days 7 and 14, the 200min incubation condition exhibit very high levels of adhesion with few statistical differences between speeds. On all days, the percent adhesion of the 200min incubation condition is statistically greater than the 20min incubation condition. The 20min incubation condition exhibits very low adhesion with no statistical differences between centrifugation speeds at any timepoint. As with the osteogenic group there is a noticeable decrease in adhesion at day 21 for all conditions. For all timepoints, chondrogenic samples exhibit very low levels of adhesion as early as day 7 (Figure 4.5). Note that the y-axes of these figures span a smaller range than for the osteogenic and adipogenic groups. At day 7, there are no differences between the groups in the

20min incubation condition, while the 200min incubation condition shows a significant decrease as centrifugation speed increases. At days 14 and 21, the percent adhesion falls lower, and there are no statistical differences between any groups.

4.3.3 Histological Analysis of Attached and Detached Fractions Following Centrifugation

All data for the osteogenic group is presented in Figure 4.6 as the percentage of calcified regions per cell. On day 7, all groups exhibit low levels of calcification, with values less than 5%. The attached fractions at all speeds in the 200min incubation condition showed statistically greater percent calcification compared to the detached fraction. At the 20min incubation condition, this was only true at the highest centrifugation speed of 500xg. On day 14, there was an increasing trend overall in the percent of calcified regions per cell. For both incubation conditions, the attached fraction at 200xg was statistically greater than the detached fraction. On day 21, there were sustained high levels of calcification. For the 20min incubation condition at 500xg, the attached fraction showed statistically greater levels of calcification compared to the detached fraction, while the 200min incubation period showed the same trend at 50 and 200xg. All data for the adipogenic group is reported in Figure 4.7 as the percent of oil red positive regions per cell. At day 7, there were very low levels of positive staining for lipid deposits. For both incubation conditions there were no statistical differences between groups. On day 14, there was an overall increase in oil red o positive regions. The only statistical difference was for the 200min incubation period, 200xg centrifugation speed which showed that the

45

attached fraction had statistically higher oil red o positive regions than the detached

fraction. Samples on day 21 exhibited the highest level of positively stained regions,

with values as high as 10%. However, there were no statistical differences. Results

for the chondrogenic group are presented as the percent of proteoglycan positive

regions per cell and shown in Figure 4.8. On day 7, there are very low levels of

proteoglycan positive regions. On day 14, there was an increasing trend in the

percentage of proteoglycan positive regions, yet still few statistical differences

between groups. For the 200min incubation condition, the attached fraction at 200xg

was statistically lower than the detached fraction. Day 21 exhibited high levels of

positively stained regions, particularly in the detached fractions. There were no

statistical differences between groups.

4.3.4 Application of Centrifugation at Day 14 to Separate Cell Populations

Using the data resulting from histological analyses, it was determined that for

all three lineages an incubation period of 200 minutes and a centrifugation speed of

200xg applied at day 14 would result in a separation between differentiating cells. For

osteogenesis and adipogenesis, results indicated that the attached fraction would

contain a greater degree of calcification and lipid deposits, respectively. For

chondrogenic samples it was predicted that the detached fraction of cells would

produce a matrix rich in proteoglycans. At day 21 (7 days after centrifugation), results

for the osteogenic group showed that the attached fraction exhibited a significantly

higher expression of osteopontin (OPN), a marker of late osteogenesis when

compared to the detached fraction (see Figure 4.9A, B). This was confirmed in Figure

4.10A with histological analysis showing a statistically greater number of calcified

regions in the attached samples compared to the detached. However, both the attached

and detached fractions showed significantly less OPN expression than the control.

This result was similar to that found in the adipogenic group. Here, the attached

fraction expressed a significantly higher amount of the adipogenic marker

adiponectin, but both fractions had significantly lower expression than the control

(Figure 4.9C, D). Gene expression results were confirmed by histological analyses of

the percentage of oil red o positive cells. At day 21, the attached fraction showed a

significantly higher level of positively stained regions compared to the detached

fraction (see Figure 4.10B). For chondrogenesis, the detached fraction at day 21

resulted in significantly greater type II collagen expression when compared to the

attached fraction as well as the control. Histological analysis using alcian blue

staining confirmed this trend, but there was no significant difference (p = 0.97)

between the attached and detached fraction at day 21 (Figure 4.9E, F and 4.10C).

A

B
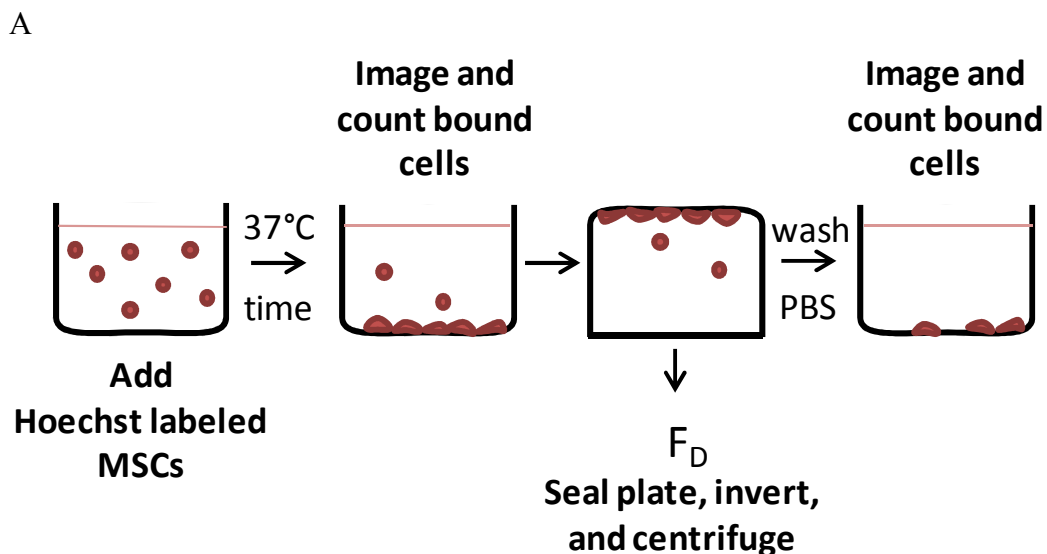
Centrifugation Speed (RCF)	Detachment Force (pN)
50	175
200	700
500	1750

Figure 4.1. Centrifugation assay. (A) Schematic of the centrifugation assay used to generate percent adhesion data for all groups throughout the 21 day differentiation period. Percent adhesion was calculated by dividing the post-spin cell count by the pre-spin count and multiplying by 100. (B) Centrifugation speeds and the corresponding detachments forces applied throughout the study. Forces were calculated based off of the formula presented in 4.2.3.
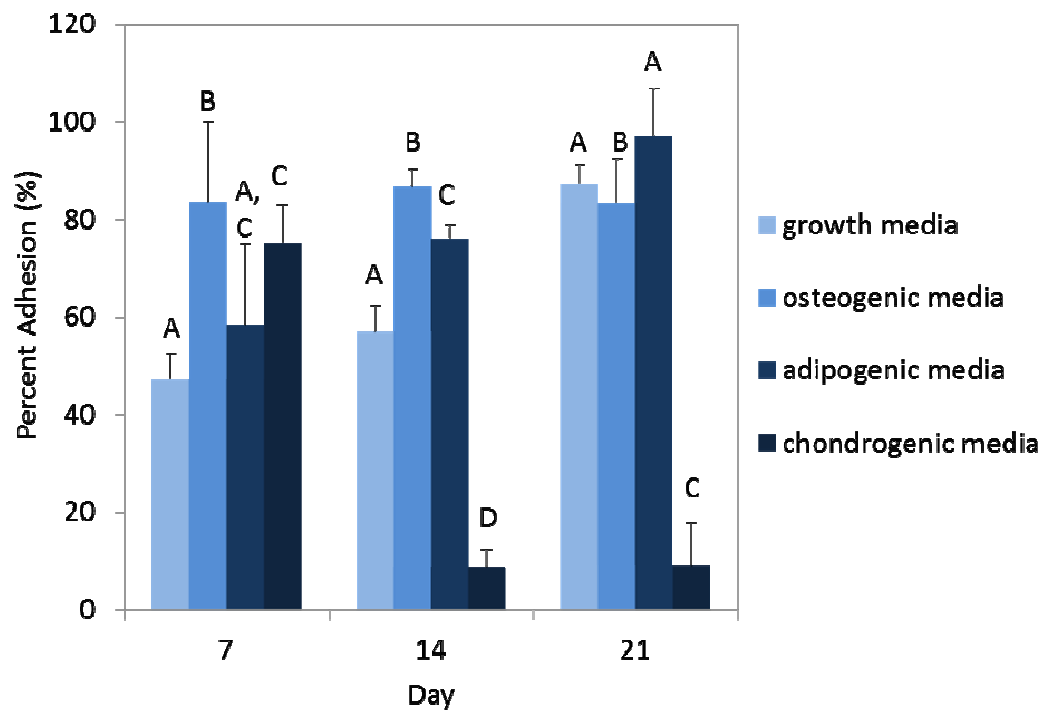
Figure 4.2. Adhesion of differentiating hMSCs over 21 days. hMSCs undergoing osteogenesis, adipogenesis, chondrogenesis, or no differentiation (growth media) were evaluated throughout the 21 day differentiation period. Cells were incubated on TCPS for 30 minutes followed by centrifugation at 200xg for 1 minute. The percent adhesion results show distinct adhesion profiles for each lineage, with the osteogenic and adipogenic groups exhibiting increased adhesion, and the chondrogenic group showing a dramatic decrease early in differentiation. Statistical analysis reveals that there are statistical differences between groups ($p < 0.05$). Groups that do not share a letter within each timepoint are statistically different.
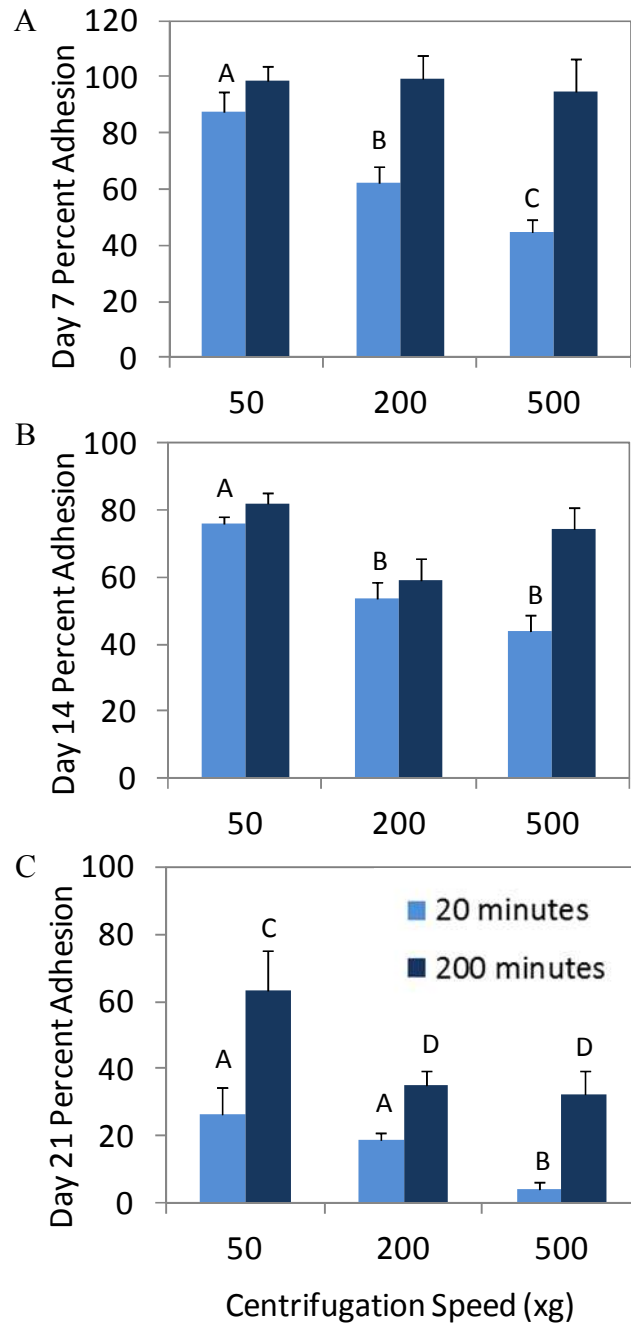
Figure 4.3. Adhesion of hMSCs undergoing osteogenesis. (A) On day 7, osteogenic samples exhibit very high adhesion levels for both incubation times and all speeds. There are no significant differences at the 200 minute incubation condition, but at 20 minutes, there is a statistically significant decrease in adhesion which corresponds to increasing speed. (B) Similarly, on day 14, there are no significant differences between the centrifugation speeds at the 200 minute incubation condition, but differences are present at the 20 minute condition. (C) On day 21, there are significant differences for both incubation conditions. Groups that do not share a letter are statistically different (p<0.05). Comparisons between centrifugation speeds within the same incubation condition are shown.
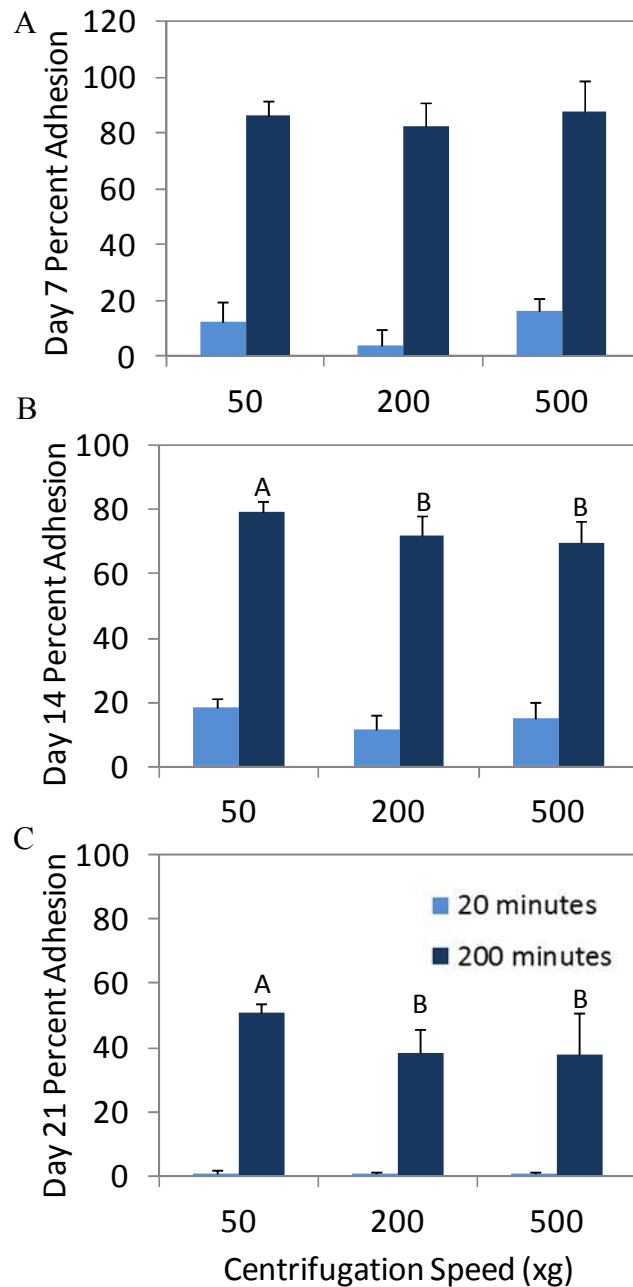
Figure 4.4. Adhesion of hMSCs undergoing adipogenesis. (A) On day 7, there are no statistical differences between centrifugation speeds at either incubation condition. (B) On day 14, there are no significant differences between the centrifugation speeds at the 20 minute incubation condition, but differences are present at the 200 minute condition. (C) The results on day 21 are similar to those on day 14, with no differences at the 20 minute incubation condition but statistical differences between speeds at the 200 minute condition. Groups that do not share a letter are statistically different ($p < 0.05$). Comparisons between centrifugation speeds within the same incubation condition are shown.
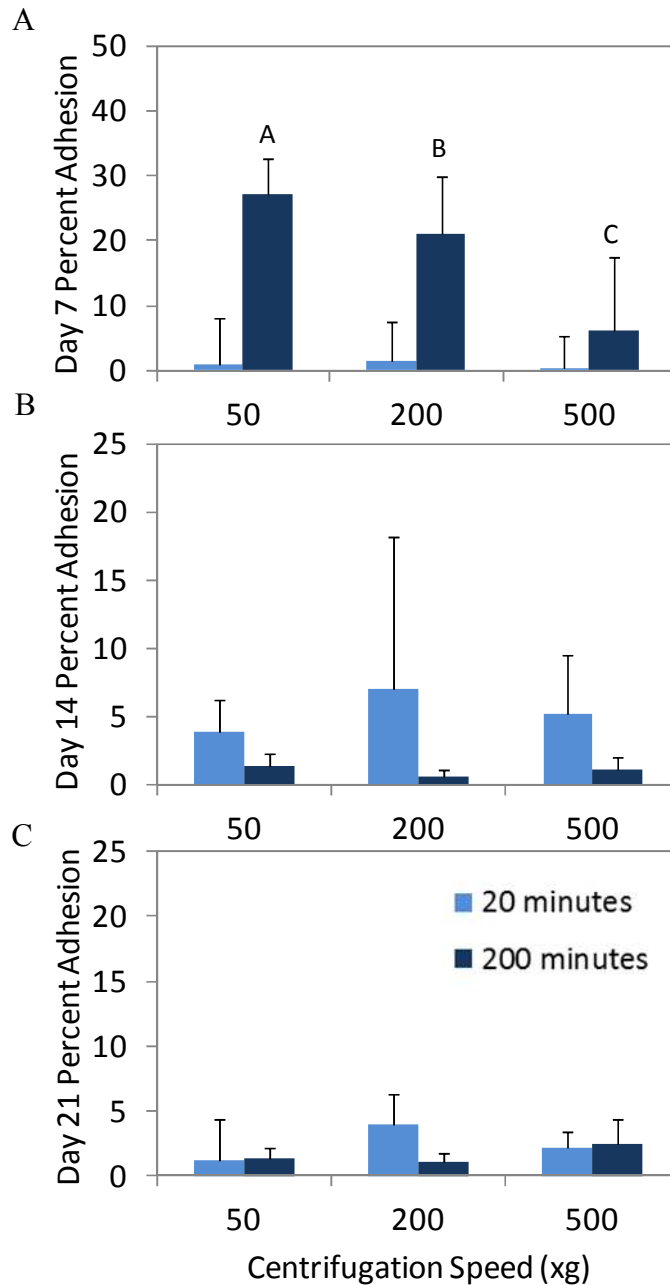
Figure 4.5. Adhesion of hMSCs undergoing chondrogenesis. (A) On day 7, there are no statistical differences between centrifugation speeds at the 20 minute incubation condition. For the 200 minute condition, there was a statistically significant decrease in adhesion with increasing centrifugation speed. (B) On day 14, there are no significant differences between the centrifugation speeds at either incubation condition. (C) The results on day 21 also show no statistical differences between groups at either incubation condition. Groups that do not share a letter are statistically different ($p < 0.05$). Comparisons between centrifugation speeds within the same incubation condition are shown.
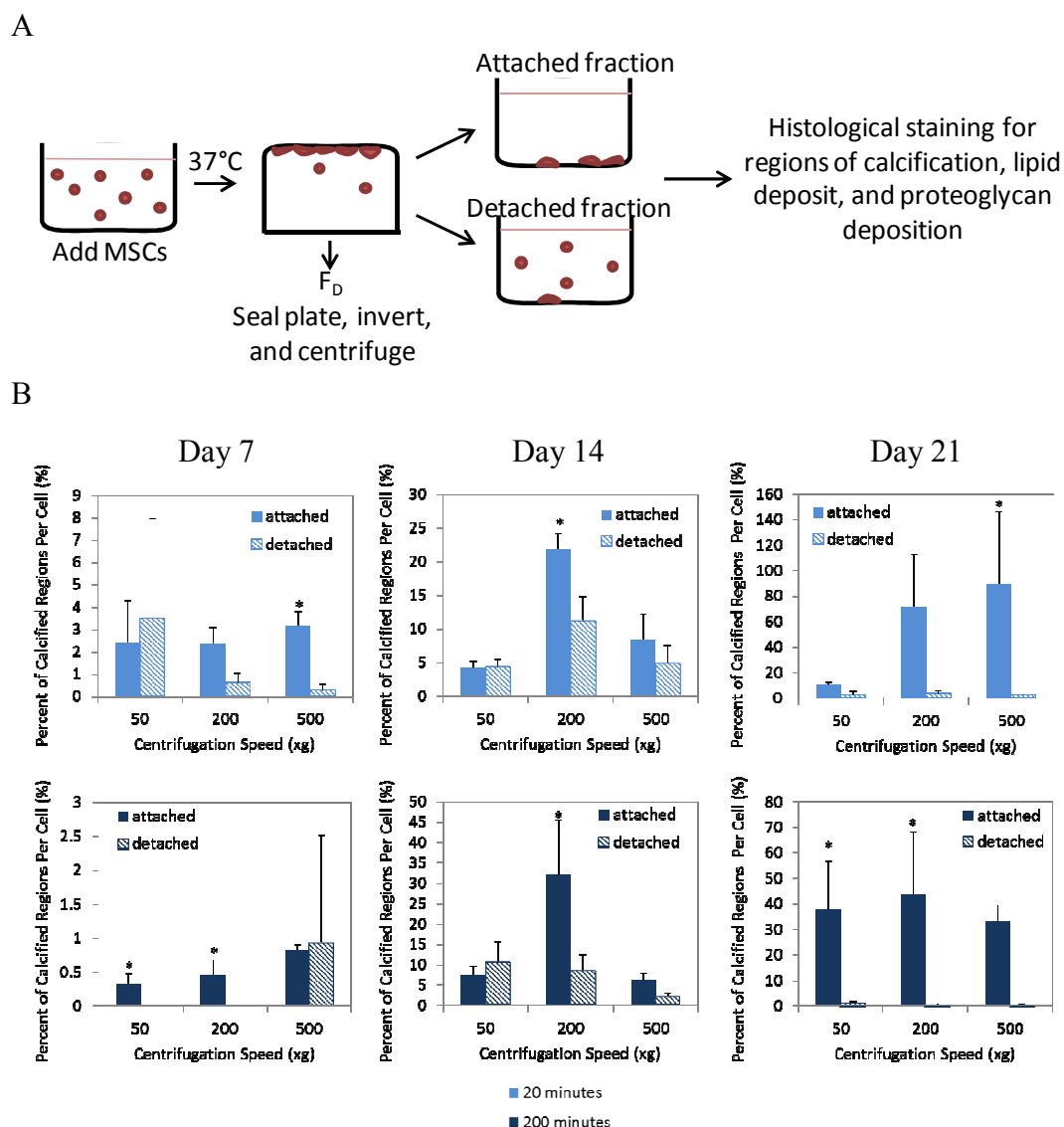
Figure 4.6. Alizarin red histological analysis for quantification of calcification. (A) Schematic of the adjusted centrifugation assay used for all histological analysis experiments (Figures 4.6, 4.7, 4.8, and 4.10). (B) Results of histological analysis using alizarin red to quantify the percent of calcified regions per cell for each condition. Alizarin red stains calcified regions a red-orange color. The top row represents the 20 minute incubation condition on all days, the bottom row is the results from the 200 minute incubation condition on all days. From right to left: day 7, day 14, and day 21. On all figures, '*' indicates the group exhibits a statistically greater percent calcification compared to the detached fraction within that condition (p<0.05). Based on this data, the 200 minute incubation condition and 200xg speed at day 14 was chosen for subsequent analysis.
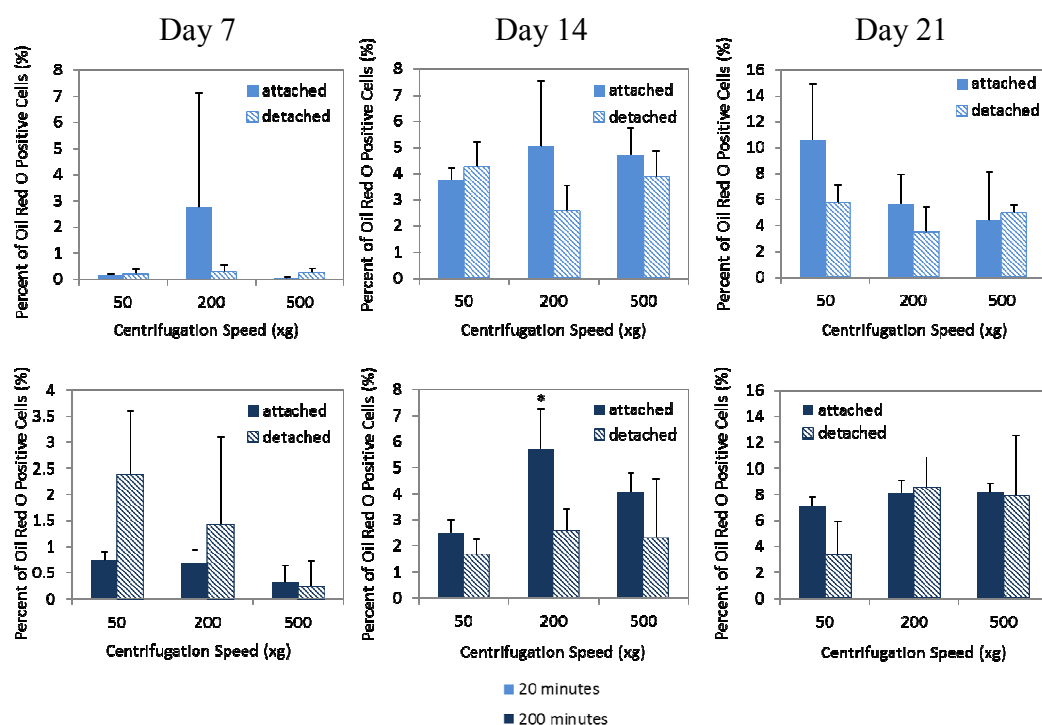
Figure 4.7. Oil red o histological analysis for quantification of lipid deposits. Oil red o stains lipid deposits red, while cell nuclei appear blue due to counterstaining with haematoxylin. Results of histological analysis using oil red o to quantify the percent of oil red o positive regions per cell. The top row represents the 20 minute incubation condition on all days; the bottom row is the results from the 200 minute incubation condition on all days. From right to left: day 7, day 14, and day 21. On all figures, '*' indicates the group exhibits a statistically greater percent of oil red o positive cells compared to the detached fraction within that condition (p<0.05). Based on this data, the 200 minute incubation condition and 200xg speed at day 14 was chosen for subsequent analysis.
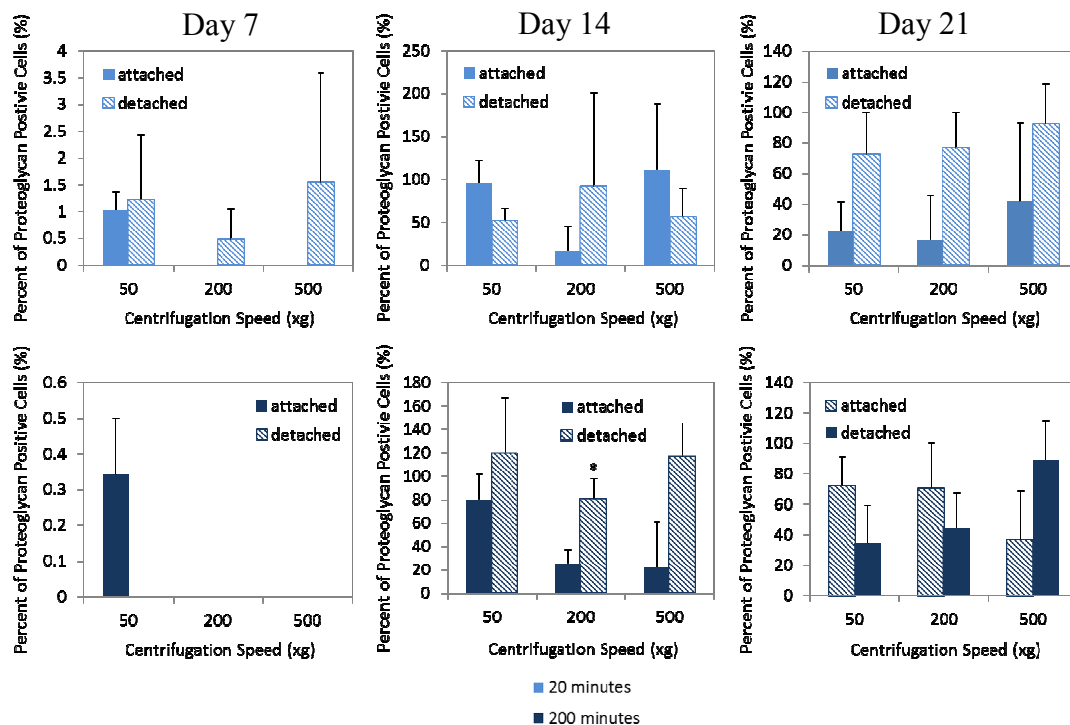
Figure 4.8. Alcian blue histological analysis for quantification of proteoglycan deposition. Alcian blue stains proteoglycan rich regions blue, while the nuclei appear pink due to counterstaining with nuclear fast red. Results of histological analysis using alcian blue to quantify the percent of proteoglycan positive regions per cell. The top row represents the 20 minute incubation condition on all days; the bottom row is the results from the 200 minute incubation condition on all days. From right to left: day 7, day 14, and day 21. On all figures, '*' indicates the group exhibits a statistically greater percent of proteoglycan positive cells compared to the attached fraction within that condition ($p<0.05$). Based on this data, the 200 minute incubation condition and 200xg speed at day 14 was chosen for subsequent analysis.
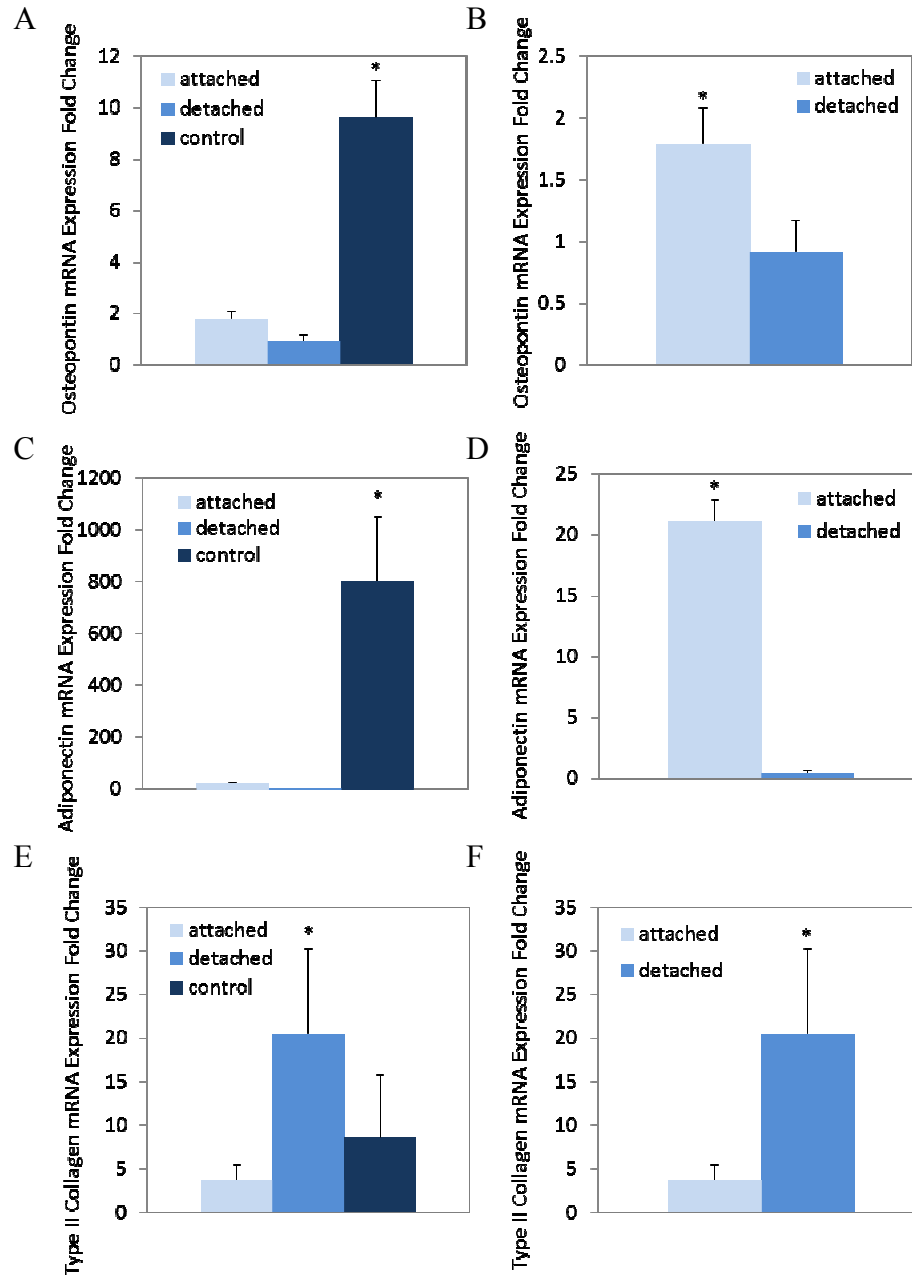
Figure 4.9. qRT-PCR results at day 21 following separation at day 14. (A) OPN expression of cells undergoing osteogenesis. OPN is a marker of osteogenesis and is typically upregulated over 21 days. (B) OPN expression of attached and detached fraction alone. (C) Adiponectin expression of all groups undergoing adipogenesis. Adiponectin is a marker of adipogenesis. (D) Adiponectin expression of the attached and detached fractions alone. (E) Type II collagen expression of all groups undergoing chondrogenesis. Type II collagen is a phenotype marker for mature chondrocytes. (F) Type II collagen expression of the attached and detached fractions alone. On all figures, '*' indicates the group exhibits a statistically greater expression of the respective marker compared to all other groups ($p < 0.05$).
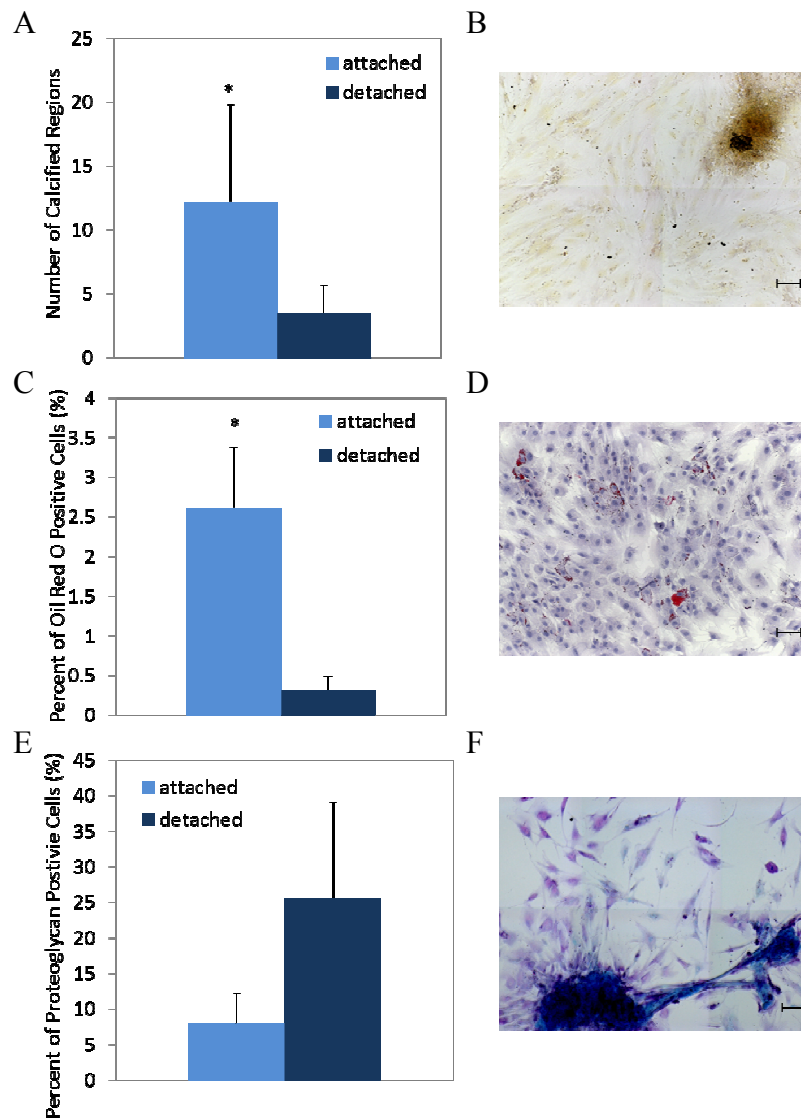
Figure 4.10. Histological analysis results at day 21 following separation at day 14. (A) The number of calcified regions for the osteogenic group as determined through alizarin red staining and quantification of calcified regions. (B) A representative image of alizarin red staining, showing red-orange regions of calcification. (C) The quantified percentage of oil red o positive regions, a measure of lipid deposits in the adipogenic group. (D) A representative image of oil red o staining, showing lipid depostis in red and nuclei counterstained blue. (E) Quantification results of alcian blue staining for the chondrogenic group. (F) A representative image of alcian blue staining for proteoglycan deposition which appeard blue and nuclei which appear pink. On all figures, '*' indicates the group exhibits a statistically greater higher level of positively stained cells compared to all other groups (p<0.05). Scale bars on all images represent 100 μm.

4.4 Discussion

During MSC differentiation down the three main mesenchymal lineages there are distinct changes in cell adhesion that can be correlated to cell differentiation. These adhesive changes can be exploited to separate cell populations based on differentiation potential, through the use of a simple, reproducible, cell adhesion based assay. Centrifugation has been used previously as a means to non-destructively monitor the phenotype of chondrocytes cultured *in vitro* [64]. It was found that increases in cell adhesion could be correlated to a loss of the chondrocyte phenotype. Through an initial study, we were able to show that MSCs undergoing osteogenesis, adipogenesis, and chondrogenesis, experience distinct variations in cell adhesion throughout differentiation. Over the 21 day differentiation period, two pathways appear to emerge. Osteogenic and adipogenic samples show an increase in the percent adhesion until maturity at day 21 is reached. Here, adhesion is sustained or somewhat decreased. Chondrogenic samples however experience an opposite trend. The percent adhesion of this lineage is dramatically decreased as early as day 7 and remains low through the remaining timepoints (see Figure 4.2).

These pathway dependent adhesive profiles may be related to the target cell phenotype. It has been shown that during osteogenesis, there are increases in the expression of key integrins responsible for cell adhesion [71], and that overall, cell morphology becomes more elongated and spread throughout the differentiation process [72]. Additionally, OPN, a key marker for osteogenesis, has been shown to play a role in the regulation of osteogenic and adipogenic differentiation [68]. It is hypothesized that this regulation is linked to the RGD motif on OPN, with blockage

58

of the motif, which is known to play a role in cell adhesion, promoting adipogenesis. Adipogenesis has previously been shown to be promoted by less adhesive environments [73-75], however, the data presented here shows an overall increase in cell adhesion through 21 days. During adipogenesis, cells undergo dramatic changes in extracellular matrix molecule expression, which impacts the adhesion of cells to their underlying substrate. Adipogenesis is supported by environments that discourage cell spreading and encourage high cell density, therefore increasing cell signaling [76]. Due to the preference for high density culture, it is possible that the increases in cell adhesion that we see here are based on increased cell-cell adhesion in addition to changing cell-matrix interactions. One of the major characteristics of the native phenotype of articular cartilage is the spherical morphology of chondrocytes [47, 77]. Chondrogenesis is promoted by environments that encourage a high level of cell-cell interaction and is typically induced with MSCs in high density pellet culture [78]. Additionally, chondrogenesis has been found to be promoted in environments where there is a disruption of the cytoskeleton [72], further supporting the dramatic decrease in adhesion that is shown here.

Centrifugation assays as a means to measure cell adhesion use simple techniques and common laboratory equipment to quantify the adhesion of a large cell population. Centrifugation assays are most sensitive at shorter adhesion times (less than 60 minutes), as cell adhesion can become saturated and the forces necessary for detachment too large with longer incubation periods [35]. For each cell type and culture condition, it is necessary to optimize assay parameters. Results shown in Figures 4.3, 4.4, and 4.5 indicate that by varying incubation time and centrifugation

speed, we can identify optimal conditions for population separation. Through the use of histological analysis of the attached and detached fractions following separation, we were able to relate the adhesive characteristics of the cells to differentiation. Figures 4.6, 4.7, and 4.8 show the results of histological analysis for the attached and detached fractions at each centrifugation assay condition. Based on these results, it is apparent that there are particular parameters for each lineage that give rise to a more homogeneously differentiated population of cells. This result is particularly apparent at days 14 or 21 when cells are more committed to each lineage.

The effectiveness of this technique for the application of purifying a differentiating cell population was successfully demonstrated by applying centrifugation at day 14. Using the optimized parameters, we were able to show that cell adhesion based separation at day 14 resulted in two distinct populations at day 21. For osteogenesis and adipogenesis, the attached fractions showed significantly greater levels of differentiation compared to the detached fractions for each group, a trend which was reversed for the chondrogenic condition. While this method was successful for identifying the populations of cells that were differentiated, there are still questions regarding the identity of the undifferentiated cells in the population. Following separation at day 14, very few cells in the detached fractions of the osteogenic and adipogenic groups underwent differentiation, exhibiting levels of differentiation markers close to what we observe after only 7 days of differentiation. A similar trend was observed with the attached fraction of the chondrogenic group, with very few cells in the attached fraction producing any proteoglycan rich regions following separation. The identity of these undifferentiated cells is uncertain. It is

hypothesized that MSCs undergo asymmetric division during the initial stages of differentiation [55], causing a heterogeneous population. Therefore, it is possible that these undifferentiated cells could be precursor or progenitor cells that have yet to undergo differentiation, but additional molecular and biochemical analysis is necessary.

To effectively separate populations, it is necessary to find parameters that result in adhesion near 50%, defined as the mean adhesive strength value [41]. For osteogenesis and adipogenesis, the parameters chosen for the assay at day 14 resulted in a percent adhesion of 59.3 and 71.9% respectively. For chondrogenesis, the mean adhesive strength value was difficult to identify. Due to very low levels of adhesion regardless of the parameters, there were no conditions that resulted in a percent adhesion near 50%. Therefore, for the purpose of comparison, the same incubation period and centrifugation speed was chosen for the chondrogenic group. For all differentiation conditions the attached and detached samples at day 21 were compared with a control group that was not subjected to centrifugation at day 14. On day 21, for both the osteogenic and adipogenic group, the attached fraction performs better than the detached, but both fractions exhibit differentiation levels significantly less than the control. This raises the question of if the separation of differentiated and undifferentiated populations by centrifugation causes too great of a disruption to the overall differentiation process. Following separation, the cell density of each fraction has decreased, which may hinder further differentiation, particularly for adipogenesis and chondrogenesis, which prefer a high cell density. Additionally, due to the large differences in cell density between the experimental and control groups, it is

somewhat difficult to compare them directly. To complete the centrifugation assay, cells must be lifted, during which the extracellular matrix and cell activity is undoubtedly disrupted. Regardless of the difficulty for direct comparison, there is potential take away from the results of the control. It is possible that the separation of differentiating cells at too early a stage eliminates necessary crosstalk between the heterogeneous populations. While from a cell therapy perspective, homogeneity prior to implantation is ideal, it is possible that during differentiation *in vitro,* the crosstalk between multipotent MSCs, precursors, progenitors, and differentiated cells is necessary to promote further differentiation.

4.5 Conclusion

In the presented study, we showed that a simple, non-destructive centrifugation assay can be used to separate a differentiating population of hMSCs. Through separation, there is a decrease in the overall heterogeneity of the cell population, which is of great importance for cell therapy applications. During chondrogenic differentiation, the application of centrifugation at day 14 resulted in a detached fraction of cells that exhibited significantly greater levels of expression for chondrogenic markers compared to the attached fraction and the control. For osteogenic and adipogenic samples, we showed that the attached fraction following separation had significantly higher expression of differentiation markers compared to the detached fraction, yet both were less than the control. This result suggests that

there is a level of crosstalk between the heterogeneous populations that is necessary

for differentiation, the details of which need to be further elucidated.

Chapter 5: Development of a Dynamic Stem Cell Culture Platform for Mesenchymal Stem Cell Adhesion and Evaluation[3]

5.1 Introduction

Significant contributions to the field of drug discovery research have been achieved using traditional *in vitro* culture of a 2D monolayer of cells seeded onto tissue culture polystyrene (TCPS) [79]. However, there are some drawbacks to TCPS in that it lacks the ability to provide a cellular microenvironment that imitates the native environment. A system which can provide environmental cues to a cultured cell population is critical for drug testing as environmental cues are found to have significant impacts on cell phenotype, function, and therefore the response of cells to drugs [80, 81]. It has been well documented that the cellular microenvironment can send signals to a cell through cell-cell and cell-matrix interactions, as well as through mechanical forces. Downstream effects of these interactions include alterations in gene expression, cell migration, proliferation, and differentiation [80, 82].

In order to develop an *in vitro* environment suitable for drug discovery applications, we chose to investigate two major components: cell-matrix interactions and mechanical cues provided by a biomaterial scaffold, and a dynamic environment provided by a perfusion bioreactor. The combination of both of these components will result in a simple *in vitro* device, the dynamic stem cell culture platform

---

(DSCCP), that can be translated to many cell types, matrix molecules, and subsequent evaluations, including investigation of cell response to drug treatments.

Biomaterials can be fabricated to control both cell-cell and cell-matrix interactions, optimizing adhesion events and the resulting downstream reactions. Cell adhesion is critical for many cellular functions, including spreading, proliferation, and migration. A key finding in cancer research discovered that integrin interactions played a major role in the resistance of breast cancer cells to paclitaxel [83], and that cell adhesion protected cancer cells from drug-induced apoptosis. The fabrication of biomaterials to include specific extracellular matrix (ECM) molecule ligands which mimic the *in vivo* integrin interactions that result in drug-resistant tumors can create a more efficient model for drug evaluation.

There have been many recent developments in the field of biomaterials for drug evaluation, including the development of modified 2D substrates as well as 3D environments for drug screening applications. Poly(dimethylsiloxane) (PDMS) 2D substrates modified to include ECM molecules have been shown to successfully increase the adhesion of the human intestinal Caco-2 cell line, and provide a foundation for creating miniaturized biomimetic environments for drug evaluation [84]. The complex 3D nature of tumors has led to the development of 3D models for drug evaluation, specifically in cancer research. Scaffold-free 3D culture of multicellular tumor spheroids (MTS) has shown that formation of 3D spheroids resulted in a significantly different outcome when spheroids are exposed to traditional cancer treatments when compared to their TCPS counterparts [85]. The cell-cell interactions that are recapitulated in the MTS system demonstrated decreased levels

of cell death following exposure to drugs commonly used for cancer treatment such as doxorubicin and paclitaxel.

Synthetic biomaterials provide a level of control over the structure and composition of the polymer that cannot be achieved when using natural materials. Tumors represent a complex *in vivo* environment, which must be studied by systematically evaluating individual interactions. In order to achieve this, recent studies have used modified poly(ethylene glycol) (PEG) hydrogels that include a specific ECM protein, exhibit specific mechanical properties, or degrade at a specific rate [86]. Studies of this nature allow researchers to break the complex tumor microenvironment into distinct parts and evaluate the effect of each of these parts on the cell response to drug treatment.

The mechanical properties of the cell microenvironment can also influence cell functions similar to those impacted by cell adhesion. Substrate stiffness has also been shown to effect cell migration [87, 88], differentiation [89, 90], and self-renewal [91]. Increasing the stiffness of PEG hydrogels has previously been shown to increase the osteogenic differentiation of mesenchymal stem cells (MSCs) [89], while soft substrates resulted in weaker adhesion and the promotion of MSC chondrogenesis [92]. It is well documented that tissue stiffness is increased in the tumor microenvironment, and several groups have sought to investigate how the substrate stiffness can impact the response of cells to drug therapy in terms of cell attachment, organization, proliferation, and survival [86, 93].

The mechanical environment is also influenced by an important factor of nutrient and drug delivery – the bloodstream. Nutrient exchange *in vivo* occurs

continuously through the diffusion of molecules from the bloodstream into the tissues. In addition to nutrient delivery, the blood also provides mechanical stimulation in the form of shear stress, which can influence cell behavior. All intravenously administered drugs reach the targeted tissue via transport in the blood, making it an important aspect of drug evaluation which cannot be ignored when creating *in vitro* drug evaluation models. We have previously developed a tubular perfusion system (TPS) bioreactor in our laboratory, which we have used extensively for the culture of MSCs, to increase nutrient transport and cell survival as well as induce osteogenic differentiation [69].

In order to develop a platform which provides a more accurate representation of the *in vivo* environment by mimicking the cell-ECM interactions, mechanical properties, and nutrient delivery of native tissue, we investigated the impact of several parameters on MSC adhesion, morphology, and pluripotency. The development of a product which can recapitulate the native cellular microenvironment is imperative for the future of drug development and evaluation. We chose to investigate MSCs because they are found in multiple tissues throughout the body including bone marrow, adipose tissue, the synovial membrane, and trabecular bone and can be differentiated into a number of lineages including chondrocytes, adipocytes, and osteoblast [56, 94]. In addition to the importance of drug evaluation on a cell type capable of downstream differentiation, the epithelial-to-mesenchymal transition (EMT) has been indicated as an important driving force for tumor development, invasion, and metastasis [95]. Recently, it has been reported that EMT may initiate the induction of a cancer stem cell (CSC) population [96, 97]. CSCs are thought to be

one of the key reasons that tumors can develop drug resistance and contribute to the unpredictable nature of tumor development [98]. Therefore, the investigation of drug treatment on a stem cell population such as MSCs is of high importance.

To develop the DSCCP, we investigated three major objectives. First, we investigated the role of stiffness on MSC adhesion and morphology by attaching non-specific amine groups to PEG hydrogels of varying stiffness. Secondly, we investigated how adhesion and differentiation may be altered by the inclusion of an MSC specific protein, fibronectin. Lastly, we examined how the inclusion of shear force and dynamic nutrient delivery, achieved by hydrogel incorporation in the TPS bioreactor impacts MSC adhesion. We hypothesize that we will see increasing MSC adhesion with increasing stiffness as well as with the inclusion of MSC-specific protein. We anticipate that the inclusion of fibronectin will not affect the pluripotency of MSCs, and that the dynamic environment provided by the TPS bioreactor will result in increased cell adhesion and survival. Overall, this will indicate that the DSCCP can serve as a fitting model for drug discovery applications.

5.2 Materials and Methods

5.2.1 Hydrogel Fabrication

Poly(ethylene glycol) diacrylate (PEGDA) hydrogels (Mn = 700, Sigma-Aldrich, St. Louis, MO) were created using free radical polymerization using a method previously established in our laboratory [99]. Hydrogels were tested at two concentrations; soft (5% w/v PEGDA) or stiff (20% w/v PEGDA). Solutions

containing 5.0 or 20.0mg PEGDA/100µl water were used to vary stiffness. 15 mM of

ammonium persulfate (APS) with a 1:2 component: solvent ratio (where the solvent

used was water) and N,N,N',N'-tetramethylethylenediamine (TEMED) (Sigma-

Aldrich) were used in a 1:1 ratio as initiators. The desired volume of PEGDA was

mixed with water, then APS and TEMED were added sequentially, vortexing after

each addition. The solution was quickly poured into a custom designed Teflon mold

to crosslink into hydrogel discs 1mm thick and 20mm in diameter. The hydrogels

finished crosslinking in 2 minutes. For surface modified gels, 25µL of 12µmol/mL

acryloyl-PEG-NH$_2$ (Nanocs, Inc., Boston, MA) solution or 0.64µmol/mL acryloyl-

PEG-fibronectin solution was added to the surface of the hydrogel, after 90 seconds

of crosslinking. Hydrogels were crosslinked for an additional 2 minutes after

modification. Acryloyl-PEG-fibronectin was fabricated by the reaction of a 50-fold

molar excess of acryloyl-PEG-NHS (Nanocs, Inc.) with fibronectin (FN) (Millipore,

Billerica, MA) in sodium biocarbonate buffer (pH = 8.5) for 2h, followed by dialysis

and drying. All hydrogels were washed in phosphate-buffered saline (PBS) for 24

hours following fabrication. Hydrogels used in cell adhesion and spreading

experiments were prepared in a sterile environment and all precursors were filtered

using a 0.22µm sterile filter.

5.2.2 Dynamic Mechanical Analysis

The bulk mechanical properties of PEGDA hydrogels fabricated at 5, 10, and

20% w/v PEGDA were calculated using the Q-800 Dynamic Mechanical Analyzer

(DMA; TA Instruments, New Castle, DE) and Q Series Explorer software. 4mm

thick samples were cyclically compressed at 1Hz to a strain of 7%. From the applied strain, the response of the material and the Young's Modulus was determined from the linear region of the stress-strain curve. Six samples at each PEGDA concentration were tested.

5.2.3 Human Mesenchymal Stem Cell Culture

hMSCs (Lonza, Walkersville, MD) were expanded prior to the study in media consisting of DMEM (Life Technologies, Frederick, MD) supplemented with 10% fetal bovine serum (Life Technologies), 1.0% v/v penicillin/streptomycin (Life Technologies), 0.1mM non-essential amino acids (Life Technologies), and 4mM L-glutamine (Life Technologies) using protocols set forth by the manufacturer and previously described [69, 99]. hMSCs were expanded on TCPS with media changes every 3 days according to the manufacturer's specifications. hMSCs at passage 4 were used for all experiments. Cell cultures were incubated at 37°C, 5% CO_2, and 80% humidity.

5.2.4 Cell Adhesion and Spreading

Prior to hydrogel seeding, adherent hMSCs were lifted with trypsin/EDTA (Life Technologies) and counted using trypan blue uptake to determine viability. Sterilized hydrogels were placed into a 12 well plate and seeded with a concentrated cell solution of 100,000 hMSCs/100μL media for 1 hour at 37°C. Additional media was added after 1 hour, and cells were cultured for 48 hours. Cells seeded onto TCPS served as a positive control for cell attachment. After 48 hours of incubation,

hydrogels were soaked in PBS containing 1mM $CaCl_2$ and 0.5mM $MgCl_2$ for 30 min to remove non-adherent cells as well as any remaining medium. To aid in the visualization of cell attachment and spreading, a live-dead assay was performed following standard protocols. Hydrogels were incubated with 2mM ethidium homodimer and 4mM calcein AM (Life Technologies) for 30min. Images were taken using a fluorescent microscope (Axiovert 40 CFL with filter set 23; Zeiss, Thornwood, NY) equipped with a digital camera (Diagnostic Instruments 11.2 Color Mosaic, Sterling Heights, MI). Images were analyzed using the Zeiss software Axiovision 4.8 to quantify relative cell number, aspect ratio, and the average cell area on each hydrogel. Six images were analyzed for each condition. If individual cells in an aggregate were indiscernible due to overlapping or aggregating, the area was counted as one cell. Figure 5.1 shows the major processing steps within the Axiovision software that were used for all images.

5.2.5 Centrifugation Assay

To quantify relative adhesion of hMSCs seeded to modified and unmodified hydrogels, a centrifugation cell adhesion assay was performed as described in Section 3.2.3 with a few exceptions. Hydrogels were fabricated directly in the wells of a 96 well TCPS-treated plate (Costar, St. Louis, MO). Labeled hMSCs were incubated for 4 hours at 37°C and 5% CO_2. Wells without hydrogels served as a positive control (TCPS). A schematic of the modified assay is shown in Figure 5. 2. Tiled images sized 2 x 2 (total tiled image area $= 0.542mm^2$) were captured on wells prior to centrifugation (pre-spin). The assay was run at a relative centrifugal force (RCF) of

50xg for 30 seconds at 22 °C. The force of detachment (FD) was approximately 18pN and was calculated as described in 3.2.3. The percent adhesion for each group was calculated following the procedure described in 3.2.3.

5.2.6 Induction of Osteogenic, Chondrogenic, and Adipogenic Differentiation

To show that the environment produced by surface modified PEGDA hydrogels neither inhibits nor induces differentiation down the three main mesenchymal lineages (osteogenesis, chondrogenesis, and adipogenesis), a differentiation study was completed to show that when induced, cells seeded on the gels underwent differentiation and cells that were not introduced to differentiation cues were not induced based on material properties alone. Cells were seeded onto modified and unmodified hydrogels as described above. After incubation for 24 hours in growth medium, cells were cultured for 21 days in osteogenic (DMEM with 10% FBS, 1mM sodium pyruvate (Life Technologies), 100U/100µg penicillin-streptomycin, 10^{-7}M dexamethasone (Sigma-Aldrich), 50µg/mL ascorbic acid (Sigma-Aldrich), and 10mM β-glycerophosphate), chondrogenic (high glucose DMEM supplemented with ITS (BD, Franklin Lakes, New Jersey), 4mM L-proline (Sigma-Aldrich), 50µg/mL ascorbic acid, 1% sodium pyruvate, 10^{-7}M dexamethasone, and 100U/100µg penicillin-streptomycin, and 10ng/µL TGF-β3 (R&D Systems, Minneapolis, MN)), or adipogenic (DMEM with 10% FBS, 1mM sodium pyruvate, 100U/100µg penicillin-streptomycin, 10^{-6}M dexamethasone, 10µg/mL insulin (Sigma-Aldrich), 0.5mM IBMX (Life Technologies), and 200µM indomethacin (Life Technologies)) media as described by Yang et al [78]. Growth

media as well as groups cultured on TCPS were used as controls. All media were changed every 3 days. After 21 days in culture, cells were lifted from the surface of the hydrogels and seeded onto chamber slides (Fisher Scientific) for 24 hours. At this time cells were fixed with 10% formalin for 10 minutes, and stored at 4°C in PBS. Histological staining was completed to show calcification, glycosaminoglycan production, and the presence of lipid droplets. Mineralization was visualized using Von Kossa staining with a Nuclear Fast Red (Poly Scientific, Bay Shore, NY) counterstain following standard protocols. Glycosaminoglycan production was visualized by staining with 0.5% Alcian Blue solution (Poly Scientific) followed by a nucleic counter stain with Nuclear Fast Red. For the visualization of lipid vacuoles in adipogenic samples, a working solution of Oil Red O (Poly Scientific) was prepared and applied to fixed monolayers, followed by counterstaining with hematoxylin.

5.2.7 Dynamic TPS Bioreactor Culture

hMSCs were seeded onto 20% w/v PEGDA hydrogels that were unmodified, amine modified, or FN modified following the procedures previously outlined. After 24 hours, a subset of each group was examined using a live-dead assay as described above. The second subset was loaded into the bioreactor. The bioreactor was set up as described previously by our laboratory [69]. Briefly, a tubing circuit comprised primarily of platinum-cured silicone tubing (Cole Parmer, Vernon Hills, IL) connected a growth chamber to a media reservoir (Figure 5.3). Prior to use, the entire tubing circuit was sterilized by autoclave. The growth chamber was made up of platinum-cured silicone tubing (ID of 1') and contained the different hydrogel groups.

Hydrogels were separated inside of the growth chamber by pieces of quarter-inch silicone tubing to prevent aggregation. hMSC growth media was pumped through the recirculating system using a peristaltic pump (Cole Parmer) at 1.0mL/min. This flow rate was chosen based on previous studies [69, 100] to prevent aggregation while still exposing cells to direct shear force. The entire system was placed in an incubator at 37°C for the duration of the study. After 48 hours in the bioreactor, hydrogels were washed in PBS and imaged using a live-dead assay and the same techniques as before. Following culture within the bioreactor, it was observed that hMSCs on modified hydrogels formed distinct clusters (see Figure 5.9). A minimum of six samples from each group were analyzed for cell number, and images of modified hydrogels without clustering were not included in analysis as they were not representative of the modified environment. As a result, the modified hydrogel groups from the bioreactor have an n=9 while all other groups have an n=6.

5.2.8 Statistics

All data was analyzed using one-way analysis of variance and Tukey's multiple-comparison test to determine statistical differences between hydrogels. A confidence interval of 95% (α=0.05) was used for all analyses, and means and SDs are shown in each figure.

5.3 Results

5.3.1 DSCCP Design

Shown in Figure 5.3, our complete device consists of a biomimetic scaffold within the TPS bioreactor. The TPS bioreactor is composed of a peristaltic pump and media reservoir that continually perfuses media through a growth chamber. The growth chamber is shown in detail below. Depicted here, unmodified (left) and modified (right) hydrogel groups can be cultured together within the same chamber at different axial positions. Hydrogel groups were separated by larger pieces of silicon tubing to distinguish groups, and individual hydrogels were separated by thin pieces of the same tubing to prevent hydrogel aggregation without inhibiting the flow of media. Our laboratory has previously completed detailed modeling of the nutrient profiles and shear forces within the growth chamber at varying flow rates, and have found that at the currently used flow rate (1.0mL/min), there are no significant differences in the nutrient profile or shear forces over a growth chamber of our size (approximately 7cm)[69, 100]. The DSCCP can be customized on many levels, as parameters such as perfusion flow rate, scaffold properties, cell type, and the perfusion media can be modified to investigate a desired cell function.

5.3.2 Dynamic Mechanical Analysis

The resulting Young's Modulus of each hydrogel formulation is shown in Figure 5.4. Hydrogels formulated at 20% w/v PEGDA were found to have a statistically greater Young's Modulus than both the 5 and 10% w/v gels. There were

no statistical differences between the softer gels. The Young's Modulus increased with increasing PEGDA concentration, from 0.1 to 1.3 to 3.4kPa for 5, 10 and 20% gels respectively.

5.3.3 Cell Adhesion and Spreading

The impact of stiffness on hMSC adhesion and spreading was first investigated by comparing unmodified PEGDA hydrogel discs at 5 and 20 w/v% with hydrogels that were modified at the surface by covalent tethering of the non-specific binding group acryloyl-PEG-NH$_2$. The amine group would create a charge at the surface of the hydrogel, mimicking the action of TCPS. Figure 5.5A shows representative images of hMSCs on the four hydrogel groups tested: unmodified 5% w/v PEGDA, unmodified 20% w/v PEGDA, amine modified 5% w/v PEGDA, and amine modified 20% w/v PEGDA. All images were taken at 10X magnification and scale bars represent 100μm. Six images of each group were analyzed using a script written with Axiovision 4.8.2. (Zeiss) to determine the average cell count per mm^2 as well as the average cell area (μm^2). Results showed that on both soft and stiff substrates, the cell number was statistically greater on modified gels when compared to unmodified (see Figure 5.5B, top). In addition to cell number, we saw that amine modified 20% w/v PEGDA hydrogels exhibited a statistically greater average cell area, indicating increased cell spreading on the surface (see Figure 5.5B bottom) which is confirmed by microscopy images in Figure 5.5A.

Based on the initial results, we proceeded with all further studies using the 20% w/v PEGDA formulation. We next examined how the inclusion of specific

binding sites on the surface of the hydrogel would impact hMSC adhesion and morphology. Acryloyl-PEG-fibronectin was fabricated through the reaction of FN and acryloyl-PEG-NHS, which was confirmed using FT-IR. Figure 5.6A shows representative images of hMSCs attached to the surface of unmodified, amine modified, and FN modified 20% w/v PEGDA hydrogels, as well as a TCPS control. Results of image analysis indicated that unmodified hydrogels exhibited a statistically lower cell number (see Figure 5.6B, top). The addition of non-specific and specific adhesion modalities increased cell number when compared to unmodified hydrogels with FN modified hydrogels demonstrating no statistical difference in cell number when compared to TCPS. Figure 5.6B, bottom shows the average cell area (μm^2) for each group. As with cell number, unmodified hydrogels had the smallest average cell area, and histological images indicate rounded cell morphology. On amine and FN modified hydrogels, there was an increase in cell area, indicating cell spreading. Again, there were no statistical differences in average cell area between modified hydrogels and TCPS. Images also revealed cell clustering on FN modified hydrogels, suggesting that the surface modification is heterogeneous and cells cluster around areas of modification. The assay also revealed that there was little or no cell death for all groups.

5.3.4 Centrifugation Assay

To compare the relative strength of adhesion to the various hydrogels, we utilized a centrifugation cell adhesion assay to apply a detachment force to hMSCs incubated on hydrogel surfaces. We investigated four groups – unmodified, amine

modified, and FN modified 20% w/v PEGDA hydrogels, as well as a TCPS control. Results indicate that the unmodified and amine modified hydrogels exhibited relatively low adhesion (9 an 26% respectively), while FN modified hydrogels and TCPS demonstrated much higher levels of adhesion (95 and 87% respectively). Both unmodified and amine modified gels had statistically lower adhesion than FN modified and TCPS groups, and there were no statistical differences between unmodified and amine modified or between FN modified and TCPS.

5.3.5 Induction of Osteogenic, Chondrogenic, and Adipogenic Differentiation

hMSCs are a valuable cell type for therapeutic applications due to their ability to readily differentiate down osteogenic, chondrogenic, and adipogenic lineages. In order to demonstrate that the inclusion of amine and FN groups on the surface of PEGDA hydrogels neither inhibits nor induces differentiation, hMSCs were exposed to growth, osteogenic, chondrogenic, or adipogenic media for 21 days. Histological images in Figure 5.8 demonstrate that hMSCs exhibit the morphology and ECM production of the expected cell type when exposed to proper differentiation signals, indicating that hMSCs seeded onto amine and FN modified surfaces are still capable of undergoing differentiation. It was similarly important to show that hMSCs that were exposed to growth media maintained the morphology of hMSCs, and remained negative for calcium deposition, glycosaminoglycan production, or the presence of lipid vacuoles, demonstrating that the hydrogel properties alone did not induce undesired differentiation. It is important to note that because cells were lifted with trypsin/EDTA prior to histological staining, there is some loss of matrix.

5.3.6 Dynamic TPS Bioreactor Culture

Image analysis (see Figure 5.9) revealed that modified hydrogel groups cultured in the bioreactor showed distinct cell clustering, further confirming that the hydrogel surface is heterogeneous. All images with cell clusters were analyzed. Analysis showed that after the initial static culture, FN modified hydrogels exhibited a significantly higher cell number, while no differences were detected between unmodified and amine modified groups. Following bioreactor culture, modified hydrogels retain a significantly higher cell number, with no differences observed between amine and FN modified groups.
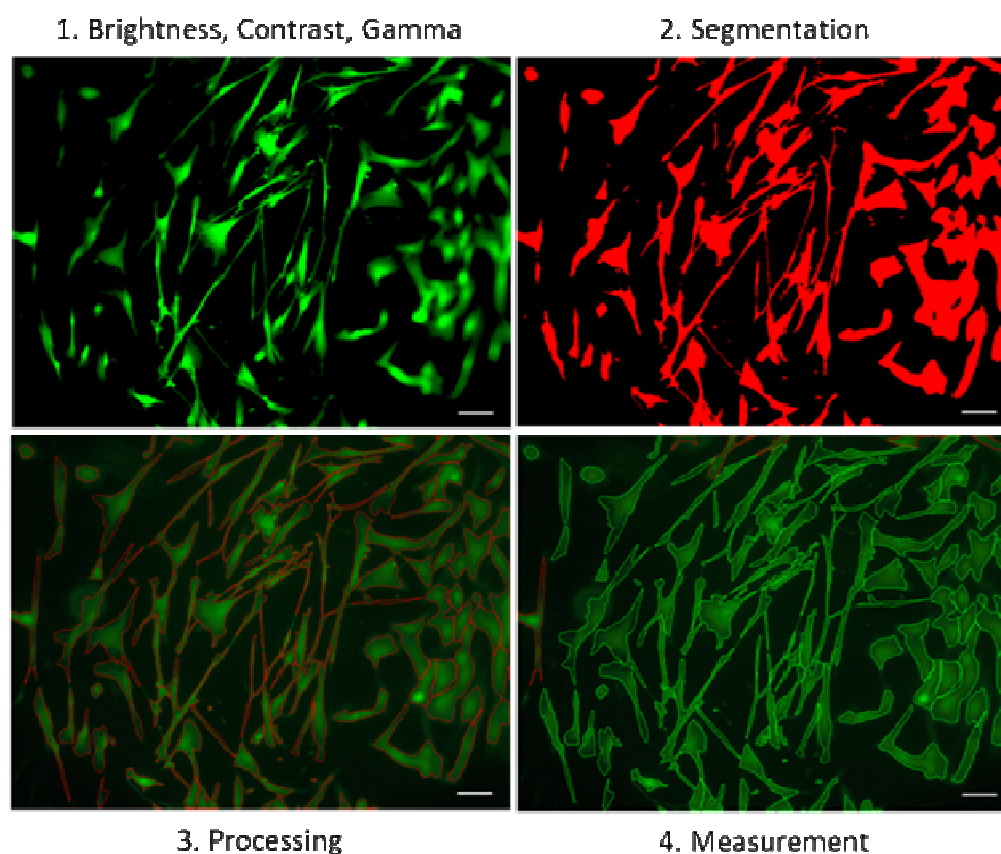
Figure 5.1. Major processing steps used to analyze all cell adhesion images. Using Axiovision software, four major steps were used to analyze images including the adjustment of brightness, contrast, and gamma, segmentation to select cells, processing to separate individual cells, and measurement of cell number and average cell area. Identical parameters were set for all images analyzed. In step 1, parameters are adjusted based on the live-dead images. Here, cells stained green indicate high levels of viability. In step 2, segmented cells appear red, and in step 3 cells outlined in red are initially selected by the program. Finally, cells outlined in green in step 4 represent cells that will be counted. Cells outlined in red in this step will not be counted due to their position along the edge of the image.
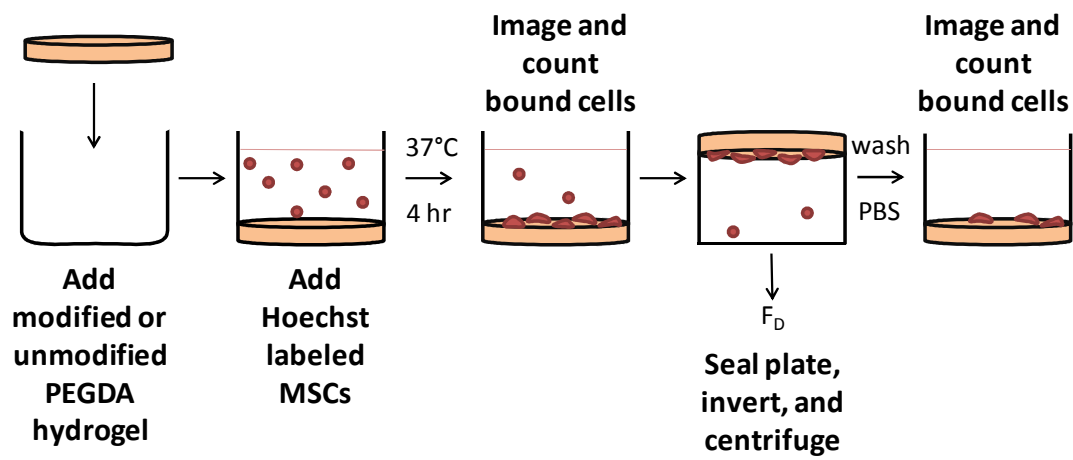
Figure 5.2. Schematic of the modified centrifugation assay. Unmodified, amine modified, and FN modified groups were tested. TCPS served as a control.
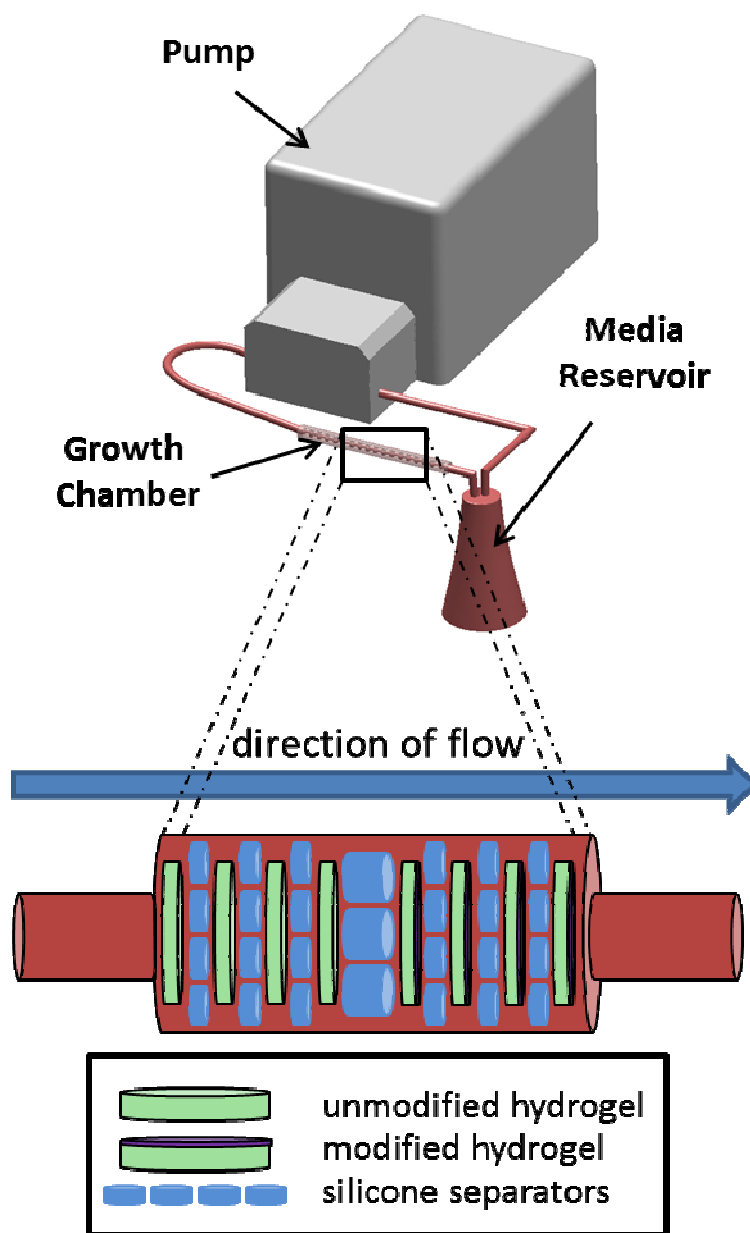
Figure 5.3. Schematic of the overall design of the DSCCP consisting of the TPS bioreactor (top) with detailed depiction of the growth chamber (bottom). Here, it is shown that unmodified (left) and modified (right) hydrogels can be cultured together within the same growth chamber to ensure evaluation under the same dynamic environment. Individual hydrogels as well as hydrogel groups were separated by pieces of autoclaved silicone tubing (blue) to prevent aggregation and maintain separation between experimental groups.
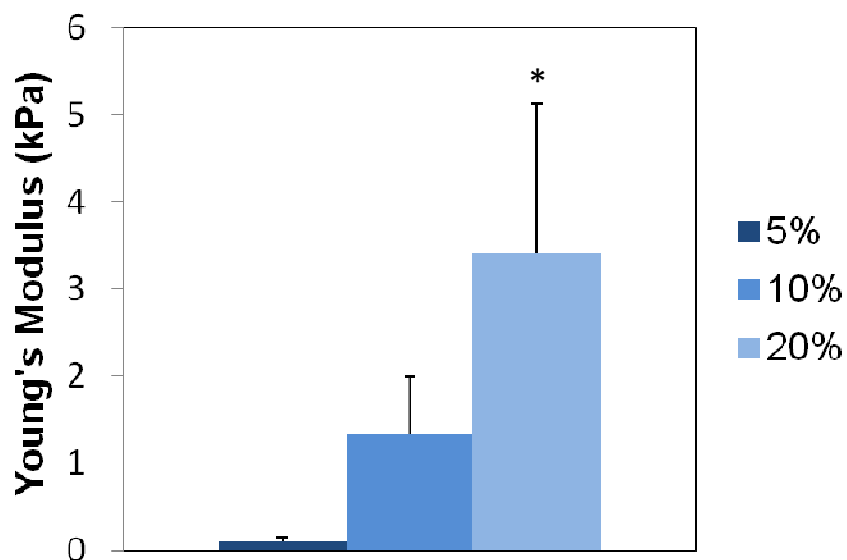
Figure 5.4. The Young's Modulus of PEGDA hydrogels fabricated at 5, 10, and 20% w/v. Six samples at each PEGDA concentration were tested. Results show that hydrogels formulated with 20% w/v PEGDA were found to have a statistically greater Young's Modulus than all other hydrogel formulations ('*', $p<0.01$).
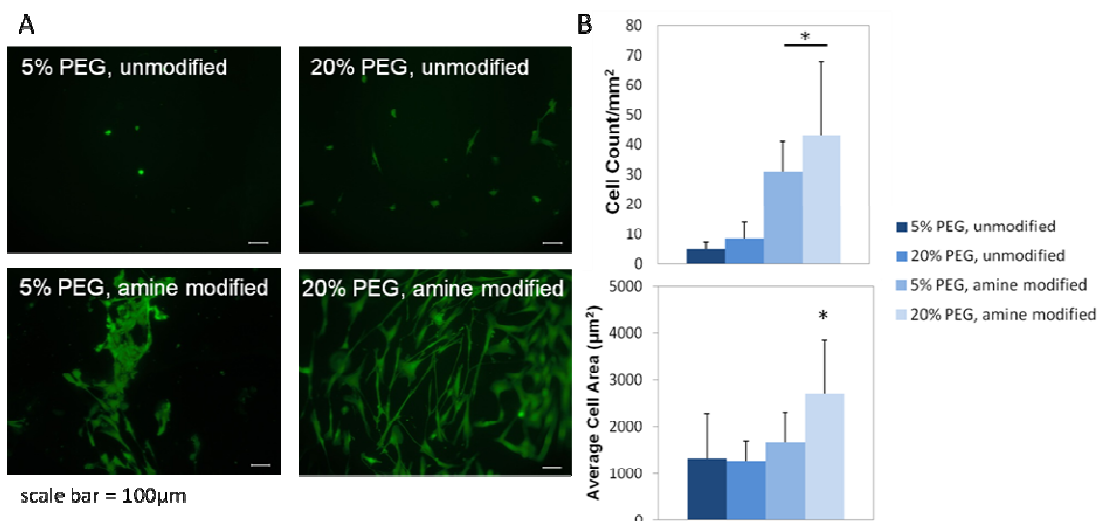
Figure 5.5. Panel A shows representative images (scale bars = 100µm) of each group showing increased adhesion and spreading on modified gels, with the greatest degree of spreading on stiff, modified hydrogels. Panel B shows the results of image analysis of hMSCs seeded onto amine modified and unmodified 5 and 20% w/v PEGDA hydrogels. On both soft and stiff substrates, the cell number (top) was statistically greater on modified gels vs. unmodified gels ('*', p<0.01). The average cell area (bottom) on amine modified 20% w/v hydrogels was statistically greater than all other groups, indicating cell spreading on the surface of the hydrogel ('*', p<0.05).
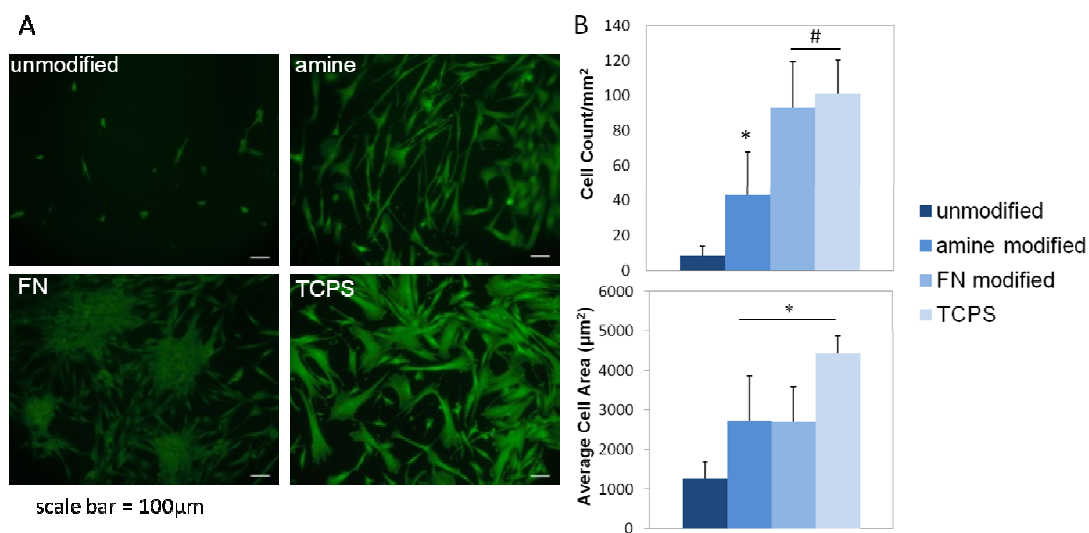
Figure 5.6. Panel A shows representative images (scale bar = 100µm) of each group showing increased adhesion and spreading on modified gels, with similar morphology to TCPS. Panel B shows the results of image analysis of hMSCs seeded onto all groups. The inclusion of amine moieties significantly increased cell number (top) over the unmodified gels ('*', p<0.01). Additionally, FN modified hydrogels and the TCPS control also showed significant increases in cell number, but demonstrated no statistical differences between them ('#', p<0.01). Modified hydrogels showed statistically greater average cell area (bottom) compared to unmodified gels, indicating a higher degree of spreading. Additionally, modified hydrogels demonstrated no statistical differences in average cell area when compared to TCPS ('*', p<0.01).
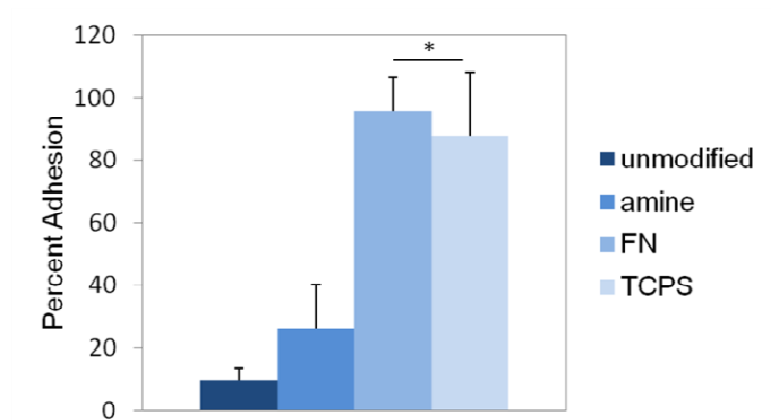
Figure 5.7. Percent adhesion resulting from the centrifugation assay. Results show that FN modified and TCPS groups had statistically greater percent adhesion compared to unmodified or amine modified hydrogels ('*', $p<0.01$). There were no statistical differences in percent adhesion between FN modified and TCPS groups.
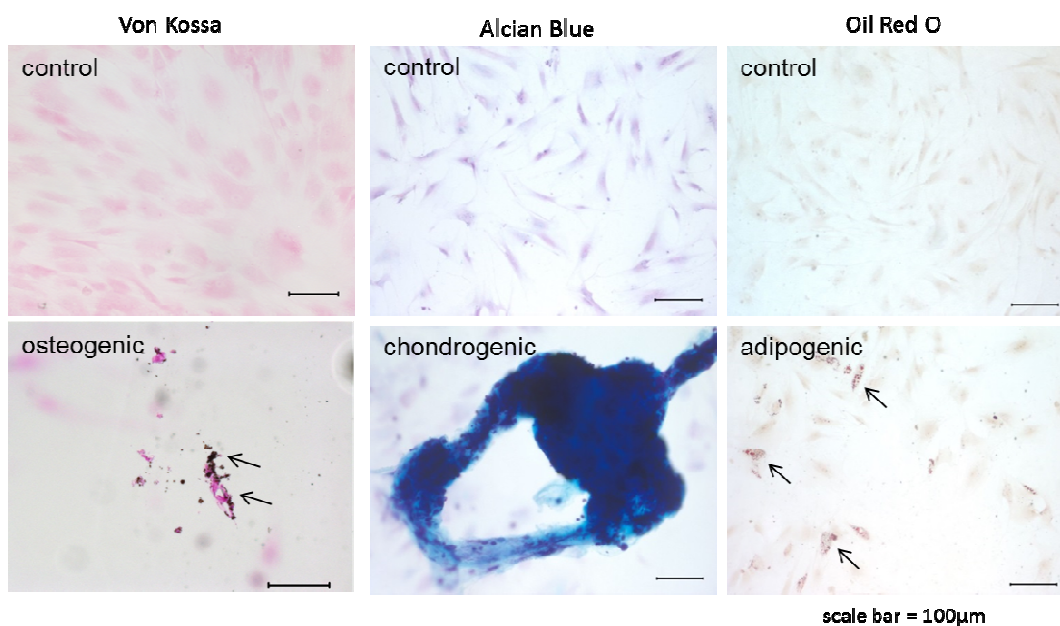
Figure 5.8. Histological images showing the results of differentiation on modified hydrogels. Results show that FN modified gels do not induce differentiation without media induction (top). Images on the bottom panel show the development of calcium deposits which are stained black in color as a result of Von Kossa, the production of a cartilaginous matrix which has stained darkly for the presence of glycosaminoglycans (blue) using Alcian Blue, or the presence of lipid vacuoles which are stained red in color with Oil Red O. All images were taken at 20X and scale bars are equal to 100 μm.
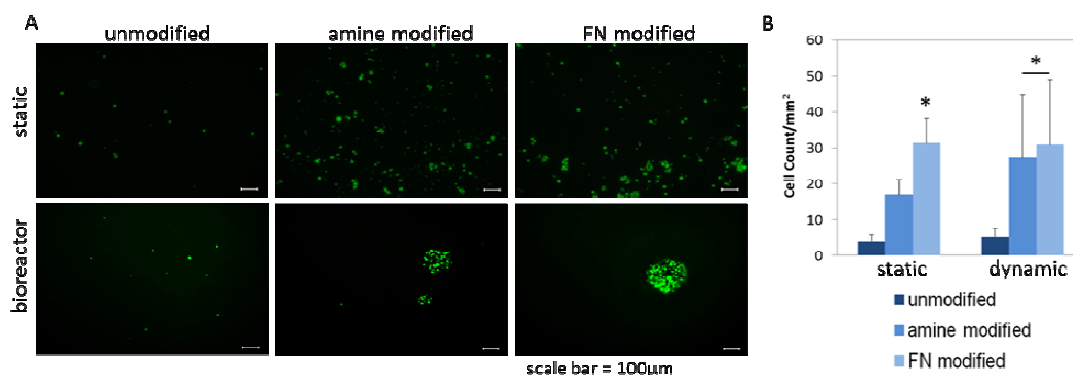
Figure 5.9. Panel A shows representative images from each group. There is distinct clustering of hMSCs on modified hydrogels following bioreactor culture. All images with clustering were analyzed (n=9 for amine and FN modified bioreactor groups). Results of image analysis (panel B) showed that after the initial static culture, FN modified hydrogels exhibited a significantly higher cell number ('*', $p<0.05$), while no differences were detected between unmodified and amine modified groups. After culture within the TPS bioreactor, hMSCs cluster on modified hydrogels and retain a significantly higher cell number ('*', $p<0.05$), with no differences between amine and FN modified groups. These results indicate that surface modified hydrogels can be used in conjunction with shear flow as a dynamic drug evaluation model, but that heterogeneity in surface modification results in cell adhesion and proliferation around points of modification.

5.4 Discussion

The development of the DSCCP which incorporated both cell-ECM interactions through the use of a biomimetic material and mechanical cues provided by the TPS bioreactor, was achieved through the investigation of three objectives. The first two objectives involved the development of a biomimetic material that is suitable to facilitate hMSC adhesion and can be used for subsequent evaluations. We first investigated the role of substrate stiffness on hMSC adhesion and morphology through the attachment of non-specific amine groups on the surface of PEGDA hydrogels of varying stiffness. The stiffness of the surrounding matrix is an important characteristic of disease states, and is still typically the method used to initially identify a potential tumor [93]. Based on the results of DMA analysis, we chose to examine 5% (E = 0.10kPa) and 20% (E=3.40kPa) w/v PEGDA gels to represent soft and stiff substrates respectively. These moduli are also comparable to the mechanical properties of normal mammary tissue (E = 0.17kPa) and the average tumor (E = 4.05kPa) [93]. Amine groups were chosen as the modifier to mimic the charge presented on TCPS, which is commonly used in 2D *in vitro* models for drug evaluation.

The results demonstrate that adhesion increased significantly on modified gels when compared to unmodified gels regardless of stiffness, indicating that cell-substrate interactions are necessary to facilitate cell adhesion. In addition to increased cell number, we also showed that amine modified 20% w/v PEGDA hydrogels exhibited a statistically greater average cell area, demonstrating increased cell spreading on the surface when compared to all other groups in the study. The

presence of amine groups on the material surface allowed us to investigate hMSC adhesion to non-specific adhesive moieties, which is similar to the function of TCPS which facilitates adhesion based on non-specific bioactive groups such as hydroxyl and carboxyl groups [101]. The results here agree with numerous studies showing that the inclusion of functional groups increases cell adhesion, proliferation, and subsequent cell responses [102-104].

Although there was increased adhesion on modified gels over unmodified for both soft and stiff substrates, there were no statistical differences in cell number between modified soft and modified stiff substrates. This indicates that the presence of charge was enough to overcome the limitations of cell binding on soft substrates, or that perhaps a larger difference in stiffness should be investigated in future studies. The Young's Modulus of polystyrene is more than 6-fold higher than the 20% w/v PEGDA gels investigated here [93], and is more in line with trabecular bone which has a modulus of approximately 50-100MPa [19]. As a platform for *in vitro* drug evaluation, the mechanical properties of our material are much more in line with the native properties of tissues at both normal and disease state when compared to TCPS. To further develop our platform, we next investigated the inclusion of a specific ECM protein, and investigated its effects on adhesion, morphology, and differentiation.

Cell-ECM interactions have been shown to effect cell adhesion, proliferation, and function, including the ability to resist some cancer therapies [83]. In order to develop a platform that accurately mimics the *in vivo* environment, we chose to include a protein from the hMSC ECM, fibronectin. Image analysis results indicated that unmodified hydrogels demonstrated the lowest level of cell adhesion, and that the

addition of non-specific and specific adhesion modalities increased cell number when compared to unmodified hydrogels. Cell adhesion experiments also revealed the heterogeneity of the modified surface, which can be confirmed visually by hMSC clustering, which is particularly evident on FN modified surfaces. The inclusion of FN on modified hydrogels exhibited no statistical difference in cell number or average cell area when compared to TCPS.

In order to compare quantitatively the strength of hMSC adhesive interactions with amine groups, FN groups, and TCPS, a centrifugation assay was used to apply a uniform detachment force. Centrifugation assays have been previously investigated for a variety of cell types and substrates, and offer a means to obtain a relative quantification of adhesion strength for a cell population [35, 36, 41, 64]. Results show relatively low levels of adhesion for unmodified and amine modified hydrogels, with percent adhesion at 9 and 26% respectively. FN modified hydrogels along with TCPS demonstrated much higher levels of adhesion, with FN mediated adhesion achieving slightly higher levels of adhesion at 95% compared to 87% on TCPS.

The observed increased adhesion when hMSCs are seeded onto FN substrates may be the result of adhesion strengthening. Strengthening can occur due to increased contact area between the cell surface integrins and the ligand of interest due to cell spreading, clustering of integrins on the cell surface to increase attachment to available binding sites, and the assembly of focal adhesions [105]. The strength of integrin binding to FN has been estimated to be 200nN, as determined through the use of a spinning disk device [105, 106]. The binding of cells to FN was also found to plateau at 4 hour incubation, indicating saturation of all available integrins for FN

binding [105]. In this study, a detachment force of 18pN was applied to all samples following a saturated incubation time of 4 hours. This detachment force is markedly lower than the estimated strength of integrin-FN adhesion, which is confirmed in the result of a 95% attachment rate of hMSCs on FN modified substrates. Non-specific binding on amine groups was still very low (26%), even at such a low detachment forces. Future studies should be completed to investigate how increasing detachment force to levels closer to the estimated integrin binding strength impacts MSC adhesion on FN modified surfaces.

Integrin binding has been found to impact a multitude of cell functions including differentiation and cell survival [1]. Recently, binding has also been shown to increase cell survival despite treatment with paclitaxel [83]. To examine the function of MSCs on our *in vitro* platform, we investigated the differentiation potential of MSCs cultured on our modified 2D surfaces. The maintenance of MSC multipotency is an important factor when considering drug discovery applications, as a multipotent population can be used to test multiple phenotypes resulting from differentiation, as well as the ability to test how a drug impacts a population of cells during differentiation [107]. The EMT has also been implicated as an important driving force for tumor development, invasion, and metastasis [95].

To investigate if the presence of an hMSC-specific protein on the biomaterial surface initiated or inhibited hMSC differentiation, cells were seeded onto modified substrates and induced down osteogenic, chondrogenic, and adipogenic lineages. Results demonstrate that hMSCs exhibit the morphology and ECM production of osteoblasts, chondrocytes, or adipocytes when exposed to proper differentiation

signals, indicating that hMSCs cultured on FN modified surfaces are still capable of undergoing differentiation. Of equal importance, hMSCs exposed to growth media alone maintained the morphology of hMSCs, demonstrating that integrin-FN interactions responsible for cell adhesion to the material surface are not enough to induce undesired differentiation.

After developing a substrate with relevant mechanical properties and modified to include functional groups representative of the native cellular microenvironment, our final objective was to examine how the inclusion of shear force and dynamic nutrient delivery impacts hMSC adhesion and survival. Together with the material properties we have developed, the inclusion of dynamic culture is the last piece in recapitulating the cell microenvironment. After a 48 hour dynamic culture period, results showed that modified hydrogels retained significantly more cells/mm^2 than unmodified gels. Distinct cell clustering was again observed on modified hydrogels, reflecting the heterogeneity of the surface modification. It appears that hMSCs that were weakly bound to the hydrogel surface were removed as a result of the direct application of shear flow, but hMSCs that were firmly adhered at areas of modification, remained and proliferated into a cluster formation. These results indicate that cells seeded onto a modified 2D substrate are able to survive and proliferate in an environment with applied shear force, as a direct result of adhesion at a point of modification.

The DSCCP we have developed here consisting of a biomimetic material cultured within the TPS bioreactor is a fitting model for drug discovery applications. Our platform allows us to evaluate a cell population which is cultured in an

environment that encourages cell-ECM interactions and delivers nutrients, growth factors, and drugs as they are delivered *in vivo*, through the perfusion flow of the bloodstream. Using the DSCCP, the response of a cultured stem cell population to growth factors that induce or inhibit differentiation could be evaluated, as well as how the incorporation of a drug into the perfusion media inhibits or enhances differentiation. The DSCCP allows for real time monitoring of drug distribution throughout the system, and can be used as a way to collect soluble molecules such as growth factors, enzymes, or proteins of interest that have been produced by the cultured cell population. The DSCCP can also be applied to any adherent cell type, ECM protein combination, or flow parameters. This versatility lends itself to several drug discovery applications such as the evaluation of a cancer cell line to treatment with doxorubicin or paclitaxel by injection into the system, while also investigating the impact of integrin binding or substrate stiffness on cell survival.

5.5 Conclusion

The use of a relevant microenvironment for *in vitro* drug discovery investigations is critical to the success of such endeavors as the interaction between cells and the surrounding environment is responsible for a multitude of downstream cell functions. In particular, the use of *in vitro* models that are capable of testing a pluripotent stem cell population is of great importance as pluripotent populations are difficult to test through the use of animal models or cadaveric tissue. Here, we successfully developed an evaluation platform, the DSCCP, consisting of two parts: a

biomimetic material in which mesenchymal stem cell adhesion was controlled by the interaction of integrins on the cell surface with hMSC specific ligands on the material surface, and a dynamic culture environment that mimics the mechanical and transport properties of the bloodstream. The microenvironment fabricated here was capable of supporting hMSC adhesion, spreading, and pluripotency. The combination of native ECM interactions, the mechanical properties achieved through manipulation of substrate stiffness, and the dynamic delivery of nutrients or desired drug treatments creates a successful platform for *in vitro* drug evaluation. The DSCCP developed here could be translated into a simple, highly controlled, and inexpensive model for *in vitro* drug discovery which could be used for numerous cell types, matrix molecules or growth factors, disease models, and drug treatments.

Chapter 6: Development of a Biofunctionalized Material Platform for Mesenchymal Stem Cell Adhesion

6.1 Introduction

Mesenchymal stem cells (MSCs) exist in very low numbers in the highly cellular and heterogeneous bone marrow. MSCs lack unique identifying markers necessary for definitive isolation and are typically isolated and characterized based on a set of established properties. These properties include adherence to tissue culture polystyrene (TCPS), the expression of a panel of positive cell surface markers and the lack of expression for a panel of negative surface markers, and the ability to undergo trilineage differentiation into osteoblasts, adipocytes, and chondrocytes [108]. The standard protocol for MSC isolation begins with extraction of whole bone marrow, followed by density gradient centrifugation, and subsequent expansion of the mononuclear cell fraction on TCPS. Despite the widespread use of this protocol for MSC culture, there is evidence to suggest that this expansion phase causes significant phenotypic changes in MSCs [55, 109]. To this end, we propose the development of a biomaterial-based platform on which bone marrow could be directly cultured and to which MSCs would selectively adhere, eliminating the need for long *in vitro* culture times prior to implantation.

To develop our platform, it is necessary to first provide the desired cell type with material properties that are similar to the native niche. The extracellular matrix (ECM) is a key component of the MSC niche, and it is well recognized that the ECM serves a role not only in cell anchorage, but also in cell function, including the

direction of stem cell fate [110]. Important ECM components can be selectively attached to the biomaterial surface through functionalization techniques. Biomaterial functionalization has been used extensively to fabricate highly controlled material surfaces to provide cells with environmental cues, and control cell-cell and cell-substrate interactions. Through the use of functionalized surfaces, adhesion events can be controlled and optimized to impact downstream signaling reactions and ultimately control cell behavior. Functionalization can also be used to encourage specific adhesive interactions, a function that would be imperative for MSC isolation from the bone marrow. Here, we hypothesize that the inclusion of ECM proteins on the material surface that are key components of both the MSC niche as well as the niche of major mesenchymal tissues such as bone, fat, and cartilage will facilitate MSC adhesion from the heterogeneous population of the bone marrow.

To investigate our hypothesis and develop our material platform, we will study three main objectives. First, we will determine the proteins and concentrations of proteins that result in increased MSC adhesion. Secondly, we will ensure that surface modification does not inhibit MSC differentiation or induce undesired differentiation. Lastly, we will assess the potential of our material platform to firmly attach MSCs when exposed to unprocessed whole bone marrow. For this purpose, we chose the polymer poly (propylene fumarate) or PPF as the base material for our platform because it is a biodegradable, non-cytotoxic material that can be UV crosslinked to form a polymer network [111-113]. PPF can be readily functionalized using chemical surface modification techniques, and the crosslinking properties of the polymer indicate that it can be translated into a 3D culture system for future

97

applications. MSC adhesion both as a single culture as well as a heterogeneous culture will be evaluated to determine the material surface properties that result in an increase of specific MSC adhesion.

6.2 Materials and Methods

6.2.1 Poly (Propylene Fumarate) Synthesis and Thin Film Fabrication

All thin films were fabricated out of a polymer resin consisting primarily of poly (propylene fumarate) or PPF. PPF was synthesized using a previously established protocol [31], and the number average molecular weight (M_n) and polydispersity index (PDI) were determined by gel permeation chromatography. The M_n of PPF used in this study was 1167-1987 Da with a PDI of 1.8-2.1. Thin films were fabricated out of polymer resin that was composed of PPF and its monomer diethyl fumarate (DEF) in a 1:0.8 ratio as well as the photoinitiator bis (2,4,6-trimethylbenzoyl) henylphosphine oxide (BAPO, 1%), and photoinhibiting dyes HMB (1%), and a-tocopherol (0.1%). Polymer resin (120μL) was dispersed evenly between two 2cm x 2cm glass slides and crosslinked under UV light (3.5mW/cm^2) for 120 minutes. After crosslinking, films were cut to the desired size (7mm x 7mm) and rinsed overnight in 70% ethanol to remove any uncrosslinked polymer resin. Films were then washed in PBS to remove any traces of ethanol and sterilized at 121°C for 15 minutes prior to surface modification and cell seeding.

6.2.2 Surface Modification of Polymer Thin Films

The surface of PPF thin films was modified using EDC/NHS chemistry. Briefly, scaffolds were immersed in 50mM MES buffer (pH = 5.5) containing 0.5M N-(3-dimethylaminopropyl)-N′-ethylcarbodiimide hydrochloride (EDC) and 0.5M N-hydrox-ysuccinimide (NHS) for 14 hours at room temperature, followed by a wash in PBS to remove any excess byproducts. For protein modification, thin films were modified with collagen I (rat tail, Corning, Corning, NY), hyaluronic acid (HA, Sigma), or a mixture of collagen I and HA at three concentrations: 0.01, 0.5 or 1mg/mL. For growth factor modification, thin films were modified with a solution of 10µg/mL of TGF-β3 (R&D Systems, Minneapolis, MN). All solutions were made up in PBS and sterile filtered prior to incubation with the EDC/NHS activated films for 1 hour at room temperature. Following modification, films were rinsed 3 times in sterile PBS to remove any unbound protein or growth factor.

6.2.3 Human Mesenchymal Stem Cell Culture and Scaffold Seeding

hMSCs (Lonza, Walkersville, MD) were cultured prior to the study as described in 4.2.1. Cells at passage 5 were used for all experiments. Prior to cell seeding, adherent hMSCs were lifted with trypsin/EDTA (Life Technologies) and counted using trypan blue uptake to determine viability. hMSCs were seeded onto sterilized films in a 48 well plate. Each scaffold was seeded with approximately 10,000 cells (approximately 20,000 cells/cm^2) in a concentrated serum-free solution of 20µL and allowed to adhere for 1 hour at 37°C before additional media was added.

Attachment and centrifugation studies were carried out entirely under serum-free conditions. For all other studies, media supplemented with serum was added after the initial 1 hour attachment period.

6.2.4 Cell Adhesion and Analysis of Cell Viability

After 4 hours of incubation in serum-free conditions, films were soaked in PBS containing 1mM $CaCl_2$ and 0.5mM $MgCl_2$ for 30 min to remove non-adherent cells as well as any remaining medium. To aid in the visualization of cell attachment and spreading, a live-dead assay was performed following standard protocols. Thin films were incubated with 2mM ethidium homodimer and 4mM calcein AM (Life Technologies) for 30min. Images were taken using a fluorescent microscope (Axiovert 40 CFL with filter set 23; Zeiss, Thornwood, NY) equipped with a digital camera (Diagnostic Instruments 11.2 Color Mosaic, Sterling Heights, MI). Images were analyzed using the Zeiss software Axiovision 4.8 to quantify relative cell number on each film. Five images were analyzed for each condition. If individual cells in an aggregate were indiscernible due to overlapping or aggregating, the area was counted as one cell.

6.2.5 Centrifugation Assay

To quantify relative adhesion of hMSCs seeded onto modified and unmodified thin films, a centrifugation cell adhesion assay was performed as described in Section 3.2.3. Thin films were placed into 48 well plates, and approximately 10,000 labeled hMSCs were added to each well, and incubated for 200 minutes at 37°C and 5% CO_2,

prior to centrifugation at 50 or 200xg for 5 minutes. Wells without films served as a

positive control (TCPS). Imaging procedures and the calculation of the percent

adhesion was computed as previously described. The F_D for each speed is reported in

Figure 6.3B.

6.2.6 Induction of hMSC Differentiation

Prior to the start of differentiation, hMSCs were seeded onto the thin films as

described above. Following incubation for 24 hours in growth medium, cells were

cultured for 21 days in osteogenic, chondrogenic, or adipogenic media as described in

Section 4.2.2. hMSCs cultured in growth media served as a control. All media were

changed every 3 days.

6.2.7 Impact of TGF-β3 Modification on Chondrogenesis of hMSCs

To investigate the impact of TGF-β3 modification on the phenotype of

hMSCs during chondrogenesis, cells were seeded onto modified and unmodified

films as described above. Following culture in growth media for 24 hours, cells were

cultured in chondrogenic media with or without exogenous TGF-β3 delivery for 21

days.

6.2.8 Histological Analysis

At days 7, 14, and 21, cells were lifted from the surface of thin films and

reseeded into wells of a 96 well plate for 24 hours. At this time cells were fixed with

10% formalin for 10 minutes, and stored at 4°C in PBS. Histological staining was completed as described in Section 4.2.4.

6.2.9 Unprocessed Human Bone Marrow Culture

To evaluate the performance of modified and unmodified thin films when exposed to a heterogeneous cell population, such as the bone marrow, whole unprocessed human bone marrow (Lonza) was seeded onto the surface of unmodified and collagen I modified (1mg/mL) films. Bone marrow had a nucleated cell density of 23.1 x 10^6cells/mL; 100µL was seeded onto each film. After 1 hour of attachment, additional culture media was added. Media was changed at 4 hours or 24 hours following cell seeding and films were cultured for an additional 7 days with media changes every 3 days. Bone marrow seeded onto TCPS and subjected to the same media changes served as a control.

6.2.10 Flow Cytometry Analysis

To analyze the cells that adhered to the modified and unmodified thin films over 7 days, cells were subjected to flow cytometry analysis using a Human MSC Analysis Kit (BD Stemflow, BD). Cells were lifted from the surface of the films or the TCPS control and resuspended at a concentration of 5 x 10^6 cells/mL. Cells were stained following the manufacturer's protocol. Briefly, 100µL of each cell suspension was mixed with 20µL of the hMSC Positive Cocktail (CD90 FITC, CD105 PerCP-Cy5.5, and CD 73 APC) and 20µL of the hMSC Negative Cocktail (CD34 PE, CD11b PE, CD19 PE, CD45 PE, and HLA-DR PE) and incubated at 4°C in the dark

for 30 minutes. Following incubation, the cell suspensions were washed 2x with 500µL of PBS containing 1% BSA. After washing, cells were resuspended in 500µL of PBS containing 1% BSA and analyzed using a BD FACSCanto II to quantify the amount of each marker present. hMSCs at P5 (Lonza) were used as a control, and to set up an analysis template for all samples.

6.2.11 Statistical Analysis

All data was analyzed using one-way analysis of variance and Tukey's multiple-comparison test to determine statistical differences between hydrogels. A confidence interval of 95% (α=0.05) was used for all analyses, and means and SDs are shown in each figure.

6.3 Results

6.3.1 hMSC Adhesion to Protein Modified PPF Thin Films

Following a 4 hour incubation under serum-free conditions, the cell number on modified and unmodified films was quantified. Three protein conditions at three concentrations were evaluated, and the results are presented as the fold change in cell number normalized to a well plate control (Figure 6.2). HA modified films exhibited some of the lowest values for cell adhesion, and showed no statistical differences between concentrations. For collagen I, there was a significant increase in cell adhesion, with the highest concentration showing a statistically greater level of

adhesion compared to all HA groups. Within the collagen I group, the lowest

concentration (0.01mg/mL) was statistically lower than the highest concentration

(1mg/mL). For the 50:50 protein mixture of collagen I and HA, there were no

statistical differences between concentrations. Overall, the mix showed increased

levels of adhesion, particularly at lower concentrations. For the low and medium mix

concentrations, there were no statistical differences between this and the highest

collagen I concentration. The collagen I group at 0.5 and 1mg/mL and the mix group

at 0.01mg/mL exhibited levels of adhesion that were statistically greater than the

control. Based on these data, we chose to move forward with modifications that

included collagen I and the mixture of collagen I with HA.

To examine the adhesion of hMSCs to thin films quantitatively, a

centrifugation assay was conducted. Cells were incubated for 200 minutes prior to the

application of centrifugation to serve as a detachment force. The detachment forces

corresponding to each centrifugation speed are listed in Figure 6.3B. The results are

shown in Figure 6.3C. There were no statistical differences between groups at either

centrifugation speed, indicating that the modified thin films resulted in cell adhesion

of comparable strength to the gold standard for adhesive cell culture, TCPS.

6.3.2 Differentiation of hMSCs on Modified Thin Films

Differentiation down the three main mesenchymal lineages was induced to

confirm that the presence of protein on the modified films did not inhibit desired

differentiation or induce unwanted differentiation. Through histological staining for

calcified regions (osteogenesis), lipid deposits (adipogenesis) and proteoglycans

104

(chondrogenesis) over 21 days of induction, results showed that hMSCs behaved identically on modified and unmodified films. There were no apparent differences between groups based on the inclusion of protein (Figure 6.4). Differentiation was readily induced for all lineages, with histological images resembling hMSCs differentiated on TCPS. Additionally, the growth condition for all groups remained undifferentiated over the 21 day period.

To investigate if the inclusion of growth factors on the scaffold surface could be used as a means to induce differentiation, hMSCs were cultured on thin films modified with TGF-β3. hMSCs on modified scaffolds were cultured in chondrogenic media without soluble TGF-β3 delivery and compared to hMSCs cultured on TCPS and unmodified films with and without TGF-β3 delivery. Results show that as early as 24 hours after seeding, hMSCs cultured on TGF-β3 modified films condense and form a cell aggregate on the surface of the thin film. This is a key characteristic of chondrogenic differentiation and is not observed on the controls with soluble TGF-β3 delivery until day 7, and is never observed on controls cultured without soluble TGF-β3 delivery over the 21 day period. Figure 6.5 shows histological images stained for the presence of proteoglycans of hMSCs on TCPS, unmodified films and films modified with TGF-β3 over 7 days. All groups were cultured with identical media formulations (chondrogenic media without TGF-β3 supplementation).

6.3.3 Bone Marrow Culture on Modified Thin Films

Cells that adhered to the modified and unmodified films over a period of 7 days were analyzed using flow cytometry for the panel of accepted markers based on

the phenotypic signature described by The Mesenchymal and Tissue Stem Cell Committee of the International Society for Cellular Therapy (ISCT) [114]. Results show (Figures 6.6, 6.7, and 6.8) that after 7 days of culture all films exhibit high percentages of positive markers, with markers for CD90 and CD105 above 75% for films with media changes at 4 hours and above 50% for films with media changes at 24 hours. These rates are comparable to bone marrow controls that were seeded onto TCPS, as well as hMSC controls. For all groups, including TCPS controls, the presence of CD73 is much lower than the other markers in the positive cocktail (less than 5%). This result was mimicked in the hMSC control group, with CD73 resulting in only 24.8% compared to 81.7% for CD90 and 70.6% for CD105. For the negative cocktail (all markers tied to PE), results show low levels around (<10%) for all groups, including the control. Thin film groups that had media changed at 4 hours appear to have slightly higher results for CD90 and CD105 than their 24 hour counterparts but this trend is not observed in the TCPS control. For CD73, the levels are increased for the 24 hour thin film groups, yet again this trend is not observed in the TCPS control. For the control there are little to no difference between groups (less than 5%).
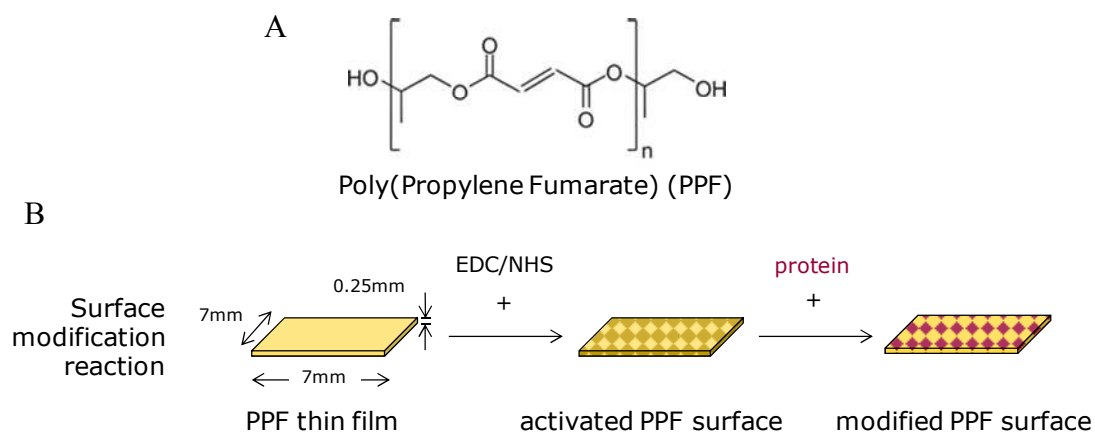
Figure 6.1. (A) Schematic of poly(propylene fumarate) or PPF. PPF contains a repeating unit of two ester groups flanking a carbon-carbon double bond. (B) Schematic of surface modification using EDC/MHS crosslinking. PPF thin films were modified through a two-step process. First, the films were immersed in a solution of EDC and NHS for 14 hours, followed by reaction in a solution of the desired protein or growth factor.
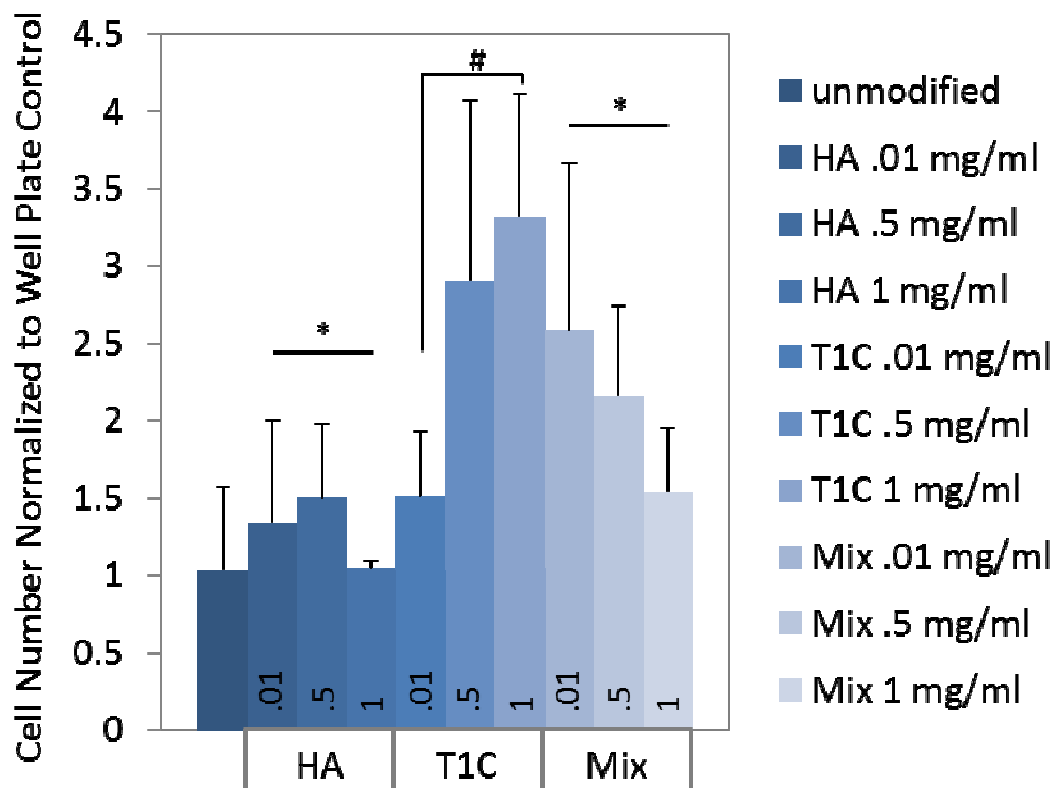
Figure 6.2. Cell adhesion to modified and unmodified PPF thin films. Films were modified with three concentrations of hyaluronic acid (HA), collagen I (T1C), and a 1:1 mixture of the two proteins (Mix). Cells were incubated in serum free conditions for 4 hours followed by washing in PBS supplemented with Ca^{2+} and Mg^{2+} and imaging using a live-dead viability assay as outlined in 6.2.4. Cell number was calculated based on analysis of live-dead images using a counting routine developed using Axiovision software.Cell number is represented here as a fold change compared to a positive control (cells of identical density seeded onto a well plate). Collagen I groups exhibited the highest levels of cell adhesion compared to all other groups. '*' indicates that there are no statistical differences between the three concentrations for the HA and Mix groups. '#' indicates that for the collagen I group, the high concentration film showed significantly increased adhesion compared to the low concentration film ($p<0.05$).

A

B

Centrifugation Speed (RCF)	Detachment Force (pN)
50	175
200	700

C
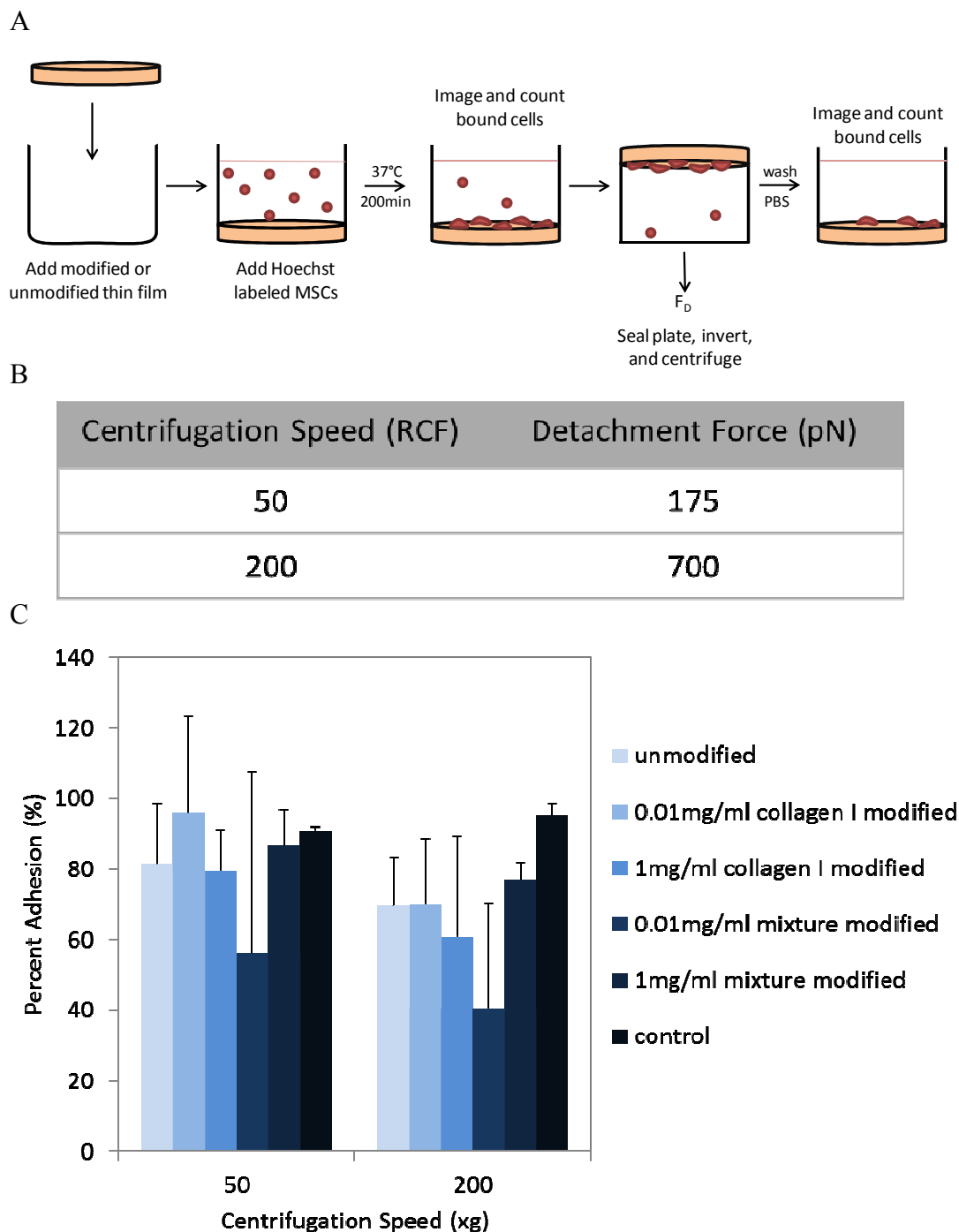
Figure 6.3. (A) Schematic of the centrifugation assay used to evaluate the adhesion of modified and unmodified films. (B) Centrifugation speeds and the associated detachment forces for the two conditions tested here. Speeds were calculated based off of the equation outlined in 4.2.3. (C) Results of the centrifugation assay. There were no statistical differences between groups at either centrifugation speed (p = 0.90). This indicates that hMSCs adhered to thin films with adhesion strength that was not significantly different from the control (TCPS).

Day 7 Growth   **Day 7 Adipogenic**
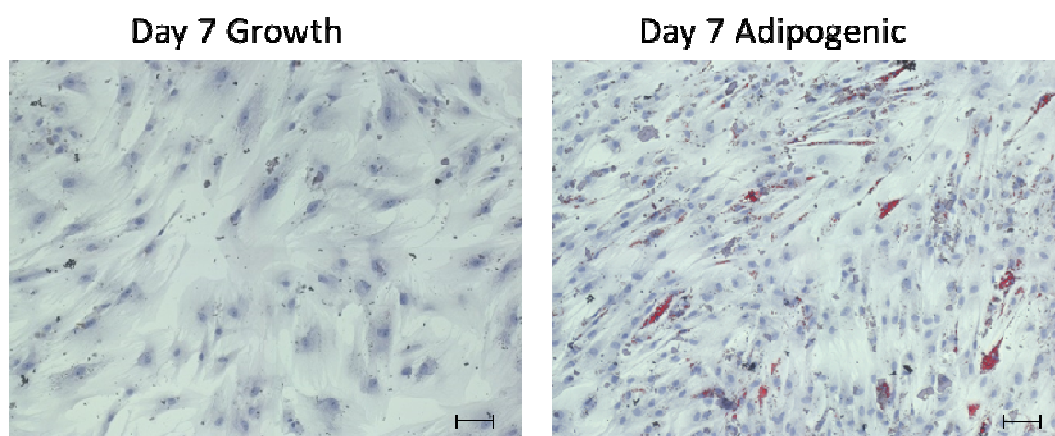
Figure 6.4. Histological staining of hMSCs on PPF thin films during differentiation. Here, oil red o staining is used to identify lipid deposits, an indication of adipogenesis. The films shown here have been modified with 1mg/mL collagen I. On day 7, cells in the control (growth) group exhibit typical hMSC morphology and do not stain positively for oil red o. Cells cultured in adipogenic media (right) stain positively for lipid deposits which are visualized as red, indicating that the inclusion of collagen I does not inhibit differentiation. Scale bar = 100 µm.
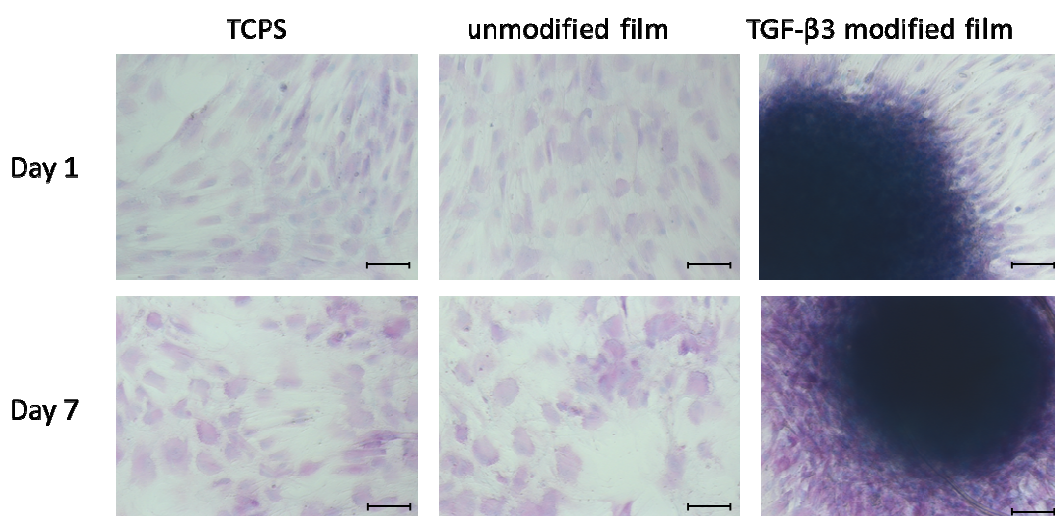
Figure 6.5. Alcian blue staining of hMSCs on undergoing chondrogenic differentiation. All groups were cultured in chondrogenic media without soluble TGF-β3 delivery. The inclusion of TGF-β3 on the material surface results in rapid condensation of cells seeded onto modified films. As early as day 1, cells are condensed and show high levels of positive staining for proteoglycans. Alcian blue stains proteoglycan rich regions blue and the nuclei of the cells appear pink. This was observed throughout the 21 day study. For cells cultured in identical media but either on TCPS or unmodified PPF films, cells did not form condensed pellets at any point during the differentiation. Scale bar = 100μm.

Cell Surface Markers
CD90 FITC (positive)
CD105 PerCP-Cy5.5 (positive)
CD73 APC (positive)
Negative Cocktail (CD34, CD11b, CD19, CD45, HLA-DR); all PE

Table 6.1. Cell surface markers used to characterize the phenotypic signature of cells recovered on PPF thin films and controls using flow cytometry to quantify the population. Samples were seeded with unprocessed bone marrow and media was changed after 4 or 24 hours in culture. Culture was maintained until day 7 and the cell population was characterized using a BD Stemflow hMSC Analysis Kit.

unmodified PPF thin film with media changed at 4 hours

unmodified PPF thin film with media changed at 24 hours
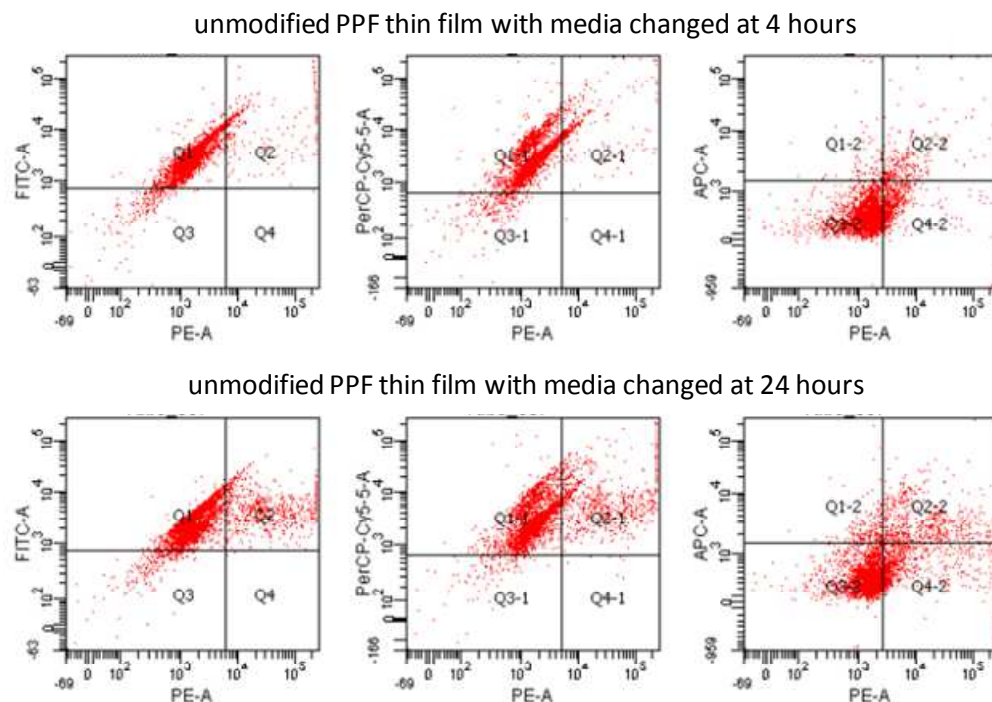
sample	FITC +	PerCP +	APC +	PE +
unmodified PPF; 4hr	87.5	84.3	1.5	6.33
unmodified PPF; 24hr	75.4	75.5	4	7.87

Figure 6.6. Flow cytometry results for cells recovered from unmodified PPF films following 7 days in culture. Media was changed after 4 hours or 24 hours and cultures were continued for 7 days. At this time, cells were lifted from the material surface, stained with a positive and negative cocktail of surface markers and analyzed using flow cytometry. Results on unmodified PPF show that the 4 hour group has increased levels of the positive markers for CD90 (FITC) and CD105 (PerCP-Cy5.5), but that both groups show low expression for CD73 (APC). Both media changes resulted in relatively low PE+ results, which suggest that the media changes sufficiently cleared away negative cells.

collagen I modified PPF thin film with media changed at 4 hours
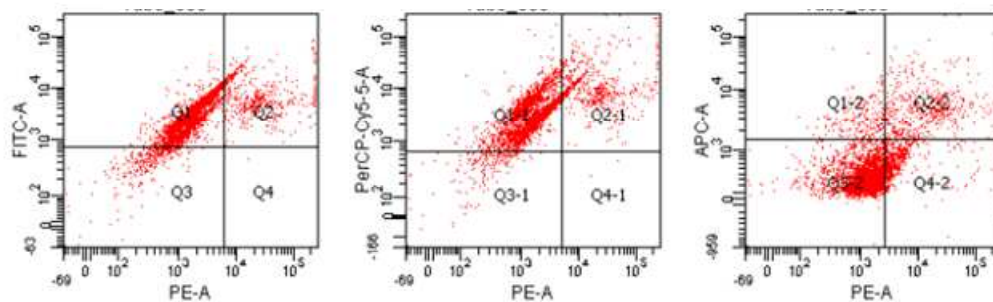
collagen I modified PPF thin film with media changed at 24 hours
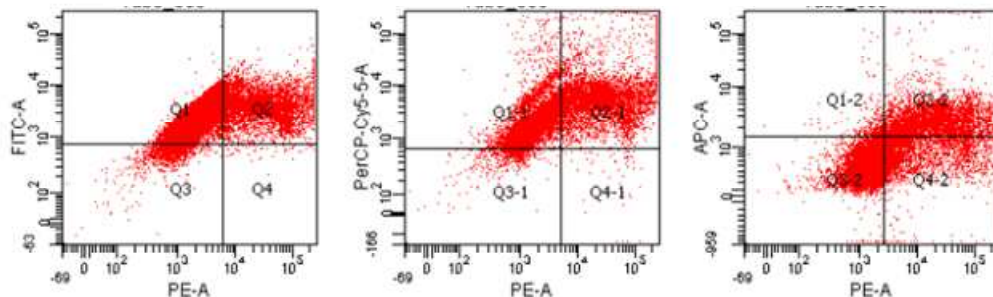
sample	FITC +	PerCP +	APC +	PE +
collagen I modified PPF; 4hr	78.1	79	4.6	5.63
collagen I modified PPF; 24hr	53.8	55.7	1.5	9

Figure 6.7. Flow cytometry results for cells recovered from collagen I modified PPF films following 7 days in culture. Results on collagen I modified PPF show that the 4 hour group exhibits high levels of the positive markers for CD90 (FITC) and CD105 (PerCP-Cy5.5) with values around 20% higher than the 24 hour group. Both groups show low expression for CD73 (APC), with the 4 hour group expressing a value around 3% higher. Both media changes resulted in low PE+ results, with the 4 hour group showing the lowest PE+ expression.

114
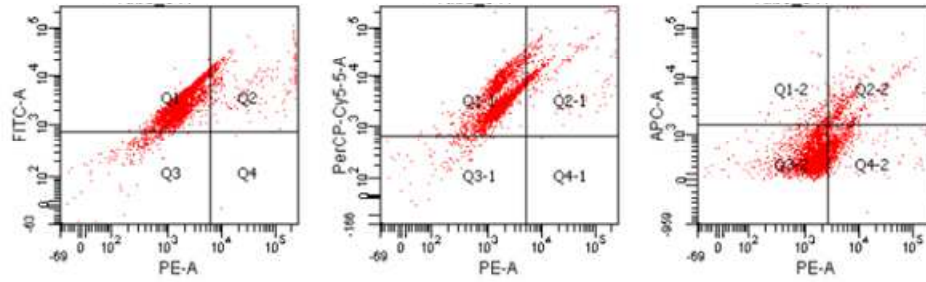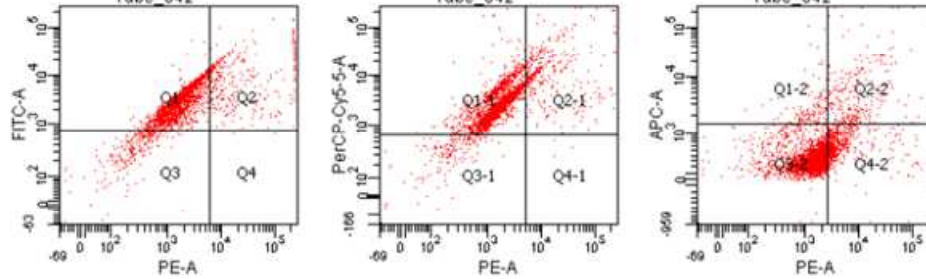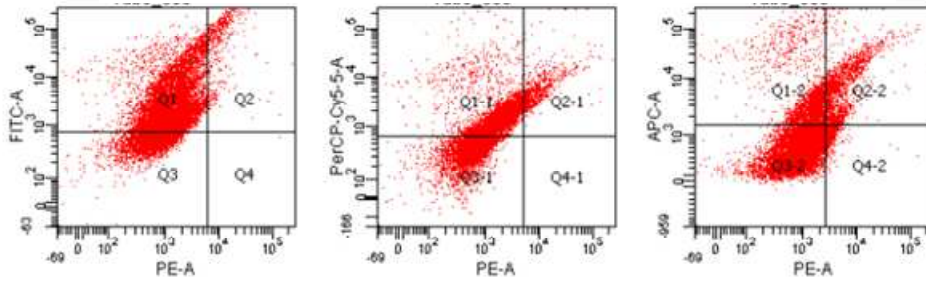
sample	FITC +	PerCP +	APC +	PE +
TCPS; 4hr	78.1	79	4.6	5.63
TCPS; 24hr	53.8	55.7	1.5	9
hMSC control	81.7	70.6	24.8	1.77

Figure 6.8. Flow cytometry results for cells recovered from the controls. TCPS seeded with bone marrow and subjected to media changes at 4 hours and 24 hours served as a control. In addition, hMSCs (Lonza) at P5 were used as a positive control for the population of interest, and to set up the flow cytometry analysis template. As with modified PPF films, bone marrow cultured on TCPS shows increased expression of positive markers for the 4 hour group when compared to the 24 hour group. Both TCPS controls show markedly lower percentages of CD73 (APC) positive staining when compared to the hMSC control. Similarly the hMSC control showed the lowest level of PE+ staining.

6.4 Discussion

The creation of a biomaterial platform capable of isolating MSCs from the heterogeneous population of the bone marrow would greatly simplify the current methods that use MSCs for cell therapy applications. The development of such a device would enable one-step isolation, which could be followed by immediate implantation or *in vitro* culture and differentiation. In the work presented here, we were able to show the ability of PPF, a biodegradable and non-cytotoxic polymer, to serve as a platform to encourage MSC adhesion *in vitro.* PPF has been used extensively for tissue engineering applications, particularly for the regeneration of bone due to its mechanical properties. PPF degrades slowly and maintains its mechanical properties throughout the initial phases of degradation [115], and could be used as a platform to deliver MSCs to the injury site. Previous studies have shown that stem cell and progenitor cell populations can be seeded directly onto the polymer surface and cultured for at least 8 days [20, 116], with results showing cell attachment, proliferation, and differentiation during this period. However, due to the hydrophobic nature of the polymer surface, it is often pre-wetted in cell culture media containing serum to increase cell attachment rates, or is formed into a composite material to improve surface hydrophilicity and protein absorption [116].

To encourage specific cell-substrate interactions, we have used surface modification techniques to achieve specific protein or growth factor attachment on the PPF surface. We wanted to investigate the impact of single proteins and combinations of proteins that are common both in the MSC niche as well as the ECM of mesenchymal tissues. Collagen I and hyaluronic acid were evaluated alone and as a

mixture at several concentrations to find the ideal protein density to encourage hMSC attachment. Overall, as shown in Figure 6.2, we observed that collagen I resulted in high levels of adhesion at all concentrations, while HA alone was not sufficient at producing adhesion levels much higher than unmodified polymer thin films. The mixture of the two proteins had increased levels of adhesion compared to HA alone, but still underperformed when compared to collagen I alone. This result could suggest that the specific binding mechanisms to these two ECM proteins occur at different rates, or that the number of receptor ligand pairs is greater for collagen I. Binding to HA is facilitated through the integrin CD44, while collagen I has been shown to interact with two integrins (α1β1 and α2β1) through the GFOGER peptide sequence [117]. This could suggest in general that the cells are interacting with the collagen I binding sequences at a much higher rate than on HA, which helps to explain the mix group results. Though it may not contribute to increase immediate cell adhesion, HA is still a major component of the MSC niche and has a vital role as a key component of the cartilage ECM. For these reasons, it is important to continue exploring the use of HA in a system that has a goal of simulating the MSC niche *in vitro*.

The quantification of cell adhesion to modified and unmodified films through the use of a centrifugation cell adhesion assay yielded no statistical differences between groups (see Figure 6.3C). This result indicates that the films are performing at a level comparable to the standard for adhesive cell culture, TCPS. Additional studies should be conducted into the parameters of the adhesion assay, as only one incubation period (200min) and two centrifugation speeds (50 and 200xg) have been evaluated here. Under these conditions, a percent adhesion between 60 and 80% is

observed for most groups. Previous studies have suggested that in order to gain a full understanding of the adhesion between a cell and its substrate, the incubation time and centrifugation speed that results in approximately 50% adhesion, or the mean adhesive strength value must be determined [41]. In the study presented here, an incubation period of 200 minutes is used, which may have resulted in saturated levels of cell adhesion and therefore higher percent adhesion values for all groups.

A key requirement for the development of a platform for MSC adhesion is that the modification techniques used to increase initial cell attachment do not negatively impact the long term culture and subsequent implantation of the device. Here, we demonstrated that the incorporation of protein on the material surface had no impact on the differentiation potential of hMSCs cultured on the surface of thin films. The results also confirmed that PPF scaffolds with or without modification are capable of supporting long-term *in vitro* culture. To create a one-step system for MSC isolation and differentiation, it is necessary to be able to use the material surface properties to drive the attached cells towards a specific lineage. Here, we showed that the incorporation of TGF-β3 onto the surface of our material platform results in cell condensation and an early onset of chondrogenic differentiation, with evidence of proteoglycan staining as early as day 1 of culture (see Figure 6.5). hMSCs that were cultured under identical media formulations on either unmodified PPF thin films or TCPS did not result in cell condensation equivalent to cells cultured either with soluble TGF-β3 delivery or on TGF-β3 modified films. By day 21, there was an observed plateau of chondrogenesis for hMSCs cultured on TGF-β3 modified films compared to groups cultured with TGF-β3 soluble delivery. This is most likely due to

the gradual degradation of TGF-β3 from the films, which was not replenished throughout the culture period. Additional studies should be completed to confirm that the initial rapid differentiation produces similar gene and protein expression as typical protocols for chondrogenesis. Supplementation with soluble TGF-β3 may be necessary at later timepoints to maintain high levels of chondrogenic tissue formation. As an initial result, it is apparent that TGF-β3 is successfully attached to the PPF surface and remains an active and potent initiator of chondrogenesis at early timepoints.

MSCs primarily reside in the bone marrow, which is a highly cellular and heterogeneous tissue composed of endothelial cells, adipocytes, macrophages, reticular cells, fibroblasts, osteoprogenitors, hematopoietic stem cells, and number progenitor cell populations [55]. The lack of a single unique identifying marker makes the definitive isolation of MSCs from this heterogeneous mixture difficult, and extensive *in vitro* expansion is necessary. However, it remains unclear if the MSCs that are cultured in these 2D *in vitro* environments are representative of the actual progenitor cells that exist *in vivo* [55]. By culturing unprocessed human bone marrow on unmodified and modified thin films, we were able to recapitulate the potential clinical applications of our biomaterial platform. Results showed that direct seeding of whole bone marrow onto the material surface produced a cell population with a phenotypic profile similar to hMSC controls based on the panel of positive and negative markers set forth by ISCT. Moreover, it appears that a media change earlier than is typically applied (4 hours versus of 24 hours) resulted in equivalent populations, with some markers increased at the 4 hour timepoint. Based on these

observations, PPF unmodified or modified at the surface to contain ECM proteins appears to result in efficient MSC isolation from the bone marrow, compared to TCPS, the current gold standard.

The work presented here is a key first step to the development of a material platform to simplify the use of MSCs for cell therapy. However, the 2D nature of the polymer thin films does not provide an environment that recapitulates the MSC niche. Additionally, implantation of the thin polymer membrane would not provide the structural and mechanical support necessary for defects of the mesenchymal lineage, such as bone or cartilage. The properties of PPF make it an ideal candidate for the translation of the technology developed here into a 3D scaffold. PPF is readily and controllably crosslinked in the presence of UV light and has recently been used in 3D printing applications to produce scaffolds with highly controlled architectures [115, 118, 119]. The combination of 3D printing technology and the surface modification methods presented here could result in the development of a 3D platform that encourages MSC adhesion, while providing an environment that is supportive of long-term culture, differentiation, and implantation.

6.5 Conclusion

In the work presented here, we were able to show that the biodegradable, non-cytotoxic polymer, PPF is a suitable material for a biomaterial platform that encourages MSC attachment and differentiation. Additionally, we were able to show in a pilot study, the feasibility of PPF as a means to isolate MSCs from the bone

marrow based on their adhesive properties. Through tethering proteins found in the MSC ECM onto the PPF surface, we were able to increase the specific adhesion of MSCs when compared to unmodified scaffolds and a positive control (TCPS). The modification techniques described here did not negatively impact cell function, and could actually be used to drive differentiation. By tethering the growth factor TGF-β3 onto the material surface, we observed rapid cell condensation and proteoglycan deposition. These results were not observed on control substrates with identical media conditions. When our biomaterial platform was cultured in the presence of unprocessed bone marrow, the resulting cell populations were phenotypically similar to TCPS and hMSC controls after 7 days of culture. Taken together, these results demonstrate the potential of modified PPF surface as an alternative to TCPS for the capture and culture of MSCs from the bone marrow. The crosslinking abilities of PPF make it a great candidate for translation of these technologies into a physiologically relevant 3D culture system for one-step MSC isolation.

Chapter 7: Influence of 3D Printed Porous Architecture on Mesenchymal Stem Cell Differentiation

7.1 Introduction

Mesenchymal stem cells (MSCs) are an adult stem cell population found in multiple tissues throughout the body including bone marrow, adipose tissue, the synovial membrane, and trabecular bone. They are of particular interest for therapeutic applications because MSCs can be differentiated into a number of lineages including chondrocytes, adipocytes, and osteoblasts [94]. Although the use of MSCs as a therapeutic agent is promising, there is still much to learn about the native MSC niche and how these properties can be exploited for regenerative medicine applications. The MSC niche is a complex and dynamic structure consisting of cellular components, secreted factors, extracellular matrix, and physical factors among others [110].

The influence of physical parameters such as substrate elasticity and geometry on MSCs is of rising interest in the field of tissue engineering, especially with the development of novel micropatterning techniques [74]. With the rise of new technologies, substrates can be controlled such that studies can be completed on the single cell level. Substrate stiffness has been shown to play a large role in stem cell differentiation, with softer substrates resulting in neurogenic or adipogenic differentiation while more rigid substrates are favorable for osteogenic differentiation [90]. The investigation of substrate shape and its relationship to cell contraction and differentiation has been well characterized [74, 75, 120] using micropatterning

techniques. These studies have shown that culturing cells in geometries that permit cell spreading and therefore higher levels of contractility promote osteogenic phenotypes, even when cells are exposed to a mixture of chemical cues. Likewise, under an identical chemical environment, rounded geometries encourage low cell tension and adipogenic phenotypes [74].

The discovery of the link between cell shape and differentiation has been critical in the design of biomaterials that can be used for cell therapy applications. However, many of these fundamental studies have been conducted in 2D or "pseudo-3D" [120] substrates, which is dissimilar to the native environment where cells may be implanted for regenerative therapy. Here, we aim to elucidate the relationship between 3D geometry and MSC differentiation through the use of 3D printed biodegradable scaffolds. 3D printing technology provides a means to fabricate highly ordered and complex scaffold structures with great reproducibility. The design criteria for scaffolds capable of supporting MSC proliferation and differentiation includes a structure that consists of an interconnected porous network with pore sizes on the range of hundreds of microns [121-123], mechanical properties in the range of mesenchymal tissues, and mechanical stability during *in vivo* degradation [115].

Here, we studied the impact of 3D pore structure using two pore architectures printed out of poly (propylene fumarate) or PPF. PPF is a biodegradable polymer that can form UV cross-linked networks and has been used extensively in tissue engineering applications [111-113, 124]. Scaffolds were designed to have an interconnected porous network with pores that exhibited cubic or cylindrical geometry. We hypothesize that the response of MSCs to chemical cues known to

induce differentiation will be influenced by the pore architecture of the 3D printed scaffold. Scaffolds with cubic or cylindrical pores were seeded with MSCs and underwent differentiation down the three main mesenchymal lineages. Gene expression and histological analysis were used to assess differences in differentiation based on scaffold geometry.

7.2 Materials and Methods

7.2.1 Scaffold Design

Three-dimensional scaffolds composed of cubic or cylindrical pore geometries were designed using SolidWorks® (Waltham, MA). All scaffolds were designed to have an ordered pattern of continuous pores, resulting in an interconnected porous network. Scaffolds were constructed to have a theoretical porosity of 80% and a pore volume of 1mm^3. Several iterations of the each design were tested until an interconnected porous network and high reproducibility were achieved, as outlined in Figure 7.1.

7.2.2 Poly (Propylene Fumarate) Synthesis and 3D Printing

All scaffolds were fabricated out of a polymer resin consisting primarily of poly (propylene fumarate) or PPF. PPF was synthesized using a previously established protocol [31], and the number average molecular weight (M_n) and polydispersity index (PDI) were determined by gel permeation chromatography. The

M_n of PPF used to synthesize all scaffolds in this study was 1167-1987 Da with a PDI of 1.8-2.1. Scaffolds were fabricated using an EnvisionTEC Perfactory® P4 with an exposure to UV light of 350mW/dm^2 for 100s per layer. Scaffolds were printed out of polymer resin that was composed of PPF and its monomer diethyl fumarate (DEF) in a 1:0.8 ratio as well as the photoinitiator bis(2,4,6-trimethylbenzoyl) henylphosphine ox-ide (BAPO, 1%), and photoinhibiting dyes HMB(1%), and a-tocopherol (0.1%). Following printing, several post-processing methods were investigated to achieve the desired scaffold properties, as outlined in Figures 7.3 and 7.4. Following optimization, it was determined that the most effective post-processing method was for scaffolds to be immediately placed in a 30min wash of isopropyl alcohol, followed by a 30min wash of acetone to remove any uncured resin from within the porous network. After these washes, scaffolds were post-cured in a 3D systems UV box for 100 flashes. Following post-curing, scaffolds were rinsed overnight in a solution of 70% ethanol to remove any remaining unreacted resin or debris. For characterization studies, scaffolds were vacuum dried overnight prior to testing. For cellular studies, scaffolds were sterilized in 70% ethanol for 4 hours followed by 4, 30min washes in sterile phosphate-buffered saline (PBS) to remove any traces of ethanol.

7.2.3 Sol Fraction Determination

To evaluate PPF crosslinking and the effectiveness of processing post-printing, the cured network sol fraction was determined using previously established methods [112]. The sol fraction is the percent of soluble polymer remaining after

post-processing. Scaffolds were weighed (W_i) prior to immersion in acetone, which served as the extraction solvent. The samples were incubated in acetone for 24 hours. Following incubation, samples were completely dried and weighed again (W_d) (n = 5). The sol fraction was calculated using the equation:

$$sol\ fraction = \frac{W_i - W_d}{W_i} \times 100\%$$

7.2.4 Compressive Mechanical Testing

Compressive mechanical testing of scaffolds was conducted using an Instron mechanical testing system (Model 858, MTS System Corporation, Eden Prairie, MN). Force and displacement were zeroed prior to compression, with the top plate slightly above the surface of the sample. Samples (n = 5) were compressed at a crosshead speed of 2 mm/min while stress and strain were monitored throughout the experiment. The experiment was halted after sample fracture. The elastic modulus for each sample was calculated using MATLAB to determine the slope of the linear region of the stress-strain curve. The linear region was calculated by using the linear fit command starting with the first 10 data points, considering a preload of 1N. The program continued to systematically add points in steps of 8 until the R^2 value dropped below 0.95. The slope of this region is representative of the modulus of the sample.

7.2.5 Micro-computed Tomography

Micro-computed tomography (µCT) was used as a means to noninvasively image and characterize actual scaffold parameters. Scanning was performed using a µCT 100 (SCANCO Medical, Brüttisellen, Switzerland) operated at 70kVp, 9mm voxels, and 200mA. The 3D datasets that resulted from each scan were segmented using predetermined thresholds (lower: 35, upper: 188, maximum: 1000), with gauss sigma (0.8) and support (1) values to distinguish pores from polymer [119]. All resulting 3D images were evaluated using the Image Processing Language (IPL) for Scanco to determine pore size and porosity. Three samples of each scaffold type were scanned.

7.2.6 Human Mesenchymal Stem Cell Culture and Scaffold Seeding

hMSCs (Lonza, Walkersville, MD) were expanded prior to the study as described in Section 4.2.1. Prior to cell seeding, adherent hMSCs were lifted with trypsin/EDTA (Life Technologies) and counted using trypan blue uptake to determine viability. hMSCs were seeded onto sterilized scaffolds in a 48 well plate. Each scaffold was seeded with approximately 42,000 cells (11,000 cells/cm^2) in a concentrated solution of 20µL and allowed to adhere for 1 hour at 37°C before additional media was added.

7.2.7 XTT Assay

To quantitatively evaluate cell metabolic activity on the scaffolds surface, a Cell Proliferation Kit II (XTT) (Roche, Mainheim, Germany) was used. XTT [2,3-bis-(2- methoxy-4-nitro-5-sulfophenyl)-2H-tetrazolium-5-carboxanilide] was used following the manufacturer's protocols. The electron coupling and XTT labeling reagents were thawed and immediately combined in a 1:50 ratio. Scaffolds were moved into new cell culture wells to avoid evaluating cells that did not attach to the scaffold surface. The XTT solution was added to cell culture wells and incubated at 37°C for 4 hours. Following incubation, absorbance was measured with a M5 SpectraMax plate reader (Molecular Devices, Sunnyvale, CA). Net absorbance was calculated (A450-A650) for each sample and reported. Cells grown on tissue culture polystyrene at the same density were used as a control. Samples were evaluated at day 1, 4, and 7.

7.2.8 Fluorescence Imaging

The viability of cells seeded onto scaffolds was qualitatively evaluated using live/dead fluorescent staining. At days 1, 4, and 7, scaffolds were soaked in PBS containing 1mM $CaCl_2$ and 0.5mM $MgCl_2$ for 30 min to remove non-adherent cells as well as any remaining medium. Following standard protocols, scaffolds were incubated with 2mM ethidium homodimer and 4mM calcein AM (Life Technologies) for 30min. Images were taken using a fluorescent microscope (Axiovert 40 CFL with filter set 23; Zeiss, Thornwood, NY) equipped with a digital camera (Diagnostic Instruments 11.2 Color Mosaic, Sterling Heights, MI).

7.2.9 Induction of hMSC Differentiation

To evaluate the impact of pore geometry on hMSC differentiation, hMSCs were seeded onto each scaffold type and induced down the three main mesenchymal lineages (osteogenesis, chondrogenesis, and adipogenesis). Cells were seeded onto scaffolds as described above. Following incubation for 24 hours in growth medium, cells were cultured for 21 days in osteogenic, chondrogenic, or adipogenic as described in Section 4.2.2. hMSCs seeded on scaffolds and cultured in growth media served as a control. All media were changed every 3 days. At days 7, 14, and 21, samples were collected for RNA isolation and histological analysis.

7.2.10 Quantitative Reverse Transcriptase-Polymerase Chain Reaction

RNA was isolated using an RNeasy Mini Plus Kit (Qiagen, Valencia, CA) following standard protocols. Isolated RNA was then reverse transcribed to cDNA using a High Capacity cDNA Archive Kit (Applied Biosystems, Foster City, CA). The sequences of the gene expression assays used (Applied Biosystems) are proprietary and listed in Section 4.2.6. Glyceraldehyde-3-phosphate dehydrogenase (GAPDH) served as an endogenous control gene for all samples. Gene expression assays were combined with the cDNA to be analyzed and TaqMan PCR Master Mix (Applied Biosystems). The reaction was performed on a 7900HT real-time PCR System (Applied Biosystems) using thermal conditions of 2 minutes at 50°C, 10 minutes at 95°C, and 40 cycles of 15 seconds at 95°C and 1 minute at 60°C. The relative gene expression level of each target gene was then normalized to the mean of the GAPDH in each group. Fold change was calculated using the $\Delta\Delta CT$ relative

comparative method as described previously [69]. Samples were completed in triplicate and standard deviations are reported (n = 3).

7.2.11 Histological Analysis

At days 7, 14, and 21, cells were lifted from the surface of the scaffolds and seeded onto 96 well plates for 24 hours. At this time cells were fixed with 10% formalin for 10 minutes, and stored at 4°C in PBS. Histological staining was completed to show calcification, glycosaminoglycan production, and the presence of lipid droplets as described in Section 4.2.4. For quantification, 5 x 5 tiled images (total tiled image area = 3.177mm^2) were captured of each well (n = 4) using an inverted microscope (Zeiss AxioVert, equipped with an AxioCam MRm digital camera; Zeiss, Inc., Thornwood, NY) and AxioVision Software (Version 4.8.2; Zeiss, Inc.). A routine was created in Axiovision for each stain to capture and calculate regions positively stained for calcification, lipid deposits, or proteoglycans.

7.2.12 Statistical Analysis

All data was analyzed using one-way analysis of variance and Tukey's multiple-comparison test to determine statistical differences between hydrogels. A confidence interval of 95% (α=0.05) was used for all analyses, and means and SDs are shown in each figure.

7.3 Results

7.3.1 Scaffold Fabrication and Characterization

Scaffolds were designed to have an interconnected cubic or cylindrical porous network with 1000μm features and 80% porosity. In order to achieve an interconnected porous network that could be reproducibly printed, several design changes were made and the progression is shown in Figure 7.1. Using μCT, we were able to evaluate the actual scaffold parameters that resulted following fabrication and post-processing (Figure 7.2). The optimized printed scaffolds showed good correlation to the designed parameters, with cubic and cylindrical scaffolds having an actual porosity of 78.8 +/- 1.8% and 70.4 +/- 11.8% respectively. Pore size also printed close to the theoretical values with cubic scaffolds resulting in a pore size of 882 +/- 68 μm and cylindrical scaffolds a pore size of 735 +/- 91 μm. By using μCT to generate a pore map of each scaffold, it was apparent that the pores regardless of architecture were continuous and interconnected throughout the scaffold.

The μCT imaging also showed that the scaffold integrity was not compromised by the use of harsh chemical solvents in post-processing, as there are few areas of the scaffold surface that are roughened by surface defects. Similarly, there is little to no remaining debris around the scaffold surface. Sol fraction testing revealed that all washes tested had a sol fraction of less than 5%, and that washes containing an overnight ethanol wash had significantly lower sol fraction when compared to the PBS control. Washes without the overnight ethanol incubation were not statistically different compared to the control, except when 100% acetone was

used. The washes used were therefore effective at removing any remaining uncured polymer resin which could be potentially damaging to cell viability (Figure 7.3).

Compressive mechanical testing (Figure 7.3 and 7.4) revealed that there were no significant differences between washes. However, significant differences were found when post-processing UV flashes were compared. There was an increase in the elastic modulus of the scaffolds with an increasing number of UV flashes. For both acetone wash conditions, 100 flashes resulted in significantly lower modulus, followed by 500 flashes. There were no statistical differences between 1000 and 2000 flashes for either acetone wash. When comparing batches of PPF, it was found that overall, there is a correlation between the molecular weight of the polymer and the elastic modulus, with higher molecular weights resulting in increased moduli of the printed scaffolds (see Figure 7.3 and 7.4). Comparing geometries, cubic scaffolds had a statistically higher elastic modulus of 25.9MPa when compared to 17.5MPa for cylindrical scaffolds.

7.3.2 Assessment of MSC Viability

The results of the XTT assay show that MSCs cultured on scaffolds over a period of 7 days exhibit levels of metabolism that are not statistically different from cells cultured on tissue culture polystyrene (Figure 7.5A). On day 7, '*' indicates there is no statistical difference between groups (p>0.05). Quantitative results were confirmed using qualitative imaging techniques. In Figure 7.5B, the majority of the cells stain positively for calcein AM (green) indicating that they are viable on the scaffold surface and within the pores of the scaffold. An increased level of

fluorescence within the pores suggests that MSCs have begun to fill the pores. Taken together, these results confirm that the post processing techniques used to remove unreacted polymer following fabrication is effective and promotes cell function on and within the scaffold architecture.

7.3.3 MSC Differentiation on Cubic or Cylindrical Scaffolds

MSC differentiation was assessed over 21 days using qRT-PCR and histological staining for markers of each mesenchymal tissue. Gene expression analysis shows that cylindrical scaffolds appear to promote an early increase in osteogenic markers (see Figure 7.6A and 7.6B) following exposure of the cells to osteogenic media. Both ALP and OPN show a statistically greater expression of the respective marker in the cylindrical group at day 7 when compared to the cubic group ('*' indicates $p<0.05$). This initial difference is diminished at later timepoints, with the results of histological analysis indicating that the cubic group appears to catch up and pass the cylindrical group in terms of calcification. Image analysis results show that at day 21, the cubic group shows a significantly greater number of calcified regions when compared to the cylindrical group.

For adipogenesis, the cubic group at day 21 shows significantly increased expression of adiponectin, when compared to the corresponding cylindrical group (see Figure 7.6C). On day 21, '*'' indicates $p<0.05$. For both geometries, the expression of adiponectin is significantly upregulated on day 21. Based on histological evidence, there appears to be no significant difference between geometries when quantifying the number of lipid deposits per cell for both groups.

As with the adipogenic group, the cubic samples showed significantly upregulated type II collagen expression compared to the cylindrical samples for the group undergoing chondrogenesis (see Figure 7.6D). At day 21, both cubic and cylindrical scaffolds show an upregulation of type II collagen expression, with cubic scaffolds resulting in the highest expression ('*' indicates $p<0.05$). Based on histological evidence, there appears to be no significant difference between geometries when quantifying the number of proteoglycan-rich regions per cell for both groups.
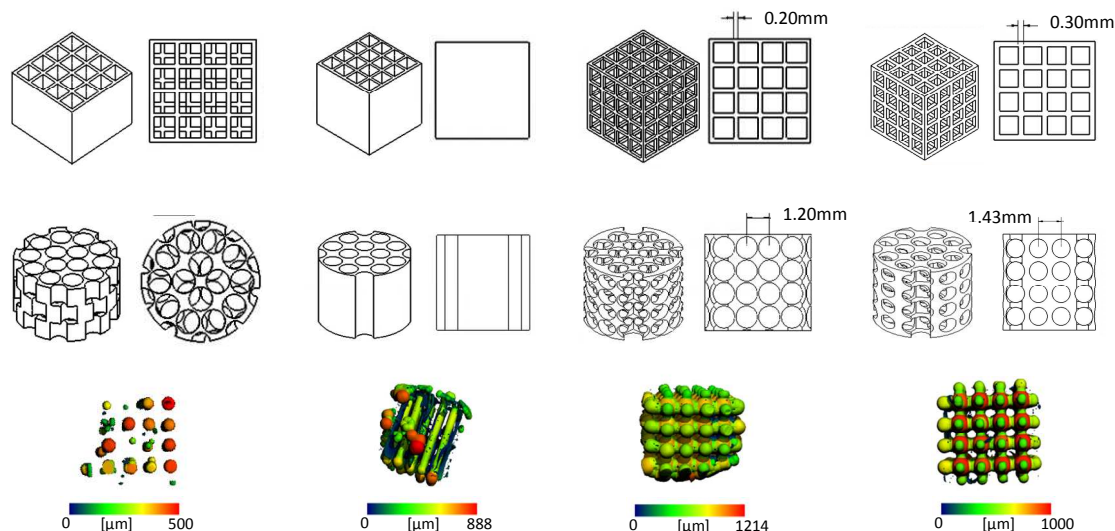
	Design A			Design B			Design C			Design D		
	Theoretical	Actual Cubic	Actual Cylindrical	Theoretical	Actual Cubic	Actual Cylindrical	Theoretical	Actual Cubic	Actual Cylindrical	Theoretical	Actual Cubic	Actual Cylindrical
Porosity (%)	80	--	51.0 ± 1.33	64%	–	–	80	68.2±10.5	–	80	78.8±1.8	70.4±11.8
Pore Side Length or Pore Diameter (µm)	1000	--	376.5 ± 119.5	1000	–	–	1000	529±203	–	1000	828±68	735± 91

Figure 7.1. To achieve a design that was capable of being reproducibly printed with an interconnected porous network, several design alterations were made. Here we show the progression of the cubic and cylindrical designs over time with pore map results from µCT. The original design (A) was based off of an offset arrangement of pores, but was difficult to print without extensive support structures and resulted in a network of disconnected pores. Design B was used for trouble shooting to validate that we could get pores of the desired size to extend throughout the entirety of the scaffold. Design C was an expansion of B, with pores extending vertically and horizontally through the scaffold. Here, the wall thickness of the scaffold (shown as measurement) was too thin for the printer to print distinct pores. Finally, design D combined the results of the previous designs to achieve a network of interconnected, relatively evenly spaced pores, which could be printed reproducibly. Note the scale of the pore maps as labeled for each design.

A
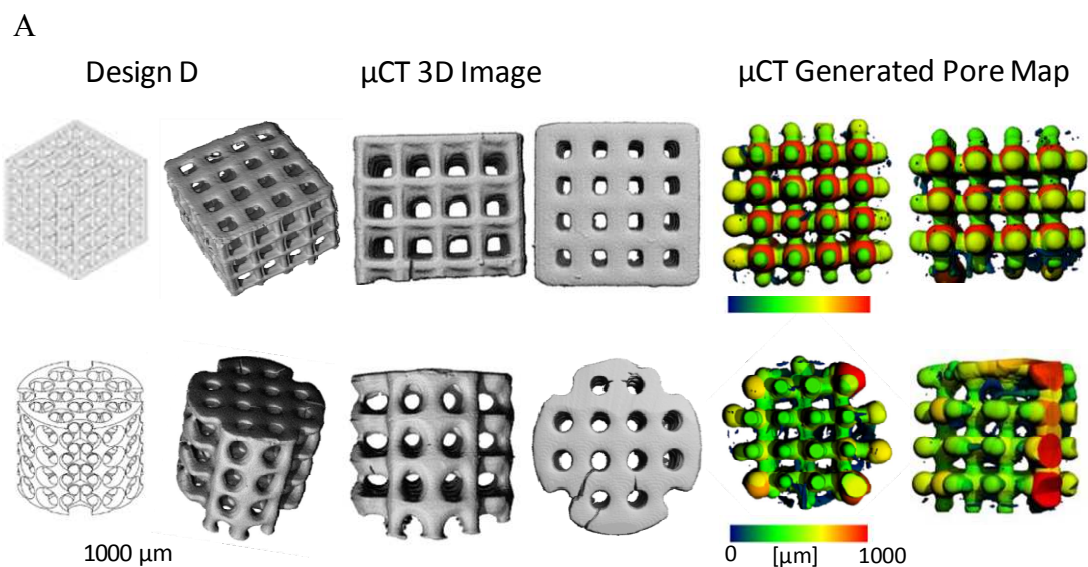
µCT Analysis	Porosity (%)	Pore Length or Diameter(µm)
Theoretical	80	1000
Actual Cubic	78.8±1.8	828±68
Actual Cylindrical	70.4±11.8	735± 91

Figure 7.2. (A) Expanded analysis of design D including 3D images resulting from µCT imaging. (B) The results from µCT show structures with highly defined and interconnecting pores. The tabulated pore size and porosity are close to the theoretical for both pore architectures. Design D was used for all subsequent experiments.

A

B

Wash Number	Post Processing	Sol Fraction (%)
1	IPA 30 min, 25% acetone 30 min, 2000 flashes, 70% ethanol 24 hr	2.43 ± 0.46
2	IPA 30 min, 25% acetone 30 min, 2000 flashes	3.93 ± 0.69
3	IPA 30 min, 50% acetone 30 min, 2000 flashes, 70% ethanol 24 hr	1.68 ± 0.16
4	IPA 30 min, 50% acetone 30 min, 2000 flashes	3.50 ± 0.37
5	IPA 30 min, 100% acetone 30 min, 2000 flashes	1.79 ± 0.86
6	PBS 1 hr, 2000 flashes	4.89 ± 0.38
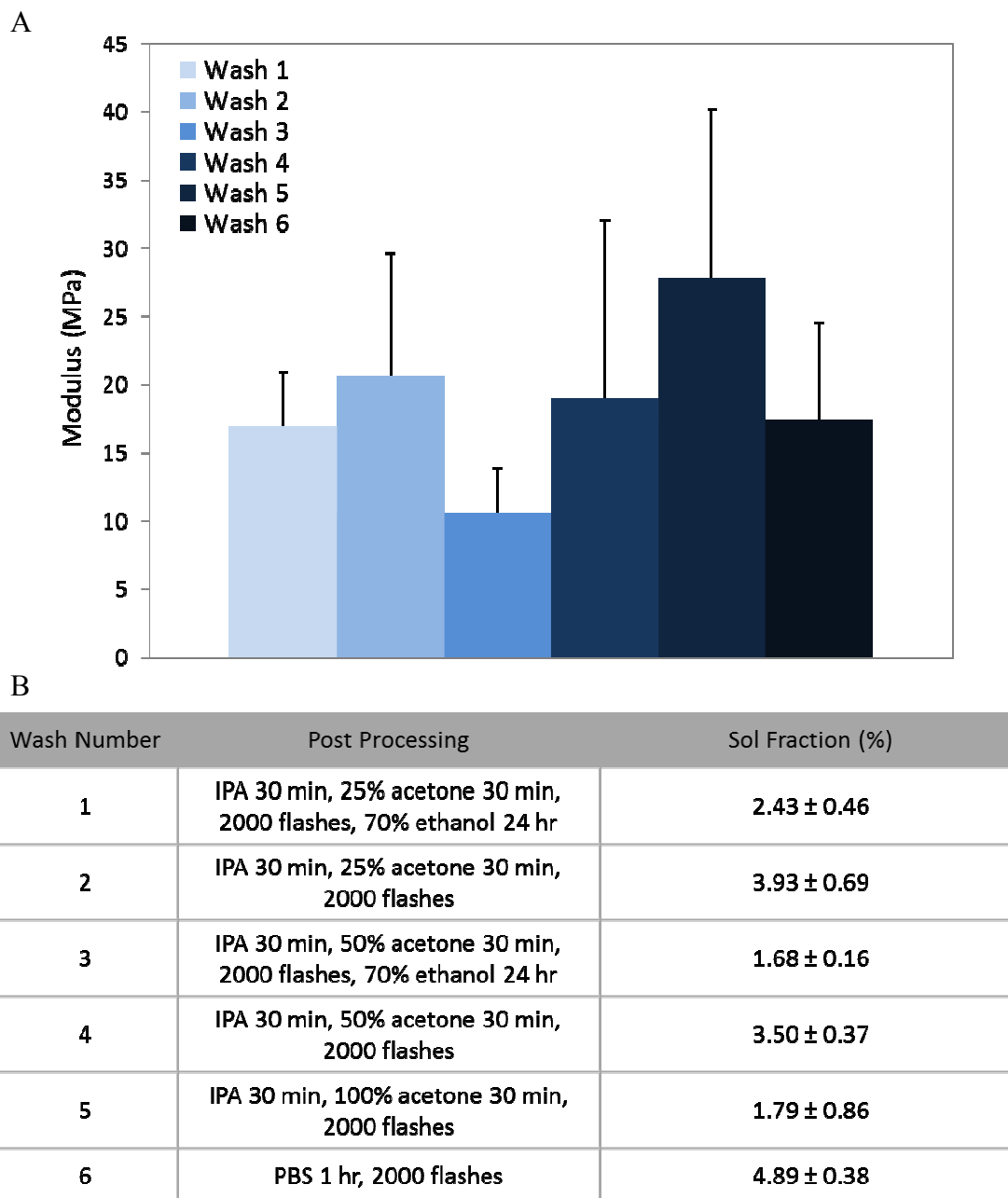
Figure 7.3. Post-processing of 3D printed PPF scaffolds. Post-processing was necessary to remove any uncrosslinked PPF resin that could result in cytotoxicity. Uncrosslinked resin was removed through the use of various solvent washes. Compressive testing was performed on scaffolds undergoing each post-processing method to determine if the solvents destroyed the scaffold integrity. (A) Modulus resulting from compressive testing of scaffolds exposed to various post processing methods. There were no statistical differences between washes ($p > 0.05$). (B) Identification of washes by number and the associated sol fractions for each post processing method. All methods resulted in very low sol fractions ($< 5\%$), indicating that the methods investigated here successfully removed uncrosslinked resin. Note, the molecular weight of PPF used for this data was 1167 Da.
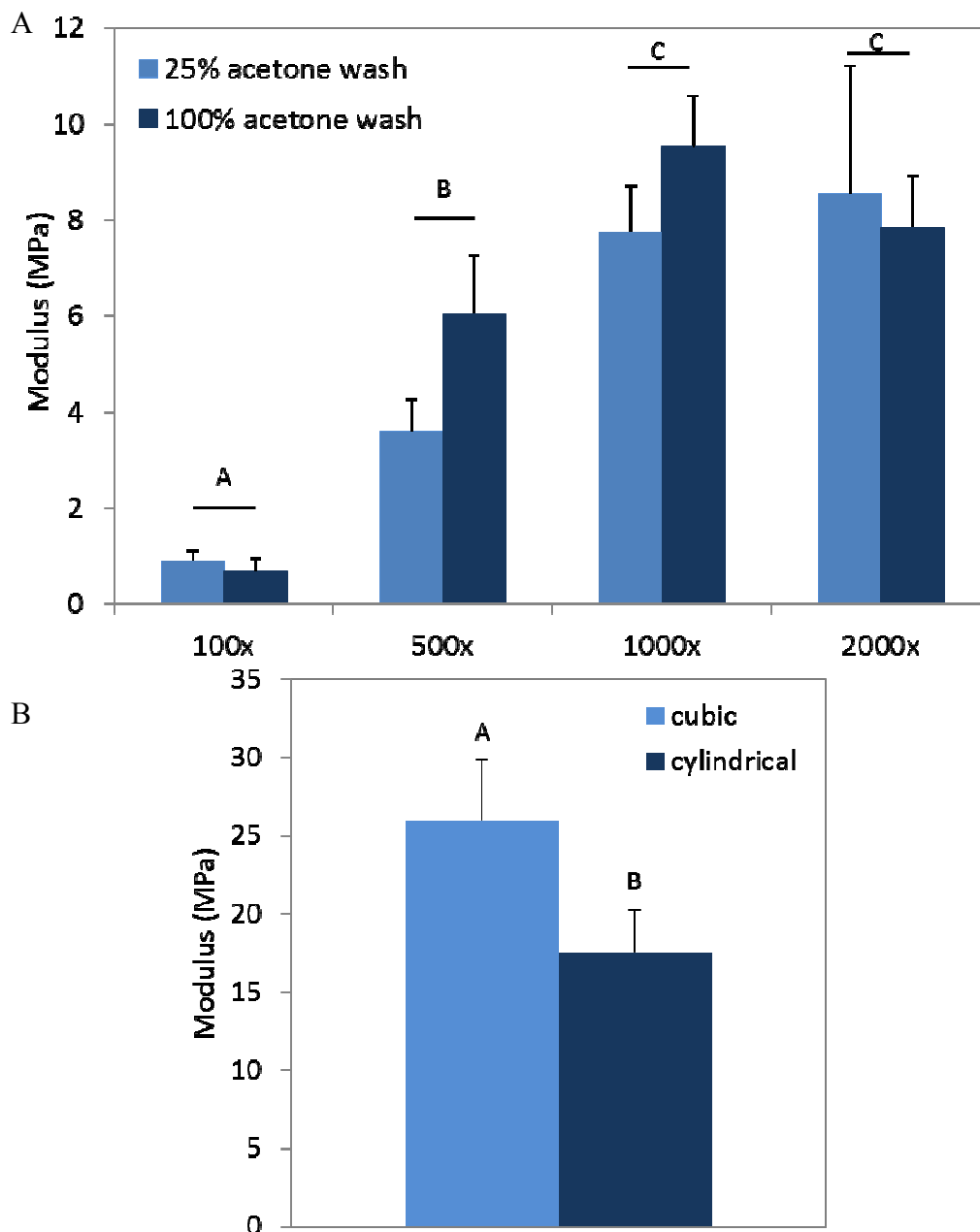
Figure 7.4. (A) Modulus resulting from compressive testing of scaffolds exposed to an increasing number of UV flashes. There were no statistical differences between 25 and 100% acetone washes, however, as the number of flashes increased there was a significant increase in the modulus of the scaffold up to 1000x ($p < 0.05$). The PPF used in this experiment had a MW = 1133 Da. (B) Modulus of cubic and cylindrical pore scaffolds subjected to a wash of 30 min IPA, 30 min 100% acetone, 100x flashes, and 24h 70% ethanol. The MW of PPF for this experiment was 1632 Da. Groups that do not share a letter in both (A) and (B) are statistically different ($p < 0.05$).
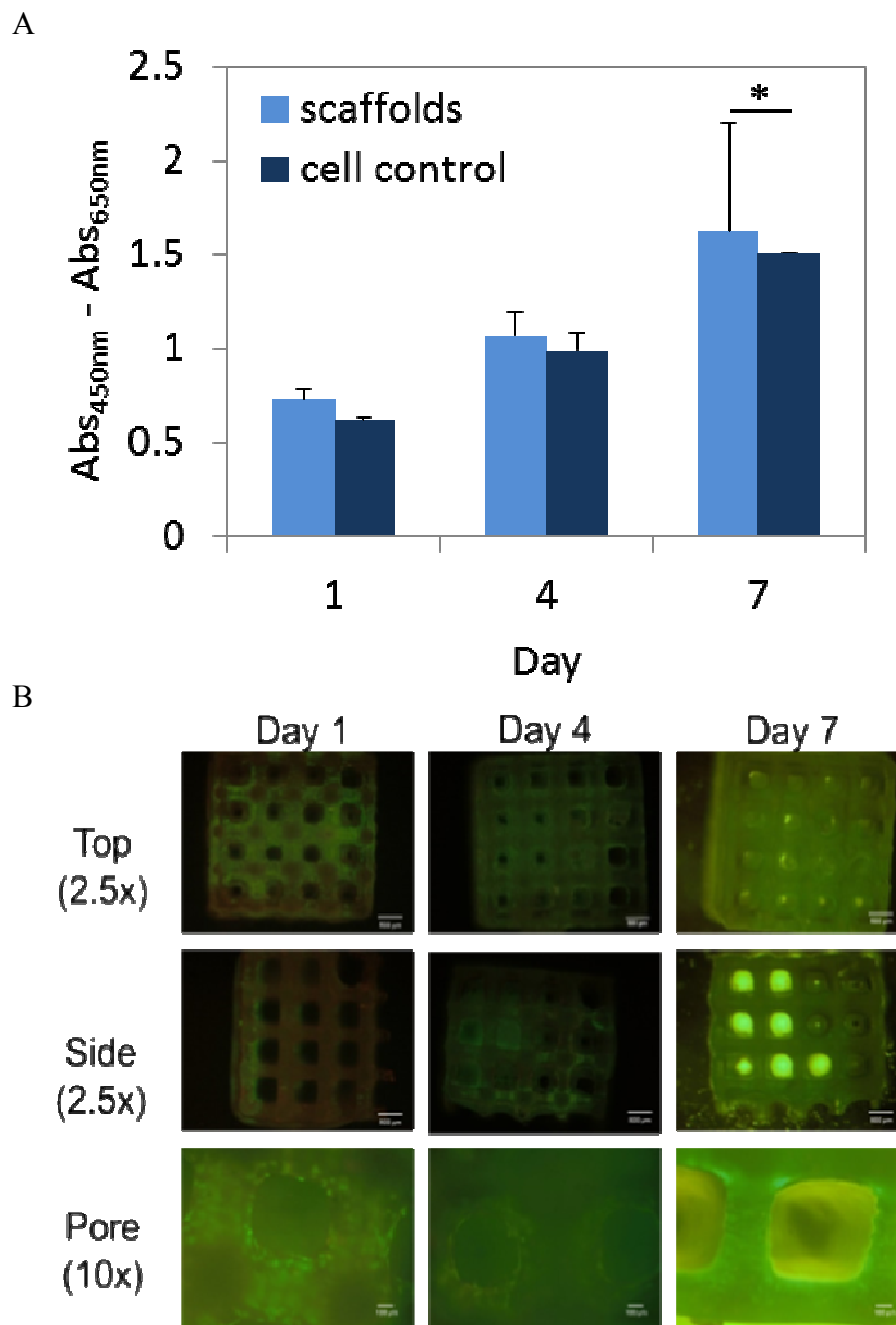
Figure 7.5. Cell viability on 3D printed PPF scaffolds. (A) XTT data following 1, 4, and 7 days of culture. '*' indicates samples on day 7 of both groups were statistically greater than day 1 ($p<0.05$). There were no statistical differences between cells grown on 3D printed scaffolds and the control at any timepoint. (B) Live-dead viability staining of samples at 1, 4, and 7 days of culture. The cells exhibit high viability (green) and localization within the pores of the scaffolds. Scale bar = 100µm.
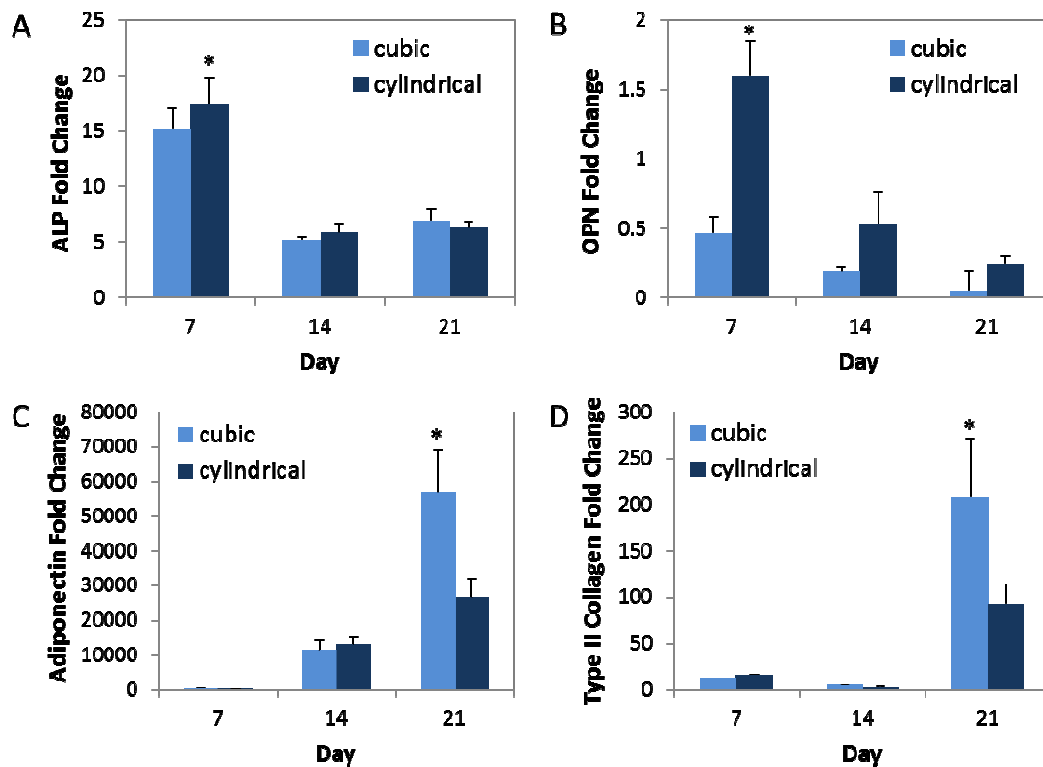
Figure 7.6. qRT-PCR results following differentiation. (A and B) Fold change in expression of osteogenic markers ALP and OPN. For both markers, the cylindrical group at day 7 exhibited a statistically greater expression level compared to all other groups. (C) Fold change in the expression of the adipogenic marker, adiponectin. At day 21, the cubic group showed the highest expression. (D) Fold change in the expression of type II collagen, a marker for chondrogenesis. At day 21, the cubic group had statistically greater expression compared to the cylindrical group. '*' indicates $p < 0.05$.
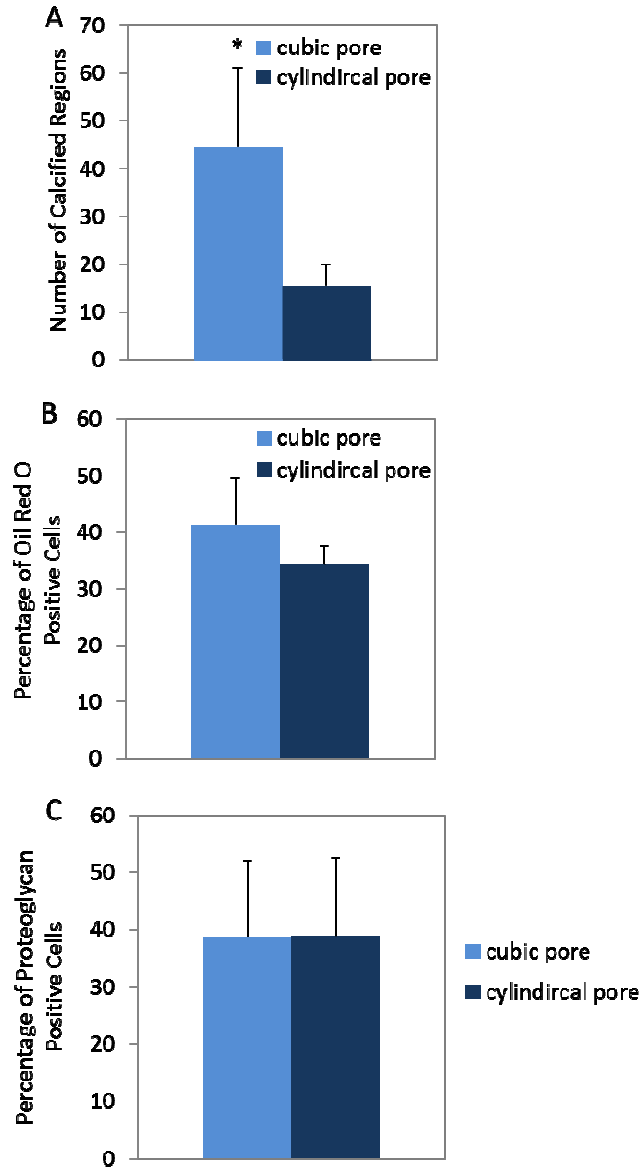
Figure 7.7. Quantification of histological staining at day 21. (A) Comparison of the number of calcified regions, an indicator of osteogenesis. At day 21, the cubic pore geometry had a statistically greater ('*' indicates p<0.05) number of calcified regions compared to the cylindrical group. (B) For adipogenic samples, the percentage of oil red o positive cells are reported. There was no statistical difference between geometries at day 21 (p>0.05). (C) Quantification of chondrogenesis was computed by dividing the number of proteoglycan positive regions by the number of cells. At day 21 there was no statistical difference between geometries (p>0.05).

7.4 Discussion

The ability to control MSC differentiation prior to and following implantation is of great importance to the field of cell therapy and regenerative medicine. In addition to chemical and biomolecular cues, MSCs have been shown to respond to scaffold parameters including substrate stiffness, surface roughness, pore size, and 2D geometry, such as curvature. In the work presented here, we used 3D printing technology to evaluate the impact of 3D pore geometry on MSC differentiation using two different pore architectures. Scaffolds were printed out of a resin of PPF, a biodegradable polymer that has previously been shown to result in accurately printed scaffolds, with parameters such as pore size, porosity, and wall thickness exhibiting accuracies of up to 91% [119]. One of the most important criteria for the culture and differentiation of MSCs on 3D scaffolds is an interconnected porous network to promote the exchange of nutrients, soluble factors, and cell signals. Here, we showed the design process used to achieve an interconnected network of evenly sized pores that could be printed with high reproducibility. Scaffolds were designed to be composed of repeatable units such that feature size and shape could be easily changed. Design parameters were altered based on the outcome of each print. PPF is a viscous polymer, a characteristic that can be troublesome for printing systems based on the use of liquid resins. Polymer resin viscosity has been noted in previous studies as a potential source of printing inaccuracies, particularly for small feature sizes [125]. Lowering of the viscosity through the use of a solvent is a simple way to combat this issue, as we have done here using DEF, the monomer of PPF. Major changes in scaffold designs can be followed in Figure 7.1. These changes were made

142

primarily to achieve successful printing of pores throughout the scaffolds. In our first design, design A, we attempted to print a series of layers with offset pores to attain interconnectivity. However, this was limited by a second printing challenge; the need for support structures. In design A, offset pores were designed to print onto areas of the scaffold that were not fully supported by the underlying layers, the result of which were pores that failed to extend throughout the scaffold (Figure 7.1). By altering both the cubic and cylindrical designs to include a set of pores extending from top to bottom interconnecting with pores extending horizontally through the scaffold, we achieved the desired connected internal structure. Design D was used for all subsequent characterization and cellular experiments.

Post-processing of the scaffold following printing is imperative to remove any uncrosslinked polymer resin as well as to preserve the features achieved through the fabrication process. In the case of PPF, uncrosslinked polymer resin has been shown to have a significantly higher sol fraction, and result in increased cell detachment and death [111]. However, the use of harsh solvents such as acetone and alcohols may result in damage to the integrity of the scaffold architecture, and therefore it is necessary to create a balance between the removal of excess polymer and the destruction of the scaffold. We tested a serial approach to washing our scaffolds, and were able to show through mechanical testing and μCT analysis that there was little to no damage to the scaffolds as a result of the post-processing methods, and that all washes resulted in very low sol fractions (less than 5%). Using compression testing to evaluate scaffold modulus, we found that there were no significant differences between washes, but that UV exposure following printing did result in significant

differences. When samples with identical washes were exposed to additional UV flashes, there was an increase in the modulus of the scaffold, indicating that there remained some amount of uncrosslinked monomers which were further crosslinked upon UV exposure. We also observed noticeable differences in the mechanical properties of scaffolds dependent on the molecular weight of PPF, despite using identical resin compositions. Increased moduli were observed with higher molecular weight, a trend that has been shown previously [118].

In order to elucidate how MSCs would respond to the two types of pore architectures presented here, cell viability had to be tested to ensure that the post-processing methods did not leave behind harsh solvents that may be cytotoxic to cells. Culture over a 7 day period showed that cells had an activity level that was not significantly different from the control, indicating that the post-processing methods used resulted in scaffolds that supported MSC cell viability and proliferation. Differentiation of MSCs down the three main mesenchymal lineages was assessed over a period of 21 days and scaffold geometries were compared for each group at each timepoint. Results indicated that there were significant differences between the gene expression of phenotypic markers depending on the 3D pore architecture of the scaffold.

The feature sizes of our scaffolds are quite large, with pore sizes around 830μm for the cubic design and 730μm for the cylindrical. Several studies have investigated the influence of pore size for each of the three target tissues – bone, fat, and cartilage. There are varying opinions on the appropriate range, however it appears that a range between 200 and 500μm has been shown to support the deposition of

extracellular matrix and tissue maturation both *in vitro* and *in vivo* [121, 122]. While the feature sizes in this study are greater than the subcellular curvatures that are commonly investigated in 2D studies of cell behavior [74, 75], it is not far above the recommended range of pore sizes, and was shown here to support MSC attachment, proliferation, and differentiation.

Based on the 2D studies that have been completed, it was hypothesized that the cubic geometry would best support osteogenesis, while the cylindrical geometry would promote the adipogenic and chondrogenic groups. Chondrogenic differentiation is typically completed using a 3D high density pellet culture system [78] which promotes increased cell-cell connections to facilitate cell signaling necessary for differentiation. Likewise, adipogenesis is induced using high density culture and has been shown to be promoted in environments with less cytoskeletal stress, such as a rounded geometry [74]. Environments with increased tension, such as a square or cubic geometry have been shown to support osteogenesis, and cytoskeletal tension has been found to be an important factor in the regulation of cell fate [75]. Here, we observe a nearly opposite trend. While the results of histological analysis show no differences between groups, the more sensitive qRT-PCR analysis shows that for both the adipogenic and chondrogenic groups, the cubic pore geometry results in a significant upregulation of the expression of key markers of cell phenotype for each respective lineage. For the osteogenic group, there is an initial upregulation of osteogenic expression in the cylindrical group at day 7, with ALP expression, a marker known to peak at day 7 during osteogenesis, significantly upregulated in the cylindrical geometry. However, by day 21, the cubic scaffold

145

geometry shows a significantly higher number of calcified regions, quantified using alizarin red staining. Overall, the cubic geometry appears to have a greater influence over the promotion of differentiation regardless of lineage.

7.5 Conclusion

In the work presented here, we were able to show the ability to successfully and reproducibly print 3D scaffolds with an interconnected porous network. Optimization of post processing methods provides a clean scaffold with little to no uncrosslinked resin remaining that encourages cell attachment and proliferation. The mechanical properties of the scaffolds can be tuned by varying the length of post curing as well as the molecular weight of the polymer. This would allow for the material properties to be altered based on the application, providing a means to match the mechanical properties of the scaffold with the target tissue. The 3D environments studied here were supportive of MSC differentiation down all three of the main mesenchymal lineages. The cubic pore geometry was shown to significantly support all three lineage commitments compared to a cylindrical counterpart. The development of a tunable 3D culture system for optimized culture of MSCs would have great potential in the field of tissue engineering and regenerative medicine.

Chapter 8: Summary and Future Directions

8.1 Summary

The overall goal of this work was to develop a 3D culture strategy to facilitate single-step MSC isolation from a heterogeneous population, such as the bone marrow. The current protocol for the isolation of MSCs is based off of the adhesive characteristics of MSCs compared to other cell types within the bone marrow, and involves an *in vitro* expansion phase following initial cell attachment to TCPS. It is hypothesized that this expansion phase significantly alters the phenotype of MSCs in culture, and therefore the use of a naïve MSC population may better serve the needs of current tissue engineering and regenerative medicine applications. Here, we show that through an understanding of the relationship between cell adhesion and phenotype, we can develop a platform that achieves direct MSC attachment, does not inhibit cell function, and encourages cell differentiation and matrix deposition.

The first objective of this work was to characterize the adhesive changes of MSCs as a result of *in vitro* culture through the use of a simple and reproducible adhesion assay. Using a centrifugation cell adhesion assay that was developed in Chapter 3 for the assessment of chondrocyte phenotypic changes, we showed in Chapter 4 that the adhesion of MSCs is altered during differentiation down the three main mesenchymal lineages and that these adhesive alterations can be detected and exploited through the use of our centrifugation assay. Populations of differentiating MSCs can be separated through the application of centrifugation, resulting in an

overall decrease in the population heterogeneity. Heterogeneity is an issue that is hypothesized to decrease the efficacy of MSCs following implantation. During chondrogenic differentiation, the application of centrifugation at day 14 resulted in a detached fraction of cells that exhibited significantly greater levels of expression for chondrogenic markers compared to the attached fraction and the control. For osteogenic and adipogenic samples, we showed that the attached fractions following separation had significantly higher expression of differentiation markers compared to the detached fractions, yet both were less than their respective controls. This result suggests that there is a level of crosstalk between the heterogeneous populations that is necessary for differentiation, the details of which need to be further elucidated. Overall, this work shows that cell populations can be separated based on phenotype to decrease cell heterogeneity prior to implantation.

The second objective was to develop a biomaterial platform that encourages specific MSC adhesion, proliferation, and differentiation. To investigate this objective we looked at two different polymer surfaces. First, in Chapter 5, we investigated the use of modified PEGDA substrates of varying stiffness on the adhesion of MSCs in both static and dynamic environments. We saw that increasing stiffness and the inclusion of ECM proteins such as fibronectin resulted in high levels of cell adhesion and spreading. Despite this success, we chose to consider another polymer, PPF, for this application. PEGDA cannot be easily translated into a 3D environment that can be fabricated with highly controlled architecture, and while biocompatible, is not biodegradable once implanted. These characteristics did not meet the criteria of our second objective, leading to the investigation in Chapter 6 of PPF as our biomaterial

148

substrate. In Chapter 6, we were able to show that PPF, a biodegradable and non-cytotoxic polymer, is a suitable material for a biomaterial platform that encourages MSC attachment and differentiation. Through the tethering of proteins found in the MSC ECM onto the PPF surface, we were able to increase the specific adhesion of MSCs when compared to unmodified scaffolds and a positive control (TCPS). The modification techniques described here did not negatively impact cell function, and could actually be used to drive differentiation. By tethering the growth factor TGF-β3 onto the material surface, we observed rapid cell condensation and proteoglycan deposition. These results were not observed on control substrates with identical media conditions. Additionally, we were able to show in a pilot study the feasibility of PPF as a means to isolate MSCs from the bone marrow based on their adhesive properties. When our biomaterial platform was cultured in the presence of unprocessed bone marrow, the resulting cell populations were phenotypically similar to TCPS and hMSC controls after 7 days of culture. Taken together, these results demonstrate the potential of a modified PPF surface as an alternative to TCPS for the capture and culture of MSCs from the bone marrow. PPF was used in a subsequent study that evaluated the translation of our substrate into 3D using 3D printing technology to fabricate reproducible, highly controlled scaffold architectures.

The third objective of this work was to translate the biomaterial platform into a relevant 3D culture system using 3D printing technology to elucidate the response of MSCs to 3D scaffold geometry. In Chapter 7, we progressively altered design parameters to achieve accurate printing of scaffolds with two distinct pore architectures and an interconnected porous network. The optimization of post

processing methods resulted in a scaffold that encouraged high levels of cell attachment, viability, and proliferation. The mechanical properties of the scaffolds can be tuned by varying the length of post curing as well as the molecular weight of the polymer. Therefore, material properties could be altered based on the application, providing a means to match the mechanical properties of the scaffold with the target tissue. The 3D environments studied here were supportive of MSC differentiation down all three of the main mesenchymal lineages. The cubic pore geometry was shown to significantly support all three lineage commitments compared to a cylindrical counterpart.

In conclusion, in an effort to increase the efficiency of the use of MSCs for clinical applications, we have shown three individual components that are necessary for the development of a one-step isolation and implantation technology. This technology would eliminate the need for time consuming and costly *in vitro* expansion and allow the procedure to remain in the clinic. Cell adhesion is critical to the isolation and phenotype of MSCs. Here, we demonstrate a relationship between MSC adhesion and phenotype, and use this relationship to separate populations of differentiating MSCs, priming the cells for implantation. We demonstrate the potential of PPF as a biomaterial substrate to facilitate specific MSC adhesion, directed differentiation, and definitive isolation from the bone marrow, with results showing a phenotypic signature similar to controls. Using 3D printing, we show that differentiating MSCs adhere, proliferate, and differentiate on PPF scaffolds, and that 3D pore architecture has an impact on cell differentiation. Taken together, the knowledge of the relationship between cell adhesion and phenotype, the use of

150

material modifications to facilitate efficient MSC adhesion, and the optimization of 3D printing technology to reproducibly fabricate 3D scaffolds, can be combined to develop a single-step biomaterial culture system for MSC capture, culture, and differentiation.

8.2 Future Directions

This work focused on the development of the main components of a single-step isolation and culture system for MSCs. These components were investigated individually, as a means to optimize the distinct parameters of a complex system. Results showed that a modified PPF substrate increased specific adhesion of MSCs on the material surface, when exposed to a population of MSCs alone or unprocessed bone marrow. The combination of the strategies presented here is an important next step in the development process. The results of Chapter 7 indicate that 3D scaffolds with a cubic pore architecture are more supportive of MSC differentiation *in vitro*, and therefore should be used in future studies. The impact of surface modification in 3D environments should be investigated and compared to the 2D results in Chapter 6, and the exposure of a modified 3D environment to unprocessed bone marrow should be evaluated for the phenotypic signature of the captured cell population. In addition to evaluating the success of the scaffold based on the phenotypic signature of the cells as determined by cell surface antigen presence, it would also be beneficial to evaluate how the genotype of the captured cell population compares to a TCPS control.

A second future objective based on the work presented here is a more in-depth look into the relationship between adhesion and differentiation, as presented in

Chapter 4. Results show that using a centrifugation assay to isolate cells based on their level of adhesion, cells could be separated during differentiation to isolate a less heterogeneous population of cells for subsequent implantation. The results were based off of histological and qRT-PCR analysis for phenotypic markers of each mesenchymal lineage. However, additional investigation into the role of integrins in the differentiation process may lead to further understanding of the adhesive changes occurring during differentiation. Evaluation of changes in integrin expression throughout differentiation as well as integrin blocking experiments to impact cell adhesion could offer further insight into the biology of the changes occurring during the *in vitro* culture of MSCs as they relate to cell adhesion. Along with studies into integrin behavior during differentiation, additional genotypic and phenotypic analysis of the heterogeneous populations before and after separation to determine if the cells in each fraction are differentiated cells, progenitors, precursors, or undifferentiated stem cells would help to elucidate if the mechanism of centrifugation is decreasing overall heterogeneity.

It is also necessary to explore the shelf-life of the final product developed here for the one-step isolation of MSCs from the bone marrow. In order for this product to be more advantageous than the current methods used today, it needs to be able to eliminate the need for an *in vitro* expansion phase, which is known to be costly and time consuming. This device would be most impactful if it could be used immediately after bone marrow harvest within the clinic, eliminating the need for additional surgical interventions. In order to successfully be used in the clinic, the device must be able to be stored in conditions that are readily available. The longevity of the

modified surfaces presented here must be evaluated, and methods to store these materials in a simple and accessible way must be developed.

Along the same lines, it is necessary to consider the overall regulatory and economic impact of the final clinical product. A product consisting of a bioactive scaffold for implantation would be regulated as a combinatorial device in the Office of Combination Products within the FDA. The development and regulation of combination products require special consideration into how the separate pieces (biological material such as ECM protein or growth factors and the scaffold device) may impact each other; such as how the combination of biologics and devices may alter the genotype or phenotype of implanted cells, how implanted cells may survive within the device following implantation, and how the inclusion of protein on the scaffold may alter the biocompatible or biodegradable properties of the combination product. While the initial economic investment during the discovery-phase and proof-of-concept portions of the product development may be increased due to the combinatorial nature of the device, the eventual economic impact of such a device would be significant. The development of a device that would allow for the elimination of the need for cell processing within a centralized good manufacturing practice (cGMP) facility would result in the reduction or elimination of several factors contributing to the overall expense of current cell therapy practices. These include reduction in staff necessary due to the product being used within the clinic and not entering a cGMP facility as well as an elimination of transportation costs and complications.

The combination of the pieces presented in this thesis, along with future refinements and optimization strategies would result in the ability to implant a 3D biofunctionalized scaffold directly into a defect site on the same day that bone marrow is harvested. This would dramatically simplify the procedure, cost, and time associated with the use of MSCs for therapeutic applications, all of which are currently holding back the widespread use of MSCs for regenerative medicine.

Bibliography

1. Takada, Y., X. Ye, and S. Simon, *The integrins.* Genome Biol, 2007. **8**(5): p. 215.
2. Hynes, R.O., *Integrins: bidirectional, allosteric signaling machines.* Cell, 2002. **110**(6): p. 673-87.
3. Petit, V. and J.P. Thiery, *Focal adhesions: structure and dynamics.* Biol Cell, 2000. **92**(7): p. 477-94.
4. Ehrlicher, A.J., et al., *Mechanical strain in actin networks regulates FilGAP and integrin binding to filamin A.* Nature, 2011. **478**(7368): p. 260-3.
5. Shih, Y.R., et al., *Matrix stiffness regulation of integrin-mediated mechanotransduction during osteogenic differentiation of human mesenchymal stem cells.* J Bone Miner Res, 2011. **26**(4): p. 730-8.
6. Tadokoro, S., et al., *A potential role for alpha-actinin in inside-out alphaIIbbeta3 signaling.* Blood, 2011. **117**(1): p. 250-8.
7. Barczyk, M., S. Carracedo, and D. Gullberg, *Integrins.* Cell Tissue Res, 2010. **339**(1): p. 269-80.
8. Humphries, M.J., *Integrin structure.* Biochem Soc Trans, 2000. **28**(4): p. 311-39.
9. Jiang, X., et al., *Self-aggregated pegylated poly (trimethylene carbonate) nanoparticles decorated with c(RGDyK) peptide for targeted paclitaxel delivery to integrin-rich tumors.* Biomaterials, 2011. **32**(35): p. 9457-69.
10. You, M., et al., *Chondrogenic differentiation of human bone marrow mesenchymal stem cells on polyhydroxyalkanoate (PHA) scaffolds coated with PHA granule binding protein PhaP fused with RGD peptide.* Biomaterials, 2011. **32**(9): p. 2305-13.
11. Sapir, Y., O. Kryukov, and S. Cohen, *Integration of multiple cell-matrix interactions into alginate scaffolds for promoting cardiac tissue regeneration.* Biomaterials, 2011. **32**(7): p. 1838-47.
12. Clements, J.M., et al., *Identification of a key integrin-binding sequence in VCAM-1 homologous to the LDV active site in fibronectin.* J Cell Sci, 1994. **107 (Pt 8)**: p. 2127-35.
13. Miyamoto, S., et al., *Integrin function: molecular hierarchies of cytoskeletal and signaling molecules.* J Cell Biol, 1995. **131**(3): p. 791-805.
14. Graf, J., et al., *A pentapeptide from the laminin B1 chain mediates cell adhesion and binds the 67,000 laminin receptor.* Biochemistry, 1987. **26**(22): p. 6896-900.
15. Niehage, C., et al., *The cell surface proteome of human mesenchymal stromal cells.* PLoS One, 2011. **6**(5): p. e20399.
16. Lee, K.Y. and D.J. Mooney, *Hydrogels for tissue engineering.* Chem Rev, 2001. **101**(7): p. 1869-79.
17. Martens, P.J., S.J. Bryant, and K.S. Anseth, *Tailoring the degradation of hydrogels formed from multivinyl poly(ethylene glycol) and poly(vinyl alcohol) macromers for cartilage tissue engineering.* Biomacromolecules, 2003. **4**(2): p. 283-92.

18. Papadopoulos, A., et al., *Injectable and photopolymerizable tissue-engineered auricular cartilage using poly(ethylene glycol) dimethacrylate copolymer hydrogels.* Tissue Eng Part A, 2011. **17**(1-2): p. 161-9.

19. Fisher, J.P., et al., *Synthesis and properties of photocross-linked poly(propylene fumarate) scaffolds.* J Biomater Sci Polym Ed, 2001. **12**(6): p. 673-87.

20. Kim, K., et al., *Effect of initial cell seeding density on early osteogenic signal expression of rat bone marrow stromal cells cultured on cross-linked poly(propylene fumarate) disks.* Biomacromolecules, 2009. **10**(7): p. 1810-7.

21. Lan, P.X., et al., *Development of 3D PPF/DEF scaffolds using micro-stereolithography and surface modification.* Journal of materials science. Materials in medicine, 2009. **20**(1): p. 271-9.

22. Roach, P., et al., *Modern biomaterials: a review - bulk properties and implications of surface modifications.* J Mater Sci Mater Med, 2007. **18**(7): p. 1263-77.

23. Ganazzoli, F. and G. Raffaini, *Computer simulation of polypeptide adsorption on model biomaterials.* Phys Chem Chem Phys, 2005. **7**(21): p. 3651-63.

24. Wilson, C.J., et al., *Mediation of biomaterial-cell interactions by adsorbed proteins: a review.* Tissue Eng, 2005. **11**(1-2): p. 1-18.

25. Yuan, L., et al., *Surface modification to control protein/surface interactions.* Macromol Biosci, 2011. **11**(8): p. 1031-40.

26. Goldstein, A.S. and P.A. DiMilla, *Effect of adsorbed fibronectin concentration on cell adhesion and deformation under shear on hydrophobic surfaces.* J Biomed Mater Res, 2002. **59**(4): p. 665-75.

27. Yoon, S.H. and M.R. Mofrad, *Cell adhesion and detachment on gold surfaces modified with a thiol-functionalized RGD peptide.* Biomaterials, 2011. **32**(30): p. 7286-96.

28. Ilagan, B.G. and B.G. Amsden, *Surface modifications of photocrosslinked biodegradable elastomers and their influence on smooth muscle cell adhesion and proliferation.* Acta Biomater, 2009. **5**(7): p. 2429-40.

29. Shekaran, A. and A.J. Garcia, *Nanoscale engineering of extracellular matrix-mimetic bioadhesive surfaces and implants for tissue engineering.* Biochim Biophys Acta, 2011. **1810**(3): p. 350-60.

30. Henslee, A.M., et al., *Degradable, antibiotic releasing poly(propylene fumarate)-based constructs for craniofacial space maintenance applications.* J Biomed Mater Res A, 2015. **103**(4): p. 1485-97.

31. Kasper, F.K., et al., *Synthesis of poly(propylene fumarate).* Nat Protoc, 2009. **4**(4): p. 518-25.

32. Wang, K., et al., *Distinct cell responses to substrates consisting of poly(epsilon-caprolactone) and poly(propylene fumarate) in the presence or absence of cross-links.* Biomacromolecules, 2010. **11**(10): p. 2748-59.

33. Petrie, T.A., et al., *Multivalent integrin-specific ligands enhance tissue healing and biomaterial integration.* Sci Transl Med, 2010. **2**(45): p. 45ra60.

34. Athanassiou, G. and D. Deligianni, *Adhesion strength of individual human bone marrow cells to fibronectin. Integrin beta1-mediated adhesion.* J Mater Sci Mater Med, 2001. **12**(10-12): p. 965-70.

35.   Garcia, A.J. and N.D. Gallant, *Stick and grip: measurement systems and quantitative analyses of integrin-mediated cell adhesion strength.* Cell Biochem Biophys, 2003. **39**(1): p. 61-73.

36.   McClay, D.R. and P.L. Hertzler, *Quantitative measurement of cell adhesion using centrifugal force.* Curr Protoc Cell Biol, 2001. **Chapter 9**: p. Unit 9 2.

37.   Simon, A. and M.C. Durrieu, *Strategies and results of atomic force microscopy in the study of cellular adhesion.* Micron, 2006. **37**(1): p. 1-13.

38.   ASTM, *Standard Guide for Assessing the Attachment of Cells to Biomaterial Surfaces by Physical Methods*, 2007, ASTM International West Conshohocken, PA

39.   Hyduk, S.J. and M.I. Cybulsky, *Role of alpha4beta1 integrins in chemokine-induced monocyte arrest under conditions of shear stress.* Microcirculation, 2009. **16**(1): p. 17-30.

40.   Konstantopoulos, K., S. Kukreti, and L.V. McIntire, *Biomechanics of cell interactions in shear fields.* Adv Drug Deliv Rev, 1998. **33**(1-2): p. 141-64.

41.   Reyes, C.D. and A.J. Garcia, *A centrifugation cell adhesion assay for high-throughput screening of biomaterial surfaces.* J Biomed Mater Res A, 2003. **67**(1): p. 328-33.

42.   Brittberg, M., et al., *Treatment of deep cartilage defects in the knee with autologous chondrocyte transplantation.* N Engl J Med, 1994. **331**(14): p. 889-95.

43.   Benya, P.D. and J.D. Shaffer, *Dedifferentiated chondrocytes reexpress the differentiated collagen phenotype when cultured in agarose gels.* Cell, 1982. **30**(1): p. 215-24.

44.   Ishaug-Riley, S.L., et al., *Human articular chondrocyte adhesion and proliferation on synthetic biodegradable polymer films.* Biomaterials, 1999. **20**(23-24): p. 2245-56.

45.   Mauck, R.L., X. Yuan, and R.S. Tuan, *Chondrogenic differentiation and functional maturation of bovine mesenchymal stem cells in long-term agarose culture.* Osteoarthritis Cartilage, 2006. **14**(2): p. 179-89.

46.   Schnabel, M., et al., *Dedifferentiation-associated changes in morphology and gene expression in primary human articular chondrocytes in cell culture.* Osteoarthritis and cartilage / OARS, Osteoarthritis Research Society, 2002. **10**(1): p. 62-70.

47.   Marlovits, S., et al., *Changes in the ratio of type-I and type-II collagen expression during monolayer culture of human chondrocytes.* J Bone Joint Surg Br, 2004. **86**(2): p. 286-95.

48.   Yates, K.E., F. Allemann, and J. Glowacki, *Phenotypic analysis of bovine chondrocytes cultured in 3D collagen sponges: effect of serum substitutes.* Cell and tissue banking, 2005. **6**(1): p. 45-54.

49.   Yoon, D.M., et al., *Addition of hyaluronic acid to alginate embedded chondrocytes interferes with insulin-like growth factor-1 signaling in vitro and in vivo.* Tissue Eng Part A, 2009. **15**(11): p. 3449-59.

50.   Gao, C., et al., *CDK5 regulates cell adhesion and migration in corneal epithelial cells.* Molecular cancer research : MCR, 2002. **1**(1): p. 12-24.

51.   Garcia, A.J. and D. Boettiger, *Integrin-fibronectin interactions at the cell-material interface: initial integrin binding and signaling.* Biomaterials, 1999. **20**(23-24): p. 2427-33.

52.   Kurtis, M.S., et al., *Integrin-mediated adhesion of human articular chondrocytes to cartilage.* Arthritis and rheumatism, 2003. **48**(1): p. 110-8.

53.   Jones, D.A., et al., *P-selectin mediates neutrophil rolling on histamine-stimulated endothelial cells.* Biophysical journal, 1993. **65**(4): p. 1560-9.

54.   Kino-oka, M., et al., *Morphological regulation of rabbit chondrocytes on glucose-displayed surface.* Biomaterials, 2007. **28**(9): p. 1680-8.

55.   Baksh, D., L. Song, and R.S. Tuan, *Adult mesenchymal stem cells: characterization, differentiation, and application in cell and gene therapy.* Journal of cellular and molecular medicine, 2004. **8**(3): p. 301-16.

56.   Pittenger, M.F., et al., *Multilineage potential of adult human mesenchymal stem cells.* Science, 1999. **284**(5411): p. 143-7.

57.   Muraglia, A., R. Cancedda, and R. Quarto, *Clonal mesenchymal progenitors from human bone marrow differentiate in vitro according to a hierarchical model.* J Cell Sci, 2000. **113 (Pt 7)**: p. 1161-6.

58.   Lo Surdo, J. and S.R. Bauer, *Quantitative approaches to detect donor and passage differences in adipogenic potential and clonogenicity in human bone marrow-derived mesenchymal stem cells.* Tissue engineering. Part C, Methods, 2012. **18**(11): p. 877-89.

59.   Lo Surdo, J.L., B.A. Millis, and S.R. Bauer, *Automated microscopy as a quantitative method to measure differences in adipogenic differentiation in preparations of human mesenchymal stromal cells.* Cytotherapy, 2013. **15**(12): p. 1527-40.

60.   Russell, K.C., et al., *In vitro high-capacity assay to quantify the clonal heterogeneity in trilineage potential of mesenchymal stem cells reveals a complex hierarchy of lineage commitment.* Stem Cells, 2010. **28**(4): p. 788-98.

61.   Seiler, C., et al., *Time-lapse microscopy and classification of 2D human mesenchymal stem cells based on cell shape picks up myogenic from osteogenic and adipogenic differentiation.* J Tissue Eng Regen Med, 2014. **8**(9): p. 737-46.

62.   Sekiya, I., et al., *Expansion of human adult stem cells from bone marrow stroma: conditions that maximize the yields of early progenitors and evaluate their quality.* Stem cells, 2002. **20**(6): p. 530-41.

63.   Gronthos, S., et al., *Molecular and cellular characterisation of highly purified stromal stem cells derived from human bone marrow.* Journal of cell science, 2003. **116**(Pt 9): p. 1827-35.

64.   Kaplan, D.S., et al., *Centrifugation Assay for Measuring Adhesion of Serially-Passaged Bovine Chondrocytes to Polystyrene Surfaces.* Tissue Eng Part C Methods, 2012.

65.   Singh, A., et al., *Adhesion strength-based, label-free isolation of human pluripotent stem cells.* Nat Methods, 2013. **10**(5): p. 438-44.

66.   LaPointe, V.L., A. Verpoorte, and M.M. Stevens, *The changing integrin expression and a role for integrin beta8 in the chondrogenic differentiation of mesenchymal stem cells.* PLoS One, 2013. **8**(11): p. e82035.

67. Frith, J.E., et al., *Tailored integrin-extracellular matrix interactions to direct human mesenchymal stem cell differentiation.* Stem cells and development, 2012. **21**(13): p. 2442-56.

68. Chen, Q., et al., *An osteopontin-integrin interaction plays a critical role in directing adipogenesis and osteogenesis by mesenchymal stem cells.* Stem Cells, 2014. **32**(2): p. 327-37.

69. Yeatts, A.B. and J.P. Fisher, *Tubular perfusion system for the long-term dynamic culture of human mesenchymal stem cells.* Tissue Eng Part C Methods, 2011. **17**(3): p. 337-48.

70. Ferlin, K.M., et al., *Development of a dynamic stem cell culture platform for mesenchymal stem cell adhesion and evaluation.* Mol Pharm, 2014. **11**(7): p. 2172-81.

71. Sista, S., et al., *Expression of cell adhesion and differentiation related genes in MC3T3 osteoblasts plated on titanium alloys: role of surface properties.* Mater Sci Eng C Mater Biol Appl, 2013. **33**(3): p. 1573-82.

72. Mathieu, P.S. and E.G. Loboa, *Cytoskeletal and focal adhesion influences on mesenchymal stem cell shape, mechanical properties, and differentiation down osteogenic, adipogenic, and chondrogenic pathways.* Tissue Eng Part B Rev, 2012. **18**(6): p. 436-44.

73. Szabo, E., et al., *Cell adhesion and spreading affect adipogenesis from embryonic stem cells: the role of calreticulin.* Stem Cells, 2009. **27**(9): p. 2092-102.

74. Kilian, K.A., et al., *Geometric cues for directing the differentiation of mesenchymal stem cells.* Proc Natl Acad Sci U S A, 2010. **107**(11): p. 4872-7.

75. McBeath, R., et al., *Cell shape, cytoskeletal tension, and RhoA regulate stem cell lineage commitment.* Dev Cell, 2004. **6**(4): p. 483-95.

76. Gregoire, F.M., C.M. Smas, and H.S. Sul, *Understanding adipocyte differentiation.* Physiol Rev, 1998. **78**(3): p. 783-809.

77. Yoon, D.M. and J.P. Fisher, *Chondrocyte signaling and artificial matrices for articular cartilage engineering.* Adv Exp Med Biol, 2006. **585**: p. 67-86.

78. Yang, Z., J.F. Schmitt, and E.H. Lee, *Immunohistochemical analysis of human mesenchymal stem cells differentiating into chondrogenic, osteogenic, and adipogenic lineages.* Methods Mol Biol, 2011. **698**: p. 353-66.

79. Elliott, N.T. and F. Yuan, *A review of three-dimensional in vitro tissue models for drug discovery and transport studies.* Journal of pharmaceutical sciences, 2011. **100**(1): p. 59-74.

80. Griffith, L.G. and M.A. Swartz, *Capturing complex 3D tissue physiology in vitro.* Nature reviews. Molecular cell biology, 2006. **7**(3): p. 211-24.

81. Kane, R.S., et al., *Patterning proteins and cells using soft lithography.* Biomaterials, 1999. **20**(23-24): p. 2363-76.

82. Discher, D.E., D.J. Mooney, and P.W. Zandstra, *Growth factors, matrices, and forces combine and control stem cells.* Science, 2009. **324**(5935): p. 1673-7.

83. Aoudjit, F. and K. Vuori, *Integrin signaling inhibits paclitaxel-induced apoptosis in breast cancer cells.* Oncogene, 2001. **20**(36): p. 4995-5004.

84. Wang, L., et al., *Chemical and physical modifications to poly(dimethylsiloxane) surfaces affect adhesion of Caco-2 cells.* Journal of biomedical materials research. Part A, 2010. **93**(4): p. 1260-71.

85. Shin, C.S., et al., *Development of an in vitro 3D tumor model to study therapeutic efficiency of an anticancer drug.* Molecular pharmaceutics, 2013. **10**(6): p. 2167-75.

86. Loessner, D., et al., *Bioengineered 3D platform to explore cell-ECM interactions and drug resistance of epithelial ovarian cancer cells.* Biomaterials, 2010. **31**(32): p. 8494-506.

87. Stroka, K.M. and H. Aranda-Espinoza, *Neutrophils display biphasic relationship between migration and substrate stiffness.* Cell Motil Cytoskeleton, 2009. **66**(6): p. 328-41.

88. Zaman, M.H., et al., *Migration of tumor cells in 3D matrices is governed by matrix stiffness along with cell-matrix adhesion and proteolysis.* Proc Natl Acad Sci U S A, 2006. **103**(29): p. 10889-94.

89. Gobaa, S., et al., *Artificial niche microarrays for probing single stem cell fate in high throughput.* Nat Methods, 2011. **8**(11): p. 949-55.

90. Engler, A.J., et al., *Matrix elasticity directs stem cell lineage specification.* Cell, 2006. **126**(4): p. 677-89.

91. Gilbert, P.M., et al., *Substrate elasticity regulates skeletal muscle stem cell self-renewal in culture.* Science, 2010. **329**(5995): p. 1078-81.

92. Park, J.S., et al., *The effect of matrix stiffness on the differentiation of mesenchymal stem cells in response to TGF-beta.* Biomaterials, 2011. **32**(16): p. 3921-30.

93. Paszek, M.J., et al., *Tensional homeostasis and the malignant phenotype.* Cancer cell, 2005. **8**(3): p. 241-54.

94. Prockop, D.J., *Marrow stromal cells as stem cells for nonhematopoietic tissues.* Science, 1997. **276**(5309): p. 71-4.

95. Heldin, C.H., M. Vanlandewijck, and A. Moustakas, *Regulation of EMT by TGFbeta in cancer.* FEBS letters, 2012. **586**(14): p. 1959-70.

96. Zubeldia, I.G., et al., *Epithelial to mesenchymal transition and cancer stem cell phenotypes leading to liver metastasis are abrogated by the novel TGFbeta1-targeting peptides P17 and P144.* Experimental cell research, 2013. **319**(3): p. 12-22.

97. Xia, H. and K.M. Hui, *MicroRNAs involved in regulating epithelial-mesenchymal transition and cancer stem cells as molecular targets for cancer therapeutics.* Cancer gene therapy, 2012. **19**(11): p. 723-30.

98. Wang, P., et al., *Identification and characterization of cells with cancer stem cell properties in human primary lung cancer cell lines.* PLoS One, 2013. **8**(3): p. e57020.

99. Betz, M.W., et al., *Macroporous hydrogels upregulate osteogenic signal expression and promote bone regeneration.* Biomacromolecules, 2010. **11**(5): p. 1160-8.

100. Yeatts, A.B., et al., *Human mesenchymal stem cell position within scaffolds influences cell fate during dynamic culture.* Biotechnol Bioeng, 2012. **109**(9): p. 2381-91.

101.   Curtis, A.S., et al., *Adhesion of cells to polystyrene surfaces.* J Cell Biol, 1983. **97**(5 Pt 1): p. 1500-6.

102.   Curran, J.M., R. Chen, and J.A. Hunt, *The guidance of human mesenchymal stem cell differentiation in vitro by controlled modifications to the cell substrate.* Biomaterials, 2006. **27**(27): p. 4783-93.

103.   Moon, J.J., S.H. Lee, and J.L. West, *Synthetic biomimetic hydrogels incorporated with ephrin-A1 for therapeutic angiogenesis.* Biomacromolecules, 2007. **8**(1): p. 42-9.

104.   Phillips, J.E., et al., *Human mesenchymal stem cell differentiation on self-assembled monolayers presenting different surface chemistries.* Acta biomaterialia, 2010. **6**(1): p. 12-20.

105.   Gallant, N.D., K.E. Michael, and A.J. Garcia, *Cell adhesion strengthening: contributions of adhesive area, integrin binding, and focal adhesion assembly.* Molecular biology of the cell, 2005. **16**(9): p. 4329-40.

106.   Garcia, A.J., P. Ducheyne, and D. Boettiger, *Quantification of cell adhesion using a spinning disc device and application to surface-reactive materials.* Biomaterials, 1997. **18**(16): p. 1091-8.

107.   Pouton, C.W. and J.M. Haynes, *Embryonic stem cells as a source of models for drug discovery.* Nature reviews. Drug discovery, 2007. **6**(8): p. 605-16.

108.   Lv, F.J., et al., *Concise review: the surface markers and identity of human mesenchymal stem cells.* Stem Cells, 2014. **32**(6): p. 1408-19.

109.   Bara, J.J., et al., *Concise review: Bone marrow-derived mesenchymal stem cells change phenotype following in vitro culture: implications for basic research and the clinic.* Stem Cells, 2014. **32**(7): p. 1713-23.

110.   Lane, S.W., D.A. Williams, and F.M. Watt, *Modulating the stem cell niche for tissue regeneration.* Nat Biotechnol, 2014. **32**(8): p. 795-803.

111.   Wang, M.O., et al., *Evaluation of the in vitro cytotoxicity of cross-linked biomaterials.* Biomacromolecules, 2013. **14**(5): p. 1321-9.

112.   Fisher, J.P., D. Dean, and A.G. Mikos, *Photocrosslinking characteristics and mechanical properties of diethyl fumarate/poly(propylene fumarate) biomaterials.* Biomaterials, 2002. **23**(22): p. 4333-43.

113.   Fisher, J.P., et al., *Soft and hard tissue response to photocrosslinked poly(propylene fumarate) scaffolds in a rabbit model.* J Biomed Mater Res, 2002. **59**(3): p. 547-56.

114.   Dominici, M., et al., *Minimal criteria for defining multipotent mesenchymal stromal cells. The International Society for Cellular Therapy position statement.* Cytotherapy, 2006. **8**(4): p. 315-7.

115.   Wang, M.O., et al., *Evaluating Changes in Structure and Cytotoxicity During In Vitro Degradation of Three-Dimensional Printed Scaffolds.* Tissue engineering. Part A, 2015.

116.   Lee, K.W., et al., *Physical properties and cellular responses to crosslinkable poly(propylene fumarate)/hydroxyapatite nanocomposites.* Biomaterials, 2008. **29**(19): p. 2839-48.

117.   Knight, C.G., et al., *The collagen-binding A-domains of integrins alpha(1)beta(1) and alpha(2)beta(1) recognize the same specific amino acid*

sequence, GFOGER, in native (triple-helical) collagens. The Journal of biological chemistry, 2000. **275**(1): p. 35-40.

118.   Wallace, J., et al., *Validating continuous digital light processing (cDLP) additive manufacturing accuracy and tissue engineering utility of a dye-initiator package.* Biofabrication, 2014. **6**(1): p. 015003.

119.   Wang, M.O., et al., *Evaluating 3D-printed biomaterials as scaffolds for vascularized bone tissue engineering.* Adv Mater, 2015. **27**(1): p. 138-44.

120.   Lee, J., et al., *Directing stem cell fate on hydrogel substrates by controlling cell geometry, matrix mechanics and adhesion ligand composition.* Biomaterials, 2013. **34**(33): p. 8140-8.

121.   Zhang, Q., et al., *Pore size effect of collagen scaffolds on cartilage regeneration.* Acta Biomater, 2014. **10**(5): p. 2005-13.

122.   Lien, S.M., L.Y. Ko, and T.J. Huang, *Effect of pore size on ECM secretion and cell growth in gelatin scaffold for articular cartilage tissue engineering.* Acta Biomater, 2009. **5**(2): p. 670-9.

123.   Woodfield, T.B., et al., *Design of porous scaffolds for cartilage tissue engineering using a three-dimensional fiber-deposition technique.* Biomaterials, 2004. **25**(18): p. 4149-61.

124.   Kim, K., et al., *The influence of stereolithographic scaffold architecture and composition on osteogenic signal expression with rat bone marrow stromal cells.* Biomaterials, 2011. **32**(15): p. 3750-63.

125.   Dean, D., et al., *Continuous Digital Light Processing (cDLP): Highly Accurate Additive Manufacturing of Tissue Engineered Bone Scaffolds.* Virtual and physical prototyping, 2012. **7**(1): p. 13-24.